THE ROLE OF CHONDROITIN SULFATE PROTEOGLYCANS AND PROTEIN TYROSINE PHOSPHATASE SIGMA IN SYMPATHETIC NERVE REMODELING AND ARRHYTHMIA SUSCEPTIBILITY AFTER MYOCARDIAL INFARCTION

By

Ryan T. Gardner

A DISSERTATION

Presented to the Neuroscience Graduate Program
and Oregon Health and Science University
School of Medicine
In Partial fulfillment of
the requirements for the degree of

Doctor of Philosophy

March 2014

School of Medicine

Oregon Health and Science University

_____

CERTIFICATE OF APPROVAL

This is to certify that the Ph.D. dissertation of

Ryan T. Gardner

has been approved

_____
Mentor/Advisor: Beth A. Habecker, Ph.D.

_____
Committee Chair/Member: Philip Copenhaver, Ph.D.

_____
Member: Sue Aicher, Ph.D.

_____
Member: Stephen Back, M.D., Ph.D.

_____
Member: Lawrence Sherman, Ph.D.

_____
Member: Larisa Tereshchenko, M.D., Ph.D.

Table of Contents

List of Figures

Chapter 1: Introduction

Chapter2: Manuscript 1

Chapter 3: Manuscript 2

Chapter 4: Summary of Results and Discussion

Appendices

List of Abbreviations

123-MIBG	123- metaiodobenzylguanadine
Ach	acetylcholine
AP	action potential
APD	action potential duration
AR	adrenergic receptor
AV	atrioventricular
BDNF	brain derived neurotrophic factor
CAM	cell adhesion molecule
cAMP	cyclic adenosine monophosphate
CaT	Calcium transient
ChABC	chondroitinase ABC
CNS	central nervous system
CNTF	ciliary neurotrophic factor
CS	chondroitin sulfate
CSPG	chondroitin sulfate proteoglycans
DAD	delayed afterdepolarization
DHBA	dihydroxybenzylamine
DMSO	dimethyl sulfoxide
ECG	electrocardiogram
ECM	extracellular matrix
ERK	extracellular signal-related kinase
Fib	fibrinogen
GRK2	G-protein coupled receptor kinase 2

HA	hyaluronan
HET	heterozygous
HMW	high molecular weight
HPLC	high performance liquid chromatography
HSPG	heparin sulfate proteoglycans
ICD	implantable cardioverter-defibrillator
IMP	intracellular mu peptide
IP	intraperitoneal
IQR	interquartile range
I-R	ischemia-reperfusion
ISO	isoproterenol
ISP	intracellular sigma peptide
JNK	c-Jun N-terminus kinase
KO	knock out
LA	left atrium
LAD	left anterior descending artery
LAR1	leukocyte antigen-related tyrosine phosphatase
LIF	leukemia inhibitory factor
LMW	low molecular weight
LV	left ventricle
MI	myocardial infarction
MMP	matrix metalloprotease
NE	norepinephrine
NGF	nerve growth factor
NgR1	nogo receptor 1

NgR3	nogo receptor 3
NT-3	neurotrophin 3
NT-4/5	neurotrophin 4/5
p75NTR	p75 neurotrophin receptor
PACAP	pituitary adenylate cyclase –activating peptide
PBS	phosphate buffered saline
PCA	perchloric acid
PI3K	phosphoinositide-3-kinase
PKA	protein kinase A
PKC	protein kinase C
PLC	phospholipase C
PLL	poly-l lysine
Prop	propranolol
PTPσ	protein tyrosine phosphatase sigma
PVC	premature ventricular complex
RA	right atrium
ROCK	Rho kinase
RV	right ventricle
RyR	ryanodine receptor
SA	sinoatrial
SCD	sudden cardiac death
SCG	superior cervical ganglion
SERCA	sarco/endoplasmic reticulum Ca^{2+} ATPase
SR	sarcoplasmic reticulum
STAT3	signal transducer and activator of transcription

TBTA	tris[(1-benzyl-1*H*-1,2,3-triazol-4-yl)methyl]amine
TCEP	tris(2-carboxyethyl)phosphine
TH	tyrosine hydroxylase
TnC	tenascin C
Trk	tropomyosin-related kinase
VIP	vasoactive intestinal peptide
V_m	membrane voltage
WT	wild type

Acknowledgements

I would like to extend a special thank you to my mentor, Dr. Beth Habecker. Her guidance and leadership throughout graduate school was essential for my development as a scientist. Beth is a great model for the type of mentor I would hope to be. She is an excellent scientist, a great writer, and a patient advisor. Throughout my training, Beth provided guidance and encouragement while also fostering independence and I can't thank her enough for her mentorship.

I would like to thank my thesis committee, Dr. Sue Aicher, Dr. Stephen Back, Dr. Philip Copenhaver, and Dr. Lawrence Sherman. Throughout my graduate training, my committee members have not only given me incredible advice in developing my project but have also been supportive and encouraging. Additionally, I am grateful to Dr. Larisa Tereshchenko for serving on my exam committee.

I would also like to acknowledge all past and present members of the Habecker lab: Dr. Christina Lorentz, Dr. Wohaib Hasan, Diana Parrish, Dr. Xiao Shi, Dr. Michael Pellegrino, Dr. William Woodward, and Antoinette Olivas. Our discussions, both scientific and not, truly fostered my graduate experience. In particular, I would like to thank Mike Pellegrino for endless support and entertainment. Thanks Mike for being totes awesome. Additionally, a special thanks to Bill Woodward. I was privileged to have the opportunity of working with Bill, one of the most intelligent people I've had the pleasure of knowing. I am

grateful for our discussions about science, power tools, and sometimes football, maybe mostly football.

Additionally, I would like to thank a number of people whose support was instrumental to me. Dr. Michael Cohen was an amazing collaborator and taught me so much about non-physiology stuff. Dr. Crystal Ripplinger and Lianguo Wang deserve so much credit for their participation in my project and teaching me one of the coolest techniques. I am grateful to Julie Walvante in the Phys-Pharm Department for endless amounts of help with scheduling, travel, and, most importantly, reimbursements. In the Neuroscience Graduate Program, Liz Lawson-Weber has been an amazing help. From the time I applied to NGP until the time I finished my thesis, Liz has helped keep me organized and registered. Also, my classmates and friends Biliana Veleva-Rotse and Molly Marra made the early years of graduate school so much more bearable, and have been fantastic friends outside the science world.

Lastly, my family deserves so much credit for everything that I do, and to whom I dedicate this work. A special thank you to my wonderful wife Ali, who has patiently listened through both the difficult and the good times. Her support has made the difficult times so much easier to deal with. Thank you, Ali, for always being there for me and remarkably reading my thesis multiple times. Finally, I am thankful to my parents, Rick and Aline, and my sister, Tessa, without whose support I wouldn't be here. They are always enthusiastic about trying to understand what I do.

Abstract

Sympathetic nerve regeneration is common after peripheral injuries. A well documented example of this is sympathetic sprouting and reinnervation after chronic cardiac ischemia. Surprisingly though, following a more common cardiac injury, ischemia-reperfusion (I-R), the resulting infarcted myocardium remains denervated. The degree of sympathetic denervation after I-R has been identified as a sensitive predictor of secondary cardiac pathologies, including sudden cardiac death and arrhythmias. Given the prevalence of I-R and incidence of secondary cardiac pathologies following this type of injury, sympathetic denervation resulting from I-R has proven to be a considerable clinical issue. In order to understand why sympathetic regeneration fails following I-R, we examined the infarct for potential inhibitory components in the extracellular matrix. We found that chondroitin sulfate proteoglycans (CSPGs) were present in the infarct after I-R and that CSPGs caused inhibition of sympathetic axon outgrowth in vitro. Furthermore, in the absence of protein tyrosine phosphatase sigma (PTPσ), a receptor for CSPGs, sympathetic innervation was restored to the infarct in vivo. Due to the importance of sympathetic denervation in determining arrhythmia susceptibility, we wanted to examine the electrophysiological consequences of sympathetic reinnervation after I-R. We found that both the absence of PTPσ using transgenic animals and pharmacologic modulation of PTPσ by the novel intracellular sigma peptide (ISP) restored sympathetic innervation to the scar and markedly reduced arrhythmia susceptibility. Using optical mapping, we observed increased dispersion of action potential duration, super-sensitivity to β-adrenergic receptor stimulation,

and Ca^{2+} mishandling following MI. However, sympathetic reinnervation prevented these changes and rendered hearts remarkably resistant to induced arrhythmias. This work is the first to show that sympathetic reinnervation is protective against electrophysiological remodeling and ventricular arrhythmias even in the presence of a scar. It also establishes Ca^{2+} mishandling as an important underlying mechanism to elevated arrhythmia susceptibility after I-R injury. More broadly, this works establishes PTPσ as a potential clinical target following a heart attack to protect the heart against arrhythmias and sudden cardiac death.

Chapter 1

Introduction

Cardiovascular disease is the leading cause of death both in the United States and worldwide, and every year approximately 1.2 million Americans suffer from a myocardial infarction (MI; heart attack) (Roger et al., 2012a). While survival and treatment of those suffering an MI has greatly improved, those who survive are much more susceptible to arrhythmias and sudden cardiac death (Solomon et al., 2005). Specifically, almost 300,000 people die annually in the United States alone from these secondary cardiac pathologies (Solomon et al., 2005). Research in both humans and animal models of MI suggest that changes in sympathetic innervation of the heart are responsible, at least in part, for this post-MI rhythm instability. Specifically, this is due to sympathetic heterogeneity that is established by sympathetic denervation of infarcted myocardium, or scar (Boogers et al., 2010;Fallavollita et al., 2013;Nishisato et al., 2010;Rubart and Zipes, 2005;Vaseghi et al., 2012). While the clinical significance of this sympathetic denervation is well established, the molecular basis for sustained sympathetic denervation of the infarct remains unclear. The focus of this thesis is to understand why sympathetic nerves fail to reinnervate into infarcted myocardium, and to examine whether sympathetic reinnervation is protective against arrhythmias.

I. The Autonomic Nervous System and Axon Regeneration

A. Autonomic Nervous System

The mammalian nervous system is composed of the central nervous system (CNS; brain and spinal cord) and the peripheral nervous system. The peripheral nervous system is further divided into the somatic nervous system and the autonomic nervous system. While the somatic nervous system transmits sensory input and controls voluntary motor behavior, the autonomic nervous system modulates the involuntary function of internal organs. For example, the autonomic nervous system modulates heart function, respiration, perspiration, digestion, and several other involuntary functions. Much like the peripheral nervous system, the autonomic nervous system can be further divided into two components: the parasympathetic and sympathetic.

1. General Anatomy

The two branches of the autonomic nervous system are largely defined anatomically but also have functional and biochemical distinctions. Although parasympathetic and sympathetic efferents both consist of pre-ganglionic and post-ganglionic neurons, each branch has a distinct spatial organization. Parasympathetic pre-ganglionic cell bodies are found within the brainstem and sacral spinal cord, while sympathetic pre-ganglionic cell bodies are found in the thoracic and lumbar regions. Pre-ganglionic axons of both branches project from the CNS to innervate post-ganglionic neurons. As the name suggests, cell bodies of post-ganglionic neurons compose a ganglion outside the CNS. Here, parasympathetic and sympathetic branches are once again anatomically distinct.

Parasympathetic ganglia are often intimately positioned adjacent to target tissue, which requires only short post-ganglionic projections. Conversely, sympathetic ganglia are located near the spinal cord and require longer post-ganglionic projections to their targets (Martin J.H., 1996).

2. Neurotransmission

Pre-ganglionic neurons of both autonomic branches transmit activity via the release of acetylcholine (ACh) onto post-ganglionic neurons that express nicotinic ACh receptors. Post-ganglionic neurons, however, have general biochemical identity based on neurotransmitter synthesis and release. Post-ganglionic parasympathetic neurons also release ACh, but here, target tissues express muscarinic ACh receptors. In contrast, most sympathetic post-ganglionic neurons release norepinephrine (NE), which activates target tissues by binding α and β adrenergic receptors (AR). This, however, is not ubiquitous; small subsets of sympathetic neurons do release ACh onto their targets. Functionally, parasympathetic and sympathetic activity results in opposing actions in many target tissues, including the heart; however, this is also not universal. Simplistically, parasympathetic activity drives “rest and digest” responses, while sympathetic activity drives “fight or flight” responses (Kandel E.R. et al., 2000).

B. Peripheral Axon Regeneration

Given the roles of sensory, motor, and autonomic nerve activity, peripheral nerve injury can create numerous deficits in physiology including analgesia, autonomic imbalance, and paralysis. However, peripheral nerves are often

capable of regenerating and reinnervating their target tissues to restore function. While peripheral nerves are capable of regeneration, the ability to do so is determined by the extracellular balance of attractive and repellant molecular signals. The composition of the local extracellular environment can create a permissive substrate for axon regeneration or a molecular barrier that prevents regeneration.

Peripheral nerve injury results in Wallerian degeneration of the axon distal to the site of injury. During the process of clearing axonal debris, Schwann cells (Funakoshi et al., 1993;Heumann et al., 1987), infiltrating monocytes (Brown et al., 1991;Dailey et al., 1998;Niemi et al., 2013), as well as the neurons themselves (Kobayashi et al., 1996;Streppel et al., 2002), produce an extracellular environment that is conducive to axon regeneration. However, even while an extracellular environment may promote axon regeneration, the ability to regenerate also depends on intrinsic adaptation of gene transcription to a state that promotes survival and axon extension.

The cellular adaptation that allows for increased axon extension following injury can be experimentally observed using a conditioning lesion paradigm (McQuarrie and Grafstein, 1973). These experiments show that an initial "priming" lesion increases the regenerative response to a second axonal injury. The switch in neuronal behavior from a transmission state to one of regeneration can include several mechanisms. For example, increased electrical activity initiated by Ca^{2+} influx at the site of injury will alter transcription at the cell body (Mandolesi et al., 2004). Other signals involve the loss of retrograde chemical

signaling, a notable example of which is reduced nerve growth factor (NGF) transport (Raivich et al., 1991). Inflammatory cytokines, like ciliary neurotrophic factor (CNTF), also play an important role in priming neurons through activation of Signal Transducer and Activator of Transcription 3 (STAT3) (Smith and Skene, 1997;Habecker et al., 2009;Liu and Snider, 2001). These environmental cues lead to activation of several signaling pathways that include mitogen activated protein kinases ERK and Jun N-terminal kinase (JNK), as well as PI3K/Akt (Lindwall and Kanje, 2005;Perlson et al., 2005;Zhou and Snider, 2006). Overall, these signaling cascades result in altered transcription at the cell body, where cytoskeletal proteins involved in axon regeneration, like actin and tubulin, are upregulated (Hoffman and Cleveland, 1988), and neurotransmission machinery, like ion channels, are reduced (Costigan et al., 2002).

1. Sympathetic Nerve Regeneration

Many early studies of peripheral nerve regeneration examined sympathetic neurons, which are incredibly dynamic in their ability to regenerate following injury, as well as during normal physiological processes. For example, in rats, sympathetic nerves denervate and reinnervate the uterus with every estrous cycle (Zoubina and Smith, 2000). Additionally, following axotomy, sympathetic nerves reinnervate several target tissues, including vasculature (Aguayo et al., 1973;Hill et al., 1985) and skin (Gloster and Diamond, 1995). The heart, in fact, is a well characterized sympathetic target where reinnervation frequently occurs.

Sympathetic nerves project throughout the entire heart and are capable of reinnervation in multiple ischemic and non-ischemic conditions. For example, sympathetic regeneration is observed using iodine-123 metaiodobenzylguanadine (123-MIBG) imaging in living patients (Bengel et al., 1999;Bengel et al., 2001;Estorch et al., 1999) and direct staining for tyrosine hydroxylase (TH) after autopsy (Kim et al., 2004) following heart transplant. Sympathetic regeneration also occurs following chemical denervation of atria (Vo and Tomlinson, 1999). In animal models of cardiac ischemia, there is extensive sympathetic sprouting and hyperinnervation throughout the damaged ventricles (Vracko et al., 1990;Zhou et al., 2004;El-Helou et al., 2008). In the heart, much of this regeneration and sprouting is due to NGF production after injury (Hasan et al., 2006;Wernli et al., 2009).

Cardiac sympathetic reinnervation is not alone in its reliance on NGF to stimulate axon outgrowth after injury. This is also true for collateral sprouting in injured skin (Gloster and Diamond, 1995) and reinnervation of arthritic joints (Ghilardi et al., 2012). NGF is often produced by target tissue after injury (Ghilardi et al., 2012;Gloster and Diamond, 1995;Hasan et al., 2006) and is thought to stabilize the growth cone cytoskeleton (Estrach et al., 2002;Veeranna et al., 1998). However, the importance of NGF is not limited to axon regeneration after injury. It is critical for both sympathetic neuron survival and axon extension during development. In order to understand sympathetic input as it relates to cardiac function, it is important to understand the role of NGF in sympathetic patterning.

2. Nerve Growth Factor (and other secreted factors)

For some peripheral nerves, namely sensory and sympathetic nerves, NGF is the primary signal for neuron survival and axon outgrowth. NGF is a member of a larger family of polypeptides called neurotrophins, which were identified for their roles in survival and axon extension (Chao, 2003;Lu et al., 2005). The neurotrophin family, in addition to NGF, includes brain derived neurotrophic factor (BDNF) (Barde et al., 1982), neurotrophin-3 (NT-3) (Hohn et al., 1990), and NT-4 (also known as NT-5) (Berkemeier et al., 1991;Hallbook et al., 1991). Synthesis of neurotrophins begins with precursors (pro-neurotrophins), which are then cleaved to become mature neurotrophins. Both the pro and mature variants are secreted factors that have distinct roles and often act in opposition via two distinct receptor types (Chao, 2003;Lu et al., 2005).

Like all other neurotrophins, NGF binds with high affinity to a tropomyosin-related kinase (Trk) receptor. There are three members of the Trk family: TrkA, TrkB, and TrkC (Chao, 2003). In general, each Trk receptor preferentially binds individual neurotrophins with high affinity. For example, TrkA binds NGF, TrkB binds BDNF and NT-4, and TrkC binds NT-3 (Chao, 2003). NGF action is mediated through activation of its high affinity receptor TrkA (Chao, 2003). Once bound, NGF induces dimerization of TrkA (Jing et al., 1992), which then enables trans-autophosphorylation of the opposing receptor and activation of downstream effectors (Cunningham and Greene, 1998;Jing et al., 1992;Reichardt, 2006). There are three primary signaling pathways activated by NGF binding to TrkA

(common to all Trk receptors) 1) phospholipase Cγ (PLCγ), 2) phosphoinostitide-3-kinase (PI3K)/Akt and 3) Ras/Raf/ERK. Although these pathways have some overlapping function, activation of the PI3K/Akt pathway primarily promotes survival and the Ras/Raf/ERK pathway primarily stimulates axon outgrowth (Figure 1.1) (Reichardt, 2006). The activity of NGF and the other neurotrophins, however, is not exclusively mediated by Trk receptor activation.

In addition to Trk receptors, neurotrophins bind the structurally distinct p75 neurotrophin receptor (p75NTR). Interestingly, p75NTR was the first neurotrophin receptor identified (Johnson et al., 1986), and, unlike Trk receptors, binds all neurotrophins with equal affinity (Rodriguez-Tebar et al., 1990). Additionally, p75NTR has distinct signaling and downstream effects that are much more complex than Trk signaling. This complexity is due to the ability of p75NTR to signal independently or in a complex with other receptors, including TrkA (Hempstead et al., 1991;Hempstead, 2002). Independently, p75NTR activation leads to inhibition of axon outgrowth and apoptosis through multiple signaling pathways, including Rho and JNK/p53 (Kaplan and Miller, 2000;Reichardt, 2006).

Developmentally, neurotrophins are critical for proper sympathetic patterning and survival. Initial axon guidance to the heart, for example, occurs along arterial vasculature where it is guided primarily by NT-3 (Francis et al., 1999). Once at the heart, cardiac derived NGF stimulates axon extension, while

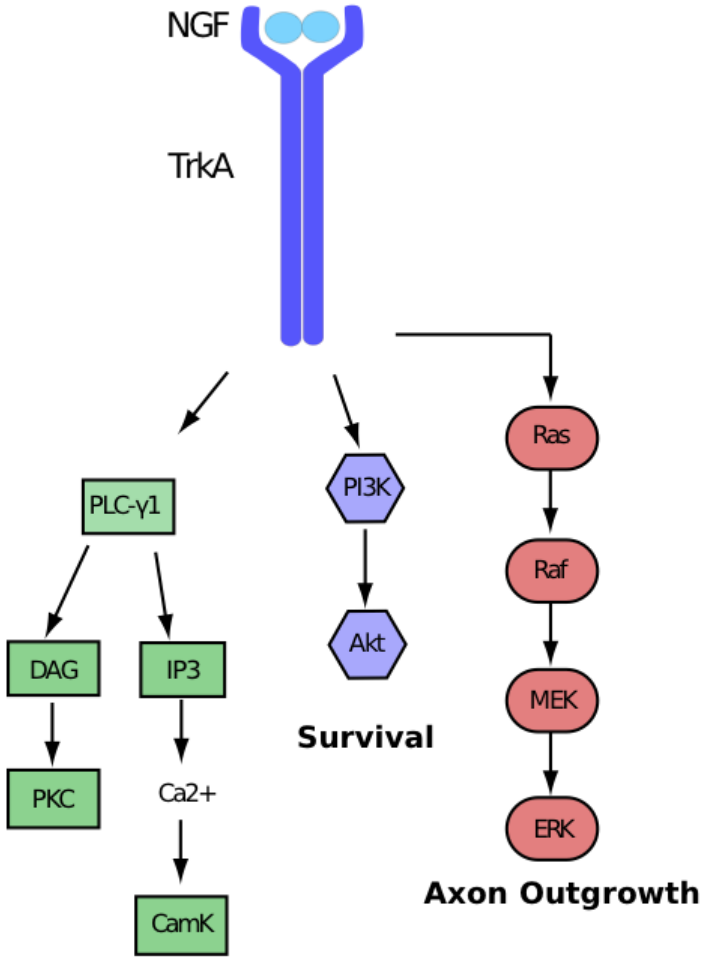

Figure 1.1 NGF/TrkA Signaling. Dimerized NGF binds to TrkA, promoting receptor dimerization and transautophosphorylation. Phosphorylation of TrkA promotes signaling via three pathways: 1) PLC-γ1/PKC/CamK, 2) PI3K/Akt, and 3) Ras/Raf/MEK/ERK. PI3K/Akt primarily promotes survival, whereas Ras/Raf/MEK/ERK primarily promotes axon outgrowth, although there is some overlapping function.

also promoting survival (Crowley et al., 1994;Glebova and Ginty, 2005;Ieda et al., 2004). At the same time, proper patterning and distribution of cardiac sympathetic innervation relies on the balance of the attractive signal of NGF and local repulsive cues. In the heart, the repulsive counterpart of NGF is Sema3a, which is highly expressed in the subendocardium of the heart (Ieda et al., 2007). This expression pattern results in high innervation density within the subepicardium (outer layer) and low density in the subendocardium (inner layer) (Ieda et al., 2007), an important pattern that will be discussed later.

Although the primary characterization of NGF and other neurotrophins was directed towards understanding their role in the development of the peripheral nervous system, it has since been established that neurotrophins are also involved in nerve regeneration in adult animals (Ghilardi et al., 2012;Gloster and Diamond, 1995;Hasan et al., 2006) and synaptic maintenance and plasticity (Maisonpierre et al., 1990;Poo, 2001). For regenerating nerves, NGF provides neurotrophic support and accelerates the rate of axon regeneration. The role of NGF following injury is not as well understood in comparison to developmental axon extension and survival. Adult sympathetic neurons no longer rely on NGF for survival (Ruit et al., 1990;Sofroniew et al., 2001) and some sympathetic regeneration occurs independently of NGF (Gloster and Diamond, 1992;Gloster and Diamond, 1995). Some tissues, however, maintain basal expression of NGF. Following injury, NGF expression is upregulated (Gloster and Diamond, 1995;Streppel et al., 2002) and promotes sprouting and reinnervation of skin (Gloster and Diamond, 1995) and the heart (Hasan et al., 2006;Wernli et al.,

2009). Furthermore, in some cases of nerve regeneration, application of exogenous NGF, or other neurotrophins, is sufficient to overcome an otherwise non-permissive extracellular environment to reinnervate the target tissue (Grill et al., 1997b;Grill et al., 1997a;Tuszynski et al., 1996).

In addition to neurotrophins, there are other stimulatory peptides and cytokines released after injury. Sympathetic nerves produce galanin (Mohney et al., 1994;Schreiber et al., 1994), pituitary adenylate cyclase-activating peptide (PACAP) (Moller et al., 1997;Klimaschewski et al., 1996), and vasoactive intestinal peptide (VIP) (Mohney et al., 1994;Klimaschewski et al., 1994) in response to injury, all of which are growth factor-like neuropeptides (Arimura et al., 1994;Said and Mutt, 1970;Tatemoto et al., 1983). In addition to these neuronally derived factors, infiltrating monocytes and localized inflammation are also stimulatory to axon regeneration. Specifically, production of cytokines like CNTF (Adler, 1993) and leukemia inhibitory factor (LIF) (Rao et al., 1993) stimulate axon growth through their receptor gp130 (Ip et al., 1992;Cafferty et al., 2001;Ekstrom et al., 2000;Leibinger et al., 2009). Interestingly, NGF/TrkA and gp130 dependent stimulation of axon outgrowth converge through STAT3 to promote maximal axon extension (Pellegrino and Habecker, 2013).

3. Extracellular Matrix

In addition to secreted factors, the extracellular matrix (ECM) is an important determinate of axon regeneration. The ECM is a protein milieu that can support neurons by providing adhesion and maintenance of synaptic structures. Additionally, the ECM, in partnership with neuronal cell adhesion

molecules (CAM), can provide attractive or repulsive cues to regenerating nerves. For much of the adult peripheral nervous system, the ECM is inhibitory to prevent sprouting and plasticity. Proteoglycans are a common inhibitory matrix component, which often act through inhibition of growth promoting ECM components (Hamel et al., 2008;Zuo et al., 1998). Although proteoglycans are also upregulated following peripheral nerve injury (Zuo et al., 1998), they are often quickly degraded in order to promote axon regeneration (Ferguson and Muir, 2000;Zuo et al., 2002).

In the absence of inhibitory or repulsive cues, peripheral nerves are capable of regenerating to the site of injury, often aided by growth promoting matrix glycoproteins collagen, laminin, and fibronectin (Babington et al., 2005;Gardiner et al., 2007;Werner et al., 2000). Much of the ability to regenerate along these glycoproteins, however, is mediated by the CAMs expressed on the neuronal membrane (Gardiner et al., 2007;Werner et al., 2000). Common neuronal CAMs include N-Cadherin (Ranscht, 2000), immunoglobulin superfamily member NCAMs (Zhang et al., 2008), and integrins (Barczyk et al., 2010). With an abundance of growth promoting ECM components and CAMs, peripheral nerve regeneration is common. In the rare cases where nerve regeneration fails, commonly in the CNS, inhibitory extracellular matrix is often the culprit.

a. Chondroitin sulfate proteoglycans

While there are several inhibitory components of ECM, chondroitin sulfate proteoglycans (CSPG) are well studied components that are active during both

development and adult axon regeneration. Structurally, CSPGs are characterized by a core protein that is covalently linked to chondroitin sulfate (CS) side chains (Kjellen and Lindahl, 1991). Although this general configuration is common to all CSPGs, there is some structural variability that allows further sub-classification. One of the most common sub-types of CSPGs are the lecticans, whose core proteins are composed of G1 and G3 domains that flank a central region containing CS side chains (Yamaguchi, 2000)(Figure 1.2). Like other ECM components, proper CSPG localization is dependent on interaction with the rest of the ECM and neuronally expressed CAMs. Much of this interaction occurs through the G1 and G3 domains. Specifically, G1 interacts with glycoaminoglycan hyaluronan (Matsumoto et al., 2003) and G3 interacts with tenascins (Grumet et al., 1994), fibronectins (Snow et al., 1996), and other cell adhesion molecules (Friedlander et al., 1994;Yamaguchi, 2000). As highly expressed and active members of the ECM, CSPGs as a whole play diverse roles throughout development and in the adult nervous system.

During development, CSPGs are expressed at high levels throughout the nervous system. Initially, they are involved in the migration of neural crest cells (Kerr and Newgreen, 1997;Perissinotto et al., 2000). Later, they are found at the ventricular zone of the developing CNS (Gates et al., 1995) where they play a role in proliferation and differentiation of stem cells (Sirko et al., 2007;von et al., 2006). More so, CSPGs are important for axon guidance and proper synapse formation (Bandtlow and Zimmermann, 2000;Landolt et al., 1995;Oakley and Tosney, 1991). As development progresses and the animal matures, CSPG

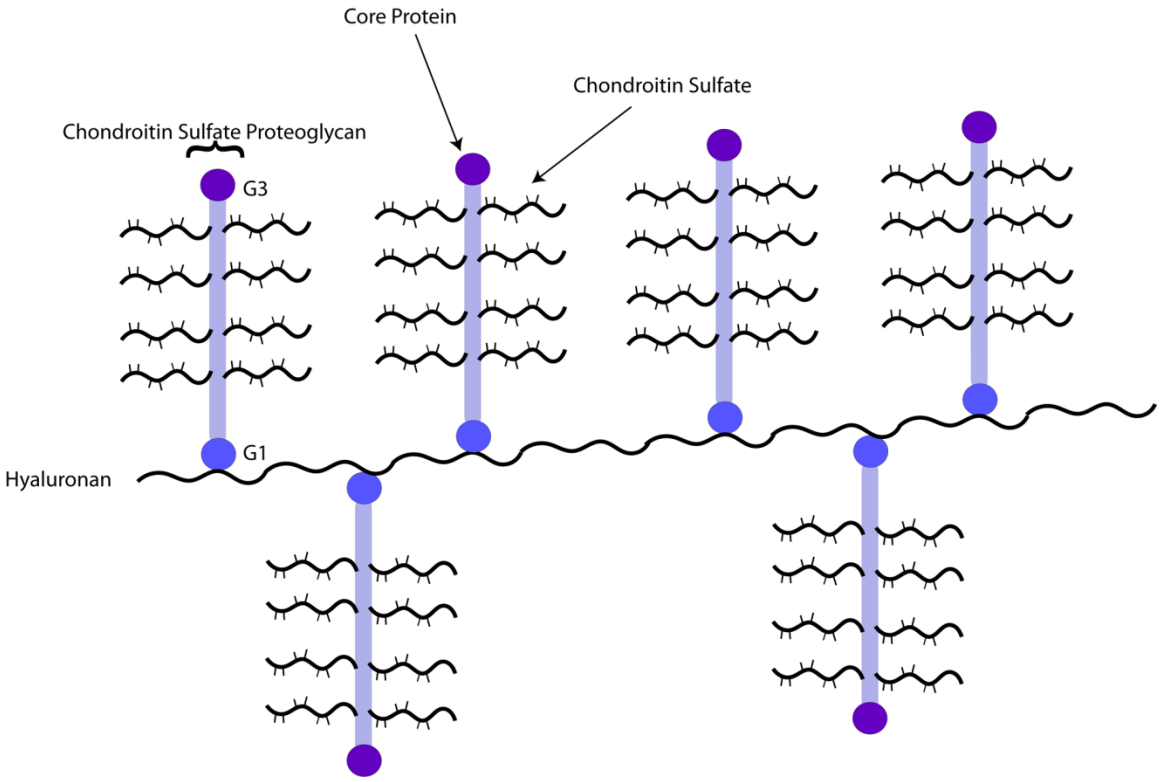

Figure 1.2 Structure and Interaction of CSPGs. CSPGs are composed of a central core protein covalently attached to chondroitin sulfate site chains. For lecticans, interaction with much of the other ECM is done via G1 and G3 domains of the core protein. Hyaluronan commonly interacts with CSPGs, which occurs via the G1 domain.

levels begin to decline, and the remaining expression becomes more localized to synapses.

In the adult animal, most notably in the CNS, CSPGs are an important component of peri-neuronal nets (Celio and Blumcke, 1994), which are lattice-like ECM configurations that encapsulate neuronal cell bodies and dendrites (Celio et al., 1998). Peri-neuronal nets are composed primarily of CSPGs, as well as HA and tenascins, and serve to stabilize synapses while limiting plasticity (Carulli et al., 2006;Celio and Blumcke, 1994;Galtrey and Fawcett, 2007). The structural integrity of peri-neuronal nets is lost by digestion of CS side chains, which allows nerve sprouting and new synapse formation in normal, healthy neurons (Pizzorusso et al., 2002). This highlights the importance of the CS-core protein covalent link in the activity of CSPGs, which has become an important focus after injury to address axon regeneration failure.

Injury in both the brain and spinal cord lead to extensive activation of astrocytes to initiate a process called reactive astrogliosis. The result of reactive astrogliosis is significant tissue remodeling and production of a scar. The scar composition, much like peri-neuronal nets, is highly enriched with CSPGs, HA, and tenascin C (Back et al., 2005;Galtrey and Fawcett, 2007;Tang et al., 2003). Acutely, production of the glial scar is protective to the surrounding tissue. The barrier created by the robust matrix of CSPGs and other components can restrict the spread of infection and cellular damage, thereby limiting the extent of the injury (Myer et al., 2006). Chondroitin sulfate itself is capable of inhibiting cytokine release from T cells *in vitro*, and may be an important regulator of the

neuroinflammatory response to injury (Rolls et al., 2006). Long term, however, neural recovery and axon regeneration beyond the scar is limited by the presence of CSPGs (Bradbury et al., 2002;Moon et al., 2001).

The role of CSPGs in preventing axon regeneration has been extensively established in studies of spinal cord injury (McKeon et al., 1995;Davies et al., 1997). As seen with peri-neuronal nets, CS side chains are required for the integrity of the glial barrier (Bradbury et al., 2002;Moon et al., 2001). Despite the numerous inhibitory components of a glial scar, targeting CSPGs alone has proven effective in allowing axon regeneration *in vitro* and *in vivo* (Lin et al., 2008;Massey et al., 2008;Nakamae et al., 2009;Tom et al., 2009) (Figure 1.3). In some cases, targeting CSPGs alone allows functional recovery of several processes including proprioceptive behaviors and locomotor capabilities (Bradbury et al., 2002). To date, studies targeting CSPGs overwhelmingly utilize chondroitinase ABC (ChABC) to cleave CS from the core protein (Bradbury and Carter, 2011). However, recent insight into CSPG signaling has provided other targets to restore nerve regeneration.

b. Protein tyrosine phosphatase sigma

Components of the ECM exert their affects through membrane bound neuronal receptors. Recently, protein tyrosine phosphatase sigma (PTPσ) was identified as a receptor for CSPGs (Shen et al., 2009). PTPσ is a member of a larger family of tyrosine phosphatases that have diverse roles in cellular function (Tonks, 2006). PTPσ is a membrane bound receptor-like tyrosine phosphatase comprised of an immunoglobulin and fibronectin-III extracellular domain and two

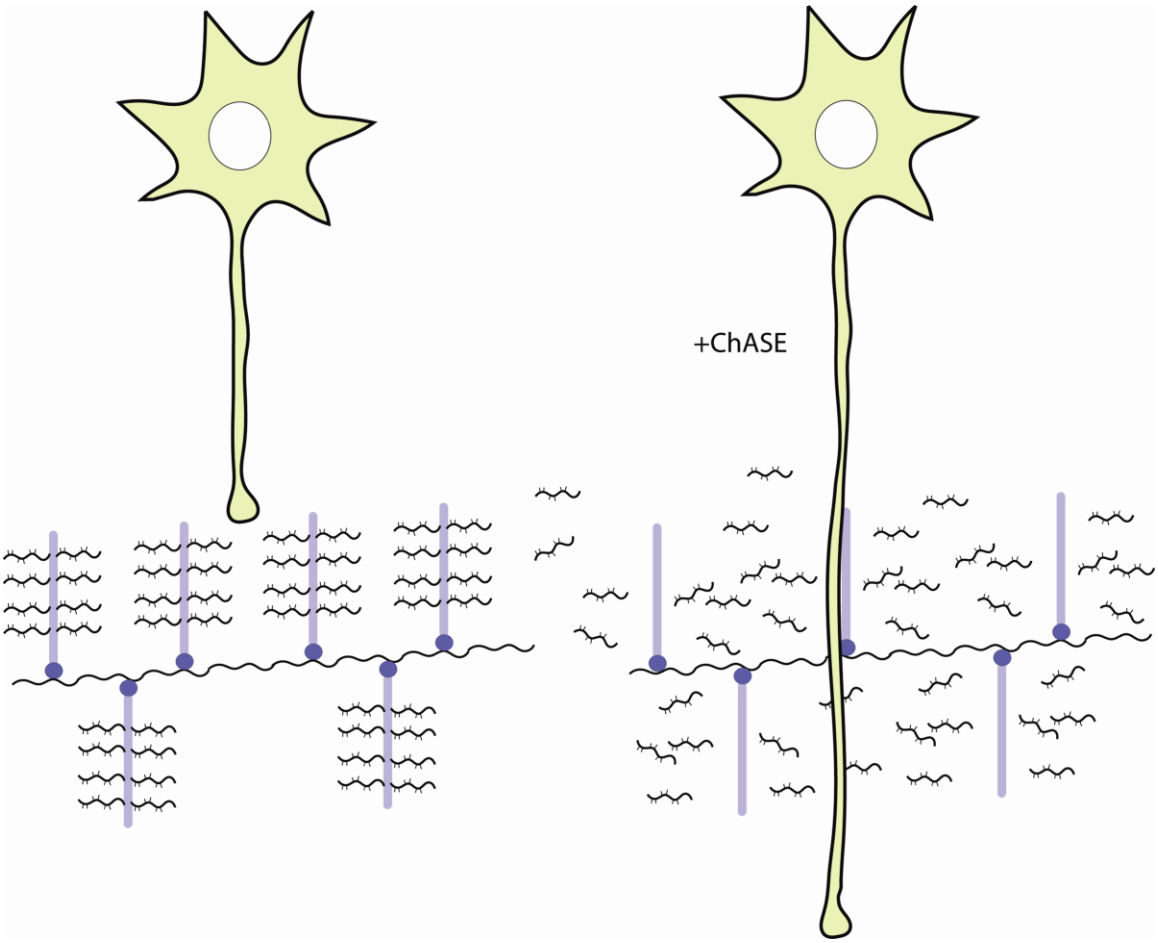

Figure 1.3 CSPGs and Axon Outgrowth. Intact CSPGs of the ECM are strong inhibitors of axon elongation. Simple digestion by ChABC, which cleaves CS from the core protein, enables axon growth through a CSPG rich substrate.

intracellular phosphatase domains (Pulido et al., 1995). Only the first phosphatase domain is active, however, while the second is regulatory (Wallace et al., 1998) (Figure 1.4). Prior to being identified as a receptor for CSPGs, PTPσ was known to restrict axon outgrowth both developmentally and after injury in adults.

In several animal systems, PTPσ plays a critical role in axon guidance and growth rate of peripheral and central neurons during development. For example, PTPσ has been shown to be important for motor neuron guidance in drosophila (Desai et al., 1996;Krueger et al., 1996), and retinal ganglion cell guidance and extension in Xenopus (Johnson et al., 2001) and chick visual systems (Ledig et al., 1999). In mice, absence of PTPσ leads to delayed and improper development of both peripheral and central nerves and structures (Elchebly et al., 1999;Wallace et al., 1999). These roles in axon guidance and extension, combined with the continued expression of PTPσ into adulthood, led to studies examining PTPσ for a role in nerve regeneration failure after injury. These studies observed that the rate of axon extension was accelerated in the absence of PTPσ following sciatic, optic, and facial nerve crush in mice. (McLean et al., 2002;Sapieha et al., 2005;Thompson et al., 2003)

Interestingly, the diverse roles for PTPσ include involvement in both axon extension and axon inhibition. These contrasting roles for PTPσ seem to be explained by ligand diveristy. Prior to identification of CSPGs as a ligand, PTPσ was identified as a receptor for heparan sulfate proteglycans (HSPG)(Aricescu et al., 2002). Developmentally, HSPGs are enriched throughout the nervous

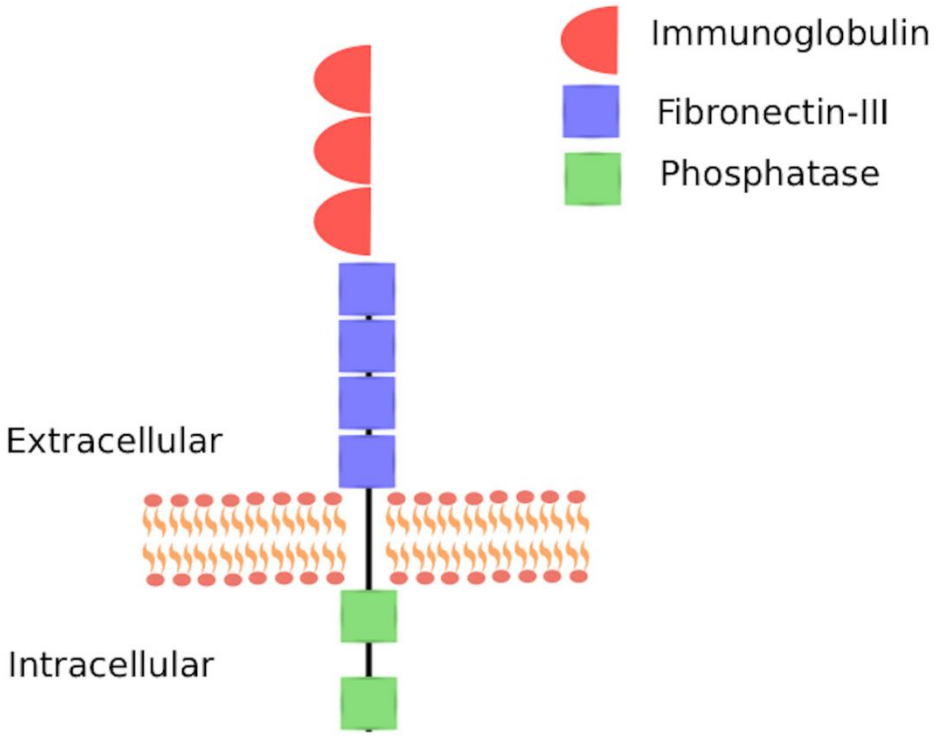

Figure 1.4 Structure of PTPσ. The structure of PTPσ resembles that of some CAMs. The extracellular domain consists of immunoglobulin and fibronectin-III repeats. The intracellular domain consists of one active phosphatase domain and one regulatory phosphatase domain

system and play diverse roles, including axon guidance (Yamaguchi, 2001). Specifically, HSPGs can promote developmental axon extension via interaction with PTPσ (Aricescu et al., 2002). This PTPσ -dependent activity is in stark contrast to nerve regeneration following injury, where PTPσ inhibts axon extension (McLean et al., 2002;Sapieha et al., 2005;Thompson et al., 2003). This PTPσ-dependent inhibition of axon outgrowth was explained by the identification of CSPGs as an endogenous ligand. This was first observed using cell free assays, which demonstrated high affinity binding of CSPGs to the extracellular domain of PTPσ. This binding is abolished by pretreatment with ChABC, which indicates that interaction occurs through the CS side chains (Shen et al., 2009). Additionally, absence of PTPσ allows increased axon extension over CSPG-rich substrates both *in vitro* and *in vivo* (Shen et al., 2009). Together, these opposing actions of PTPσ suggest that the extracellular ratio of HSPGs and CSPGs would play an important role in determining PTPσ-dependent axon regeneration.

While there is clear interaction between CSPGs and PTPσ in preventing axon regeneration after injury, the signaling mechanism by which this occurs is not known. Interestingly, HSPGs promote oligomerization of PTPσ in growth cones, while CSPGs prevent this interaction (Coles et al., 2011). Although receptor oligomerization of PTPσ may be important for axon outgrowth, it does not address the intracellular signaling mechanisms involved. Recent studies have determined that PTPσ binds and activates p250GAP (Chagnon et al., 2010), a known regulator of small Rho GTPases (RhoA, Rac, and Cdc42)

involved in cytoskeletal dynamics (Nakamura et al., 2002;Moon et al., 2003;Okabe et al., 2003). RhoA, Rac, and Cdc42 all modulate Rho kinase (ROCK), which destabilizes the cytoskeleton and inhibits axon outgrowth (Duffy et al., 2009;Fournier et al., 2003). Interestingly, p250GAP inhibits Rac and Cdc42, which are both inhibitors of ROCK, while p250GAP activates RhoA, a stimulator of ROCK (Figure 1.5) (Chagnon et al., 2010). CSPGs have also been independently linked to ROCK activity, providing strong support that this is a common pathway (Monnier et al., 2003).

In addition to ROCK activation, PTPσ directly binds all three Trk receptors (Faux et al., 2007). Dephosphorylation of Trk by PTPσ is sufficient to suppress NGF-dependent increases in axon outgrowth (Faux et al., 2007). This idea is supported by the observation that p-ERK and p-Akt increase following axon transection of retinal ganglion cells in the absence of PTPσ (Sapieha et al., 2005). These increases in Trk effector activity are coupled with increased axon regeneration at the site of the lesion (Sapieha et al., 2005). Although further examination is needed to fully understand how the CSPG-PTPσ interaction inhibits axon extension, it is clear that the absence of PTPσ allows axon regeneration across CSPG rich substrates and that PTPσ has proved to be an effective target in overcoming regeneration failure after nerve injury.

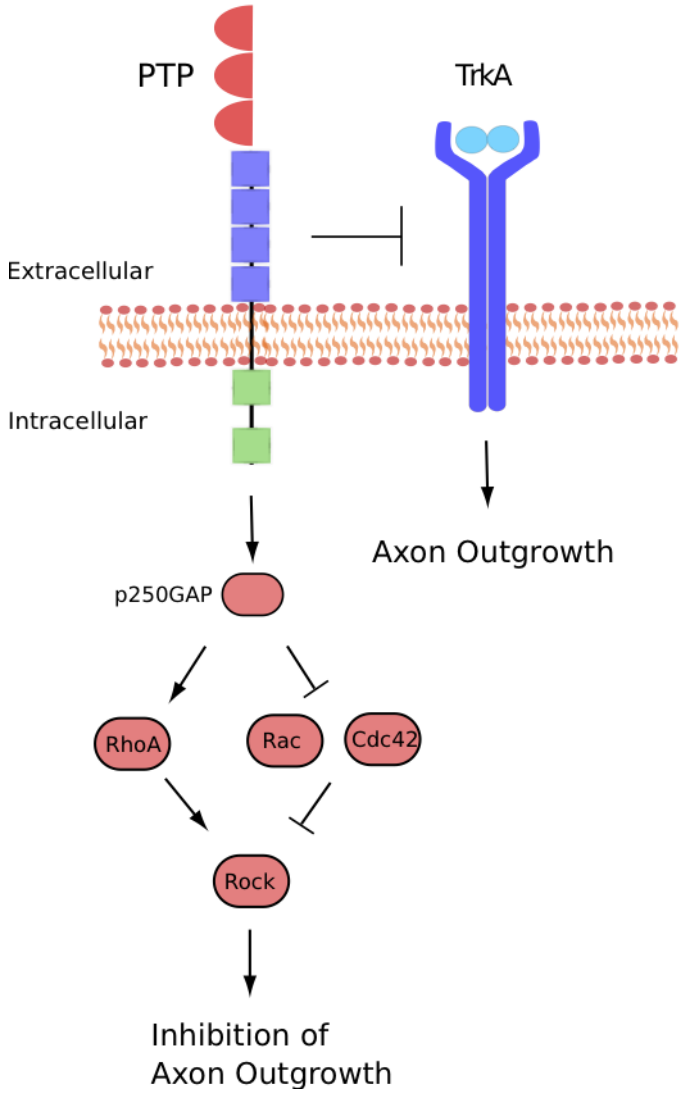

Figure 1.5 PTPσ Signaling. There are two known PTPσ signaling pathways directly involved in axon outgrowth: 1) stimulation of ROCK through modulation of Rho GTPases RhoA, Rac, and Cdc42. Rock activation leads to inhibition of axon growth by destabilizing the cytoskeleton. 2) PTPσ dephosphorylates TrkA, and inhibits NGF-dependent stimulation of axon outgrowth.

II. Cardiac Function and Innervation

A. Basic Cardiac Function

The heart is the mechanical center of the cardiovascular system. Proper blood circulation and oxygen/nutrient delivery relies on a cardiac cycle that takes deoxygenated blood, delivers it to the lungs to be oxygenated, and returns back to the heart so it can then be distributed throughout body. This process involves the four chambers of the heart acting in specific coordination and timing, beginning in the right atrium (RA). Deoxygenated blood returning to the heart via the vena cava enters into the right atrium and is quickly dumped into the right ventricle (RV) following atrial contraction. Ventricular contraction ejects blood from the RV into the pulmonary artery for delivery to the lungs. As blood passes through the lungs, it captures oxygen and returns to the left atrium (LA) of the heart via the pulmonary veins. Once again, atrial contraction empties the LA and fills the left ventricle (LV). Finally, ventricular contraction ejects oxygenated blood from the LV via the aorta, where it can be delivered to the body. This cycle then begins again as deoxygenated blood returns to the heart via the vena cava. Overall, there are two main contractile phases of this cycle that occur in quick succession. Atrial contraction allows simultaneous emptying of the RA and LA to fill the RV and LV, respectively. Ventricular contraction then causes ejection of blood from the heart by the RV and LV that allows oxygen capture and oxygen delivery, respectively. Collectively, the period in which the heart undergoes atrial and ventricular contraction is termed systole, while the period at rest is termed diastole.

In order for the heart to function properly, there must be concerted contraction of billions of specialized involuntary muscle cells called cardiomyocytes. There are two primary components of the heart that allow such action: 1) gap junctions and 2) a highly organized conduction system. Gap junctions are specialized intercellular complexes that create a tunnel structure between adjacent cells that allows transfer of many cytoplasmic components (Bernstein and Morley, 2006). In ventricular myocytes, the primary component of gap junctions is connexin 43 (Beyer et al., 1987). The presence of gap junctions between all adjacent cardiomyocytes creates a heart that is a functional syncytium, where cells are chemically and electrically linked so that the heart resembles one large muscle cell. While gap junctions enable simple transfer of cytosolic material from cell to cell, efficient coordinated pumping still requires temporal and spatial organization of activation. Here, the intrinsic cardiac conduction system is crucial.

B. Cardiac Conduction

Efficient contraction and ejection of blood relies on organized excitation that results in atrial contraction followed by ventricular contraction. The cardiac conduction system provides the path that ensures this sequence. Excitation begins in the RA, initiated by a group of specialized cardiomyocytes that are capable of generating cardiac action potentials (APs) autonomously. Collectively, these specialized cells are called the sinoatrial (SA) node. The frequency of SA node firing determines heart rate, earning it the moniker “pacemaker.” Beginning at the SA node, APs transmit to the atrioventricular (AV) node across atrial

myocytes through gap junctions. Conduction is slightly delayed at the AV node to allow complete contraction and emptying of the atria before eliciting ventricular contraction. From the AV node, APs travel through the Purkinjie fibers located in the subendocardium of the interventricular septum, which allow rapid conduction to the apex of the heart. Upon reaching the apex, the signal transmits back towards the base of the heart through the ventricular free walls (Figure 1.6). Conduction through the ventricular free walls in this direction causes contraction of the ventricles from apex to base, pumping blood from the heart. Interruption of this normal electrical conduction can profoundly limit the ability to efficiently eject blood (Anderson et al., 2009;Spach and Kootsey, 1983).

1. Cardiac Action Potentials

Not only does cardiac function rely on organized conduction of activity, but it also relies on organized activity within each cardiomyocyte. Normal electrical activity of each cardiomyocyte is dependent on the spatial and temporal coordination of several ions and ion channels. Collectively, this activity forms the cardiac AP. APs can be lumped generally into two categories: 1) Slow responding and 2) fast responding. Pacemaking cells (those capable of initiating APs) produce slow responding APs, whereas all other myocytes undergo fast responding APs. Slow responding APs are characterized by slow, autonomous depolarization during diastole (also called phase 4) and relatively slow depolarization upon activation (phase 0) during systole. Conversely, fast response APs are characterized by stable diastolic membrane potential (phase 4) and rapid depolarization upon activation (phase 0). Rapid depolarization

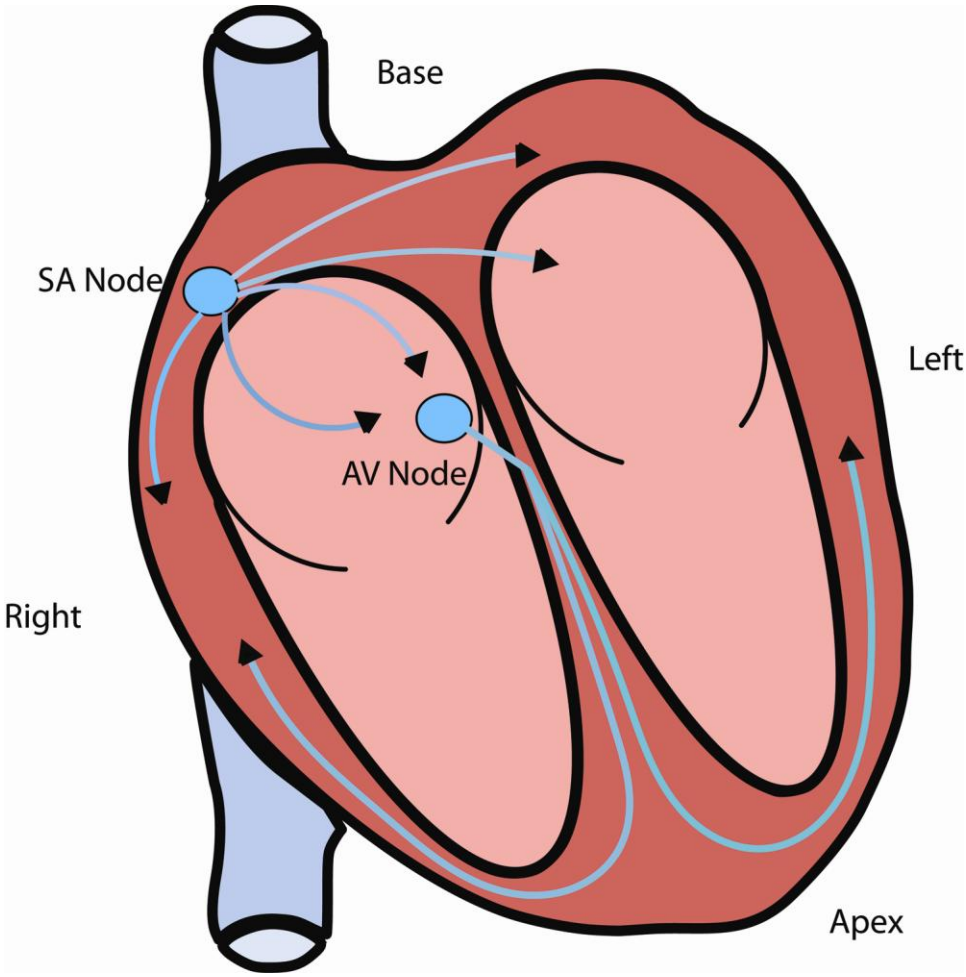

Figure 1.6 Cardiac Conduction. Electrical impulses are generated by the pacemaking SA node within the right ventricle. This signal propagates through the atrial myocardium toward the AV node at the atrioventricular junction. From the AV node, the Purkinjie fibers in the interventricular septum rapidly conduct the stimulus towards the apex of the heart. Propagation then continues from apex to base through the ventricular walls.

occurs as a result of voltage-gated Na^+ channel opening, which allows a large influx of Na^+. Phase 0 is quickly followed by a slight repolarization due to a transient outward K^+ current (phase 1). This initial repolarization is slowed by a large cytosolic Ca^{2+} increase (phase 2), predominately through release of intracellular Ca^{2+} stores in the sarcoplasmic reticulum. As Ca^{2+} is removed from the cytosol, the repolarizing K^+ current takes over (Phase 3) and the membrane potential is restored to resting (Mohrman and Heller, 2013)(Figure1.7).

2. Excitation-contraction coupling

While the cardiac action potential relies on multiple ions and currents, contraction of cardiomyocytes is dependent on the Ca^{2+} component. Specifically, muscle contraction occurs in response to elevation of cytosolic Ca^{2+} in a process called excitation-contraction coupling. Excitation-contraction coupling begins with depolarization of the myocyte membrane, triggering voltage gated L-type Ca^{2+} channels to open (Bers, 2002). A small influx of Ca^{2+} through L-type Ca^{2+} channels triggers a bulk release of Ca^{2+} from the sarcoplasmic reticulum (SR) via ryanodine receptors (RyR) in a process called Ca^{2+} induced Ca^{2+} release (Fabiato, 1985). The resulting increase in cytosolic Ca^{2+} causes the myocyte to shorten by interacting with the contractile machinery of the cell. Free Ca^{2+} is then rapidly sequestered, primarily back into the SR through the ATP-dependent sarcoplasmic reticulum Ca^{2+} pump (SERCA) or pumped out of the cell

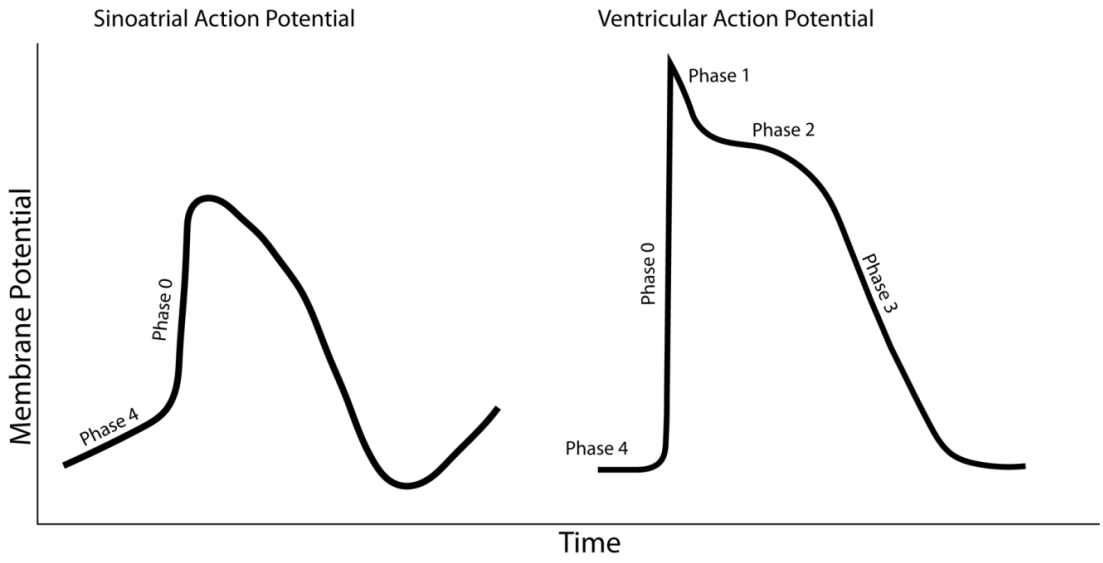

Figure 1.7 Cardiac Action Potentials. Autonomous APs of the SA node are considered slow response APs. Slow response APs are characterized by slow diastolic depolarization (phase 4) and slow Ca2+ driven phase 0 depolarization in comparison to ventricular APs. Ventricular APs, or fast response APs, have stable diastolic membrane potential followed by rapid phase 0 depolarization governed by Na+ influx. Transient K+ currents allow slight phase 1 depolarization, followed by a depolarizing Ca2+ influx of phase 2. Finally, delayed K+ currents allow final phase 3 repolarization and return to resting membrane potential.

by the Na^{+}/Ca^{2+} exchanger on the cell membrane (Bers, 2002)(Figure1.8). Rapid sequestration of Ca^{2+} is important, as it allows the myocyte to recover and be primed for the next cycle.

3. *Electrocardiogram*

A composite view of cardiac electrical activity and conduction can be visualized by electrocardiogram (ECG), which can be recorded by placing electrodes on the surface of the body. Because ECGs take into account the direction of conduction and the amplitude of current, the placement of the recording electrodes determines the form of the ECG trace. Perhaps the most recognizable configuration is lead II, where a negative electrode is placed on the right arm, and a positive electrode is placed on the left leg. Lead II configuration ECGs are composed of a p-wave (atrial depolarization), QRS complex (atrial repolarization and ventricular depolarization), and a t-wave (ventricular repolarization) (Mohrman and Heller, 2013).

As ECGs capture the electrical activity of the heart, they are also an important tool in diagnosing arrhythmias. Premature ventricular complexes (PVC), for example, are a common type of ventricular arrhythmia that arise within ventricular myocardium. They are characterized by the absence of a p-wave and early onset of a broader QRS-like complex (Figure 1.9). This waveform results from the absence of atrial depolarization, and, because PVCs are not triggered by the SA node, they do not transmit through the normal conduction pathway, but instead through the less conductive gap junctions between cells.

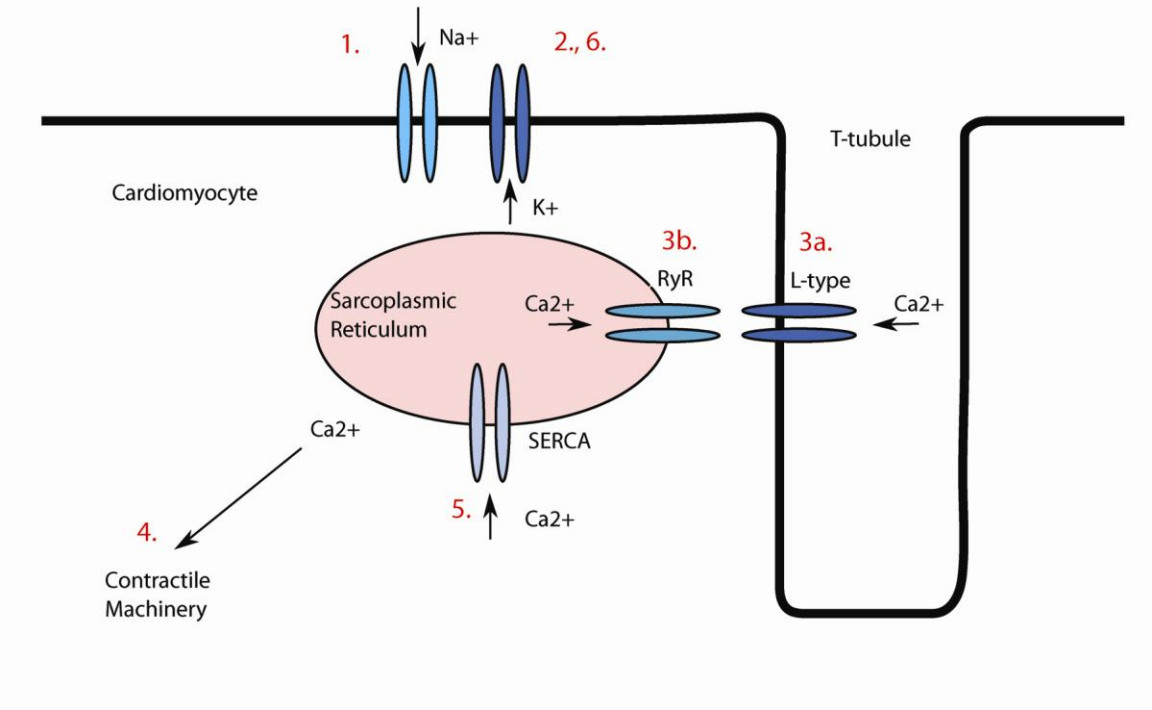

Figure 1.8 Excitation-Contraction Coupling. Ventricular APs begin by activation of voltage gated Na+ channels (1) on the cell membrane. Depolarization also activates transient outward K+ channels to slightly repolarize the cell(2), competing against depolarizing Ca2+ influx from L-type Ca2+ channels located in T-tubules(3a) and from intracellular stores via RyR (3b). Cytosolic Ca2+ elevation allows contraction of the myocyte (4), and is then quickly sequestered by SERCA into the sarcoplasmic reticulum (5), or extracellulary via the Na+/Ca2+ exchanger.

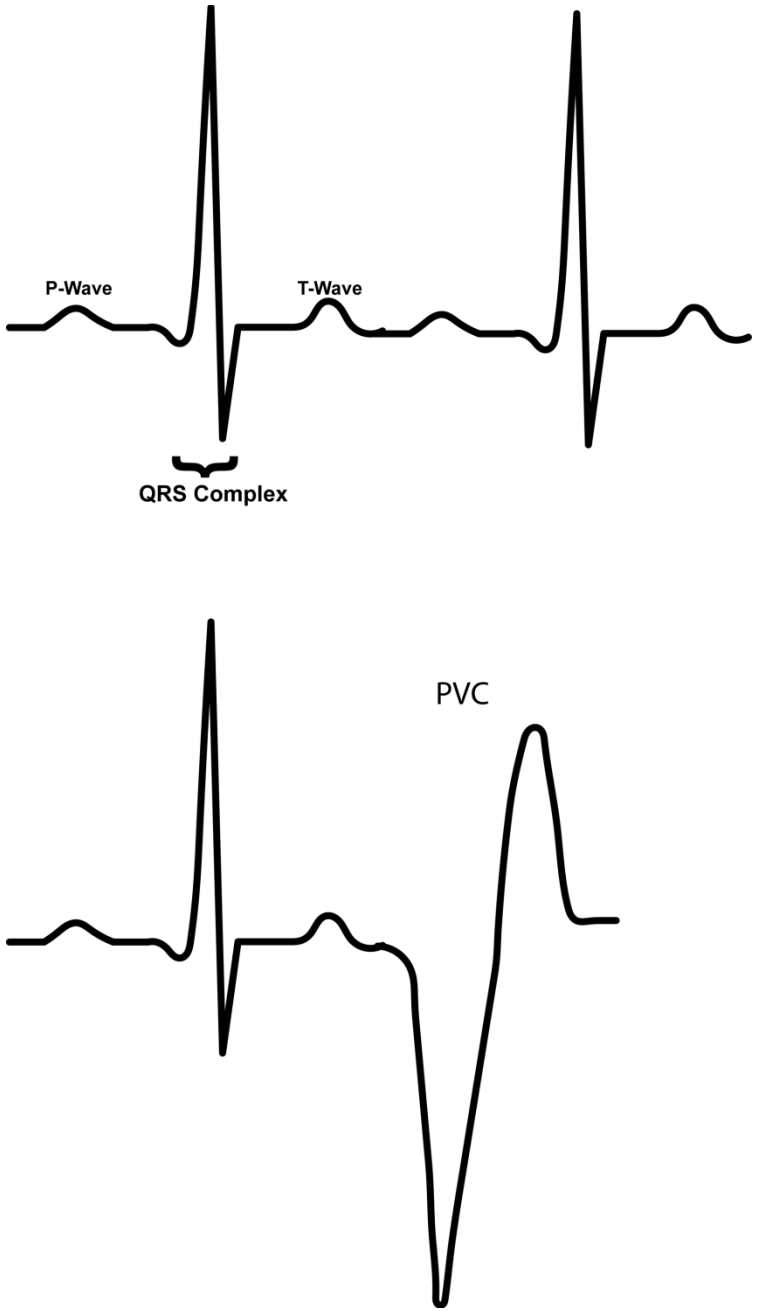

Figure 1.9 The Electrocardiogram. The upper trace depicts a normal lead-II ECG of two cardiac cycles. The P-wave represents atrial depolarization, the QRS complex is ventricular depolarization and atrial repolarization, and the T-wave is ventricular repolarization. The bottom trace depicts one normal cardiac cycle followed by a PVC. A PVC is characterized by absence of a P-wave, early onset, and a broad QRS-like complex.

C. Sympathetic Innervation of the Heart

As the mechanical driver of oxygen and nutrient delivery, the heart must respond to the changes in metabolic need of the body. For example, increased energy use by skeletal muscle during exercise requires increased delivery of oxygen and nutrients to maintain homeostasis. At the level of the heart, homeostasis is maintained by increasing cardiac output to meet these demands. The primary control of the dynamic output of the heart is through autonomic innervation.

Both branches of the autonomic nervous system are present in the heart. Parasympathetic nerves predominately innervate the SA node and the AV node, with minimal innervation throughout the ventricles (Crick et al., 1994). Increased parasympathetic activity to the SA and AV node leads to reduced heart rate and conduction velocity, respectively. Similarly, sympathetic nerves innervate both the SA node and AV node (Pardini et al., 1989). In contrast to parasympathetic nerves, however, sympathetic nerves extensively innervate both ventricles (Randall et al., 1968) (Figure 1.10). Sympathetic activation in the heart leads to increased cardiac output by stimulating heart rate, conduction velocity, and contractility (Mohrman and Heller, 2013).

1. Sympathetic neurotransmission

Sympathetic nerve activity is primarily transmitted through production and release of the neurotransmitter NE. Synthesis of NE begins with conversion of tyrosine to L-Dopa by the enzyme TH, the rate limiting enzyme in NE production. L-Dopa is then converted to dopamine by L-aromatic amino acid decarboxylase.

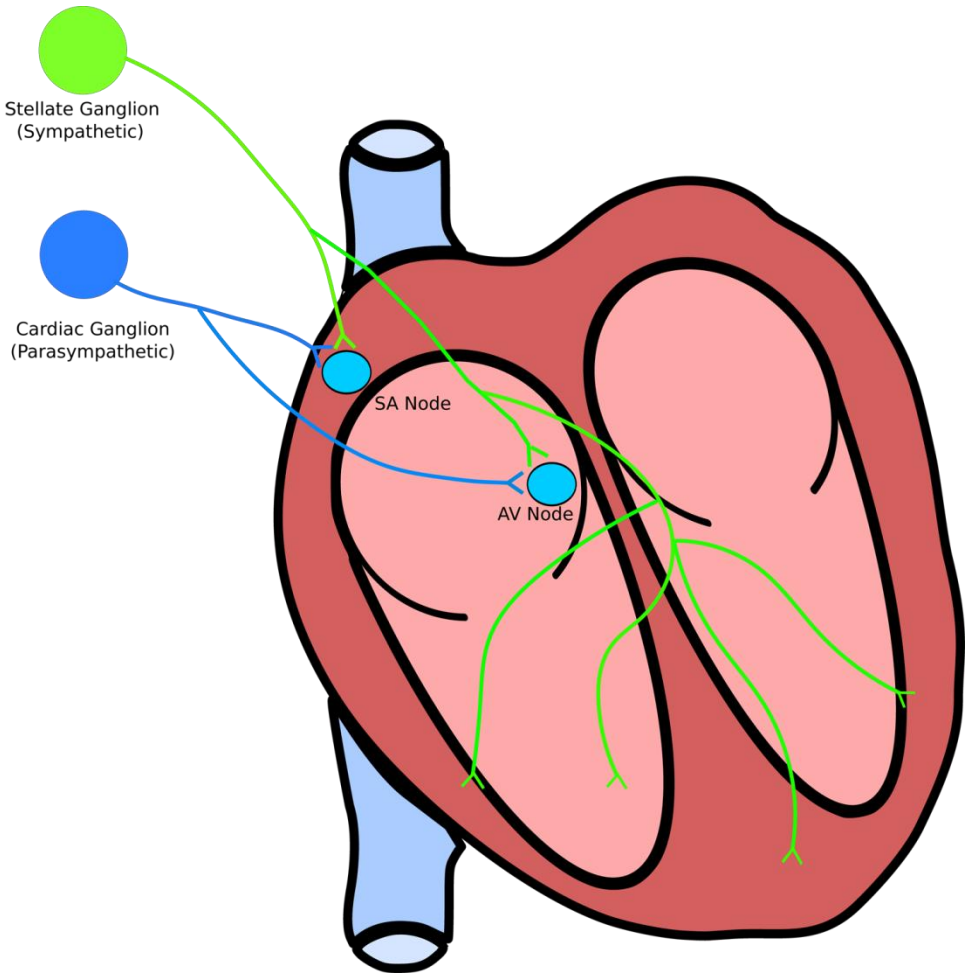

Figure 1.10 Autonomic innervation of the heart. Parasympathetic neurons, whose cell bodies are located in the cardiac ganglion, predominately innervate the SA node and AV node. Sympathetic neurons from the left and right stellate ganglia also innervate both the SA node and AV node, but are also found throughout both ventricles.

Dopamine is transported into vesicles by the vesicular monoamine transporter, where it is then converted into NE by dopamine-β-hyrdoxylase. Vesicular release of NE allows binding and activation of post-synaptic ARs. NE-dependent neurotransmission is completed by NE re-uptake by the NE transporter found on the pre-synaptic membrane (Kandel E.R. et al., 2000).

Although NE is the primary neurotransmitter, sympathetic nerves also produce and release several neuropeptides (Cane and Anderson, 2009;Lindh et al., 1989). For sympathetic nerves of the heart, this is generally neuropeptide Y and galanin (Kummer, 1987;Richardson et al., 2006). Neuropeptide release can have diverse effects on the heart. For example, neuropeptide Y is an important developmental regulator of L-type Ca^{2+} channel expression (Protas et al., 2003), and in adults can stimulate the heart similarly to norepinephrine in an AR-independent manner (Lundberg et al., 1984). Additionally, both neuropeptide Y and galanin limit the release of ACh from cardiac parasympathetic nerves (Herring et al., 2008;Herring et al., 2012).

While the heart is responsive to neuropeptides, much of the sympathetic input to the heart is transmitted by NE release from nerves and epinephrine from circulation, both of which activate cardiac ARs. There are three main classes of ARs, α1ARs, α2ARs, and βARs. βARs are the predominant class of ARs found in the heart, and are further classified into three subtypes. β1ARs are the most common cardiac subtype, comprising approximately 75% of total cardiac β-AR expression, followed by β2ARs which comprise the bulk of the remaining 25% (Bristow et al., 1986), and a very limited presence of β3ARs (Wheeldon et al.,

1993). While βARs are the predominate class of cardiac ARs, α1ARs are also present in the heart. However, they only account for approximately 10% of total AR expression (Bristow et al., 1986).

2. Sympathetic regulation of the heart

Increased metabolic demand of the body requires heightened delivery of oxygen and nutrients to the periphery. In order to accomplish elevated nutrient delivery, sympathetic input to several tissues, including the heart, must increase. Increased sympathetic input to the heart stimulates cardiac output by increasing heart rate, contractility, and relaxation. Many of these actions are through modulation of Ca^{2+} handling and ion channels involved in excitation-contraction coupling (Bers, 2008;Cutler et al., 2011;Thomas et al., 2004).

The excitation-contraction cycle can be robustly modulated by activation of ARs on the cardiomyocyte membrane. Since ARs are G-protein coupled receptors, activation can produce broad downstream effects and, indeed, this occurs in cardiomyocytes. α1AR is associated with the G-protein G_q, and stimulation of the receptor activates protein kinase C (PKC) in a Ca^{2+} dependent process (Rockman et al., 2002). Additionally, β1 and β2AR activation both lead to activation of the G-protein G_S (Rockman et al., 2002). This leads to an increase in cytosolic cyclic adenosine monophosphate (cAMP) levels by activation of adenylate cyclase. cAMP then leads to activation of protein kinase A (PKA), which allows PKA to phosphorylate its targets.

There are several targets of PKA, many of which are involved in Ca^{2+} handling. These include RyR (Valdivia et al., 1995), the SERCA modulator

phospholamban (Colyer, 1998), L-type Ca^{2+} channels (Kamp and Hell, 2000), and many others (Lundby et al., 2013). PKA modulation of these proteins results in a larger influx and faster sequestration of intracellular Ca^{2+} (Viatchenko-Karpinski and Gyorke, 2001). Together, this enhances Ca^{2+} influx to increase contractility and stimulates sequestration to quicken relaxation (Viatchenko-Karpinski and Gyorke, 2001). This reduces the duration of the Ca^{2+} transient, which shortens action potential duration (APD) by shortening phase 2 of the AP (Mohrman and Heller, 2013).

In addition to modulating Ca^{2+} dynamics, β-AR stimulation regulates other ion channels involved in the cardiac AP. Much like its influence in Ca^{2+} dynamics, much of the β-AR dependent modulation is mediated by PKA. Downstream effects include phosphorylation of voltage gated Na+ channels (Matsuda et al., 1992) and voltage gated K^+ channels (Yue et al., 1999), as well as regulation of subcellular localization of these channels (Shibata et al., 2006). These modulations, much like with Ca^{2+} dynamics, enhance the excitability of myocytes, while also shortening APD (Figure1.11).

A common abnormality of excitation-contraction coupling is a phenomenon called delayed after depolarizations (DAD) (Bozler, 1943). DADs are depolarizations that occur following complete repolarization of a myocyte but prior to rapid phase 0 depolarization of the AP. While normal phase 0 depolarization is dependent on voltage-gated Na+ channels, DADs are often Ca^{2+} driven (Kass et al., 1978), and can develop due to localized and acute β-AR stimulation (Myles et al., 2012). Specifically, the Ca^{2+} influx and sequestration

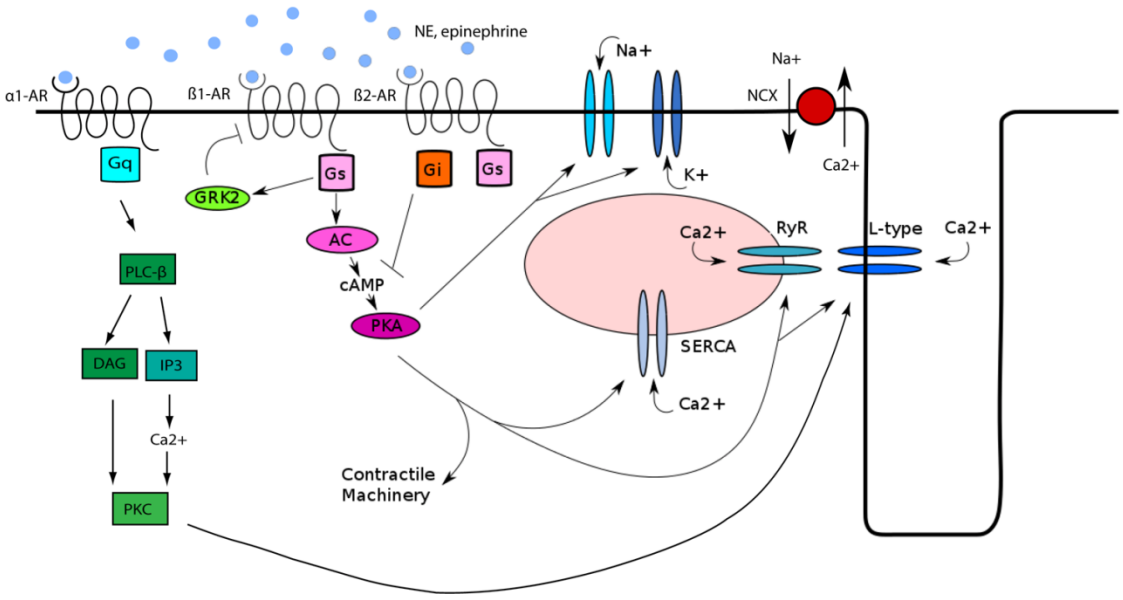

Figure 1.11 Sympathetic modulation of excitation-contraction coupling. Modulation of excitation-contraction is mainly mediated via the β-AR downstream effector PKA. Activation of PKA leads to phosphorylation of several ion channels, including voltage gated Na+, K+, and Ca2+ channels, as well as RyR, SERCA, and the contractile machinery. α1-AR activation of PKC also modulates L-type Ca2+ channel activity. Phosphorylation by PKA and PKC increase excitability and relaxation, which together shorten APD.

response to β-AR stimulation is so strong that Ca^{2+} overload of the SR can occur, resulting in diastolic dump of Ca^{2+} into the cytosol. If this Ca^{2+} dump is significant, myocytes will depolarize via the electrogenic Na^{+}/Ca^{2+} exchanger at the membrane and trigger a PVC (Zygmunt et al., 1998;Myles et al., 2012).

D. Myocardial Infarction

Cardiovascular diseases affect millions of people and are the leading cause of death in the United States. Myocardial infarction (MI; heart attack) is a common cardiovascular disease that occurs in approximately one million people annually (Roger et al., 2012b). MIs occur due to a coronary artery block, most often due to atherosclerosis, leaving the distal myocardium ischemic. Cardiac ischemia is treated by removing the coronary blockage to allow reperfusion of the ischemic tissue. While reperfusion greatly improves mortality, the result is significant remodeling of the myocardium and nerve fibers (Dobaczewski et al., 2006). Those who survive an MI remain with substantial risk of suffering from secondary cardiac pathologies including arrhythmias and sudden cardiac death (Rubart and Zipes, 2005;Solomon et al., 2005).

1. Myocardial Remodeling

Cardiac ischemia-reperfusion (I-R) results in necrosis of cardiomyocytes and the production of a collagen based scar, or infarct (Dobaczewski et al., 2006). Local inflammation in response to injury precipitates infiltration of immune cells (Nian et al., 2004), causing significant production of cytokines and growth factors, which activate resident cardiac fibroblasts (Porter and Turner, 2009). Following activation, resident fibroblasts proliferate and migrate to the site of

injury, where they secrete matrix metalloproteases (MMPs) and collagen. MMPs break down the previous ECM so that it can be replaced with a very dense collagen based infarct (Porter and Turner, 2009). The time to reach a fully mature infarct is dependent on the animal, but for mice this occurs approximately 10 days after injury (Dobaczewski et al., 2006). Initially, this remodeling response is protective as the collagen provides structure and support to heart. However, over time the infarct can lead to development of cardiac dysfunction, including heart failure (Porter and Turner, 2009).

2. Sympathetic Nerve Remodeling

In addition to myocyte necrosis and ECM remodeling, sympathetic nerve activity and patterning are also altered following I-R injury (Li et al., 2004). As noted previously, sympathetic nerves undergo dynamic cardiac remodeling under several conditions (Bengel et al., 1999;Hasan et al., 2006;Vo and Tomlinson, 1999). This is true following I-R injury as well. Sympathetic nerves quickly begin to degenerate following reperfusion of the myocardium (Inoue and Zipes, 1988;Lorentz et al., 2013) . This initial denervation is observed not only within the area of remodeling and scar production but also in the most proximal viable myocardium, termed the peri-infarct. In mice, by approximately three days following injury, the infarct is fully denervated while the proximal peri-infarct is hypoinnervated (Lorentz et al., 2013). Interestingly, more distal peri-infarct is hyperinnervated at this time. By seven days, however, innervation in both the proximal and distal peri-infarct is not significantly different than sympathetic innervation density in normal, uninjured myocardium (Lorentz et al., 2013). The

infarct itself, however, remains fully denervated, which is quite surprising given the high levels of NGF (Hiltunen et al., 2001;Zhou et al., 2004) and more so given extensive cycle of sympathetic die-back, regeneration, and pruning observed in viable myocardium after the same injury (Lorentz et al., 2013).

Overall, the result of sympathetic remodeling after MI is a heart with heterogeneous sympathetic innervation (Li et al., 2004;Stanton et al., 1989). The molecular mechanism that underlies this sustained sympathetic denervation of the infarct remains unclear, but we do know it results independently of the mechanism of denervation in the peri-infarct. In mice lacking the p75 neurotrophin receptor, the peri-infarct remains innervated following I-R, while the infarct is still fully denervated (Lorentz et al., 2013).

3. Sympathetic Heterogeneity and arrhythmias

Those who survive an MI remain at a substantial risk for developing arrhythmias and sudden cardiac death (SCD) (Rubart and Zipes, 2005;Solomon et al., 2005). Although the infarct itself is a substrate for arrhythmias, there is a large body of animal and human evidence that indicates altered sympathetic input plays a key role in the development of arrhythmias (Basu et al., 1997;Billman et al., 1997;Exner et al., 1999;Nademanee et al., 2000;Schwartz et al., 1992). Recent human evidence suggests that sympathetic heterogeneity (via MI-induced regional denervation) is the underlying link between sympathetic transmission and arrhythmias (Boogers et al., 2010;Fallavollita et al., 2013;Nishisato et al., 2010;Rubart and Zipes, 2005;Vaseghi et al., 2012). It is clear that sympathetic heterogeneity develops and persists after MI as the infarct

remains denervated and adjacent to normally innervated tissue (Li et al., 2004;Lorentz et al., 2013;Stanton et al., 1989).

It is not fully understood how sympathetic heterogeneity results in arrhythmias, but it is thought that dispersion of repolarization is key (Killeen et al., 2008;Vaseghi et al., 2012;Yoshioka et al., 2000). Dispersion, or variance, represents variability in repolarization time across the heart. This can be represented in dispersion of APD. In a healthy heart, APD is highly regulated, and in fact, some variance is essential for normal rhythmicity (Antzelevitch et al., 1991). As discussed previously, the heart has a transmural sympathetic innervation gradient, with highest innervation in the subepicardium, and the lowest in the subendocardium (Ieda et al., 2007;Randall et al., 1968). This innervation gradient is combined with a gradient of K^+ channel expression, which follows the same pattern (Brunet et al., 2004). This pattern results in longer APD in the subendocardium and shorter APD in the subepicardium, which ensures that the subendocardium cannot be excited until the subepicardium has recovered (Antzelevitch et al., 1991;Brunet et al., 2004). This organized heterogeneity is important for efficient conduction and contraction, and disruption in normal hearts leads to arrhythmias (Ieda et al., 2007;Lorentz et al., 2010). Similar to changes in sympathetic innervation, ion channel expression and patterning is regionally disrupted following MI (Kaprielian et al., 2002;Lukas and Antzelevitch, 1993). Together, the remodeling that occurs after MI establishes disorganized heterogeneity with greater dispersion of repolarization, which is prone to arrhythmias (Vaseghi et al., 2012). It is unclear whether these changes

in ion channel expression and physiology are related to sympathetic denervation, however, given the importance of sympathetic heterogeneity in arrhythmogenesis, it remains likely they are.

III. Purpose and Hypotheses

Given the extensive evidence of sympathetic reinnervation following injury, it was unexpected that following a common cardiac injury, I-R, that sympathetic nerves failed to reinnervate the scar. This was particularly surprising given that sympathetic hyperinnervation is observed following ischemia alone and that I-R results in robust production of NGF. These observations are similar to the remodeling and regeneration failure following injury in the CNS, where known inhibitory ECM components are highly expressed. Specifically, these include CSPGs, HA, and tenascin C; however, CSPGs were identified as the primary inhibitors. Similarly, cardiac I-R results in production of both HA and tenascin C, while CSPGs have not been examined in this context.

Hypothesis I: Cardiac I-R triggers CSPG production, which prevents sympathetic reinnervation of infarcted myocardium.

Sympathetic heterogeneity, specifically the degree of denervation, has been identified as the most sensitive predictor of arrhythmia susceptibility for people who have suffered an MI. MIs regionally alter ion channel activity and

expression and results in dispersion of repolarization. To date, it is unknown whether these changes occur due to altered sympathetic innervation. However, given the regulatory ability of β-AR activation, it remains a possibility that electrophysiological remodeling is due to sympathetic denervation and that re-establishing innervation could restore normal electrophysiological dynamics.

Hypothesis II: Sympathetic reinnervation of infarcted myocardium limits I-R-induced electrophysiological remodeling and prevents arrhythmias.

Chapter 2

Infarct-derived chondroitin sulfate proteoglycans prevent sympathetic reinnervation after cardiac ischemia-reperfusion injury

Ryan T Gardner MS and Beth A Habecker PhD

Department of Physiology & Pharmacology, Neuroscience Graduate Program
Oregon Health and Science University, Portland, OR 97239

Published in The Journal of Neuroscience
April 24th, 2013
Volume 33 Issue 17

Acknowledgments: This work was supported by NIH HL093056 (BAH) and an Oregon Brain Institute Neurobiology of Disease Fellowship (RTG). The authors thank Dr. Stephen Back (OHSU, Portland OR) for high and low molecular weight hyaluronan and Dr. Michael Cohen (OHSU, Portland OR) for assistance with microfluidic chambers. The authors also thank Dr. Aviva Symes (USUHS, Bethesda MD) for the suggestion to examine CSPGs in the cardiac scar, thank Dr. Herb Geller (NINDS, Bethesda MD) for helpful comments on the manuscript, and thank Alexandra Brown for technical assistance.

I. Abstract

Sympathetic nerve can regenerate after injury to re-innervate target tissues. Sympathetic regeneration is well documented after chronic cardiac ischemia, so we were surprised that the cardiac infarct remained denervated following ischemia-reperfusion (I-R). We used mice to ask if the lack of sympathetic regeneration into the scar was due to blockade by inhibitory extracellular matrix within the infarct. We found that chondroitin sulfate proteoglycans (CSPGs) were present in the infarct after I-R, but not after chronic ischemia, and that CSPGs caused inhibition of sympathetic axon outgrowth *in vitro*. Ventricle explants after I-R and chronic ischemia stimulated sympathetic axon outgrowth that was blocked by NGF antibodies. However, growth in I-R co-cultures was asymmetrical, with axons growing toward the heart tissue consistently shorter than axons growing in other directions. Growth toward I-R explants was rescued by adding chondroitinase ABC (ChABC) to the co-cultures, suggesting that I-R infarct-derived CSPGs prevented axon extension. Sympathetic ganglia lacking Protein Tyrosine Phosphatase Sigma (PTPσ; *ptprs*) were not inhibited by CSPGs or I-R explants *in vitro*, suggesting PTPσ is the major CSPG receptor in sympathetic neurons. To test directly if infarct-derived CSPGs prevented cardiac reinnervation, we carried out ischemia-reperfusion in *ptprs-/-* and *ptprs*+/- mice. Cardiac infarcts in *ptprs-/-* mice were hyperinnervated, while infarcts in *ptprs+/-* littermates were denervated, confirming that CSPGs prevent sympathetic reinnervation of the cardiac scar after I-R. This is the first example of CSPGs preventing sympathetic

reinnervation of an autonomic target following injury, and may have important consequences for cardiac function and arrhythmia susceptibility after myocardial infarction.

II. Introduction

Nerve regeneration is often minimal in the central nervous system, but peripheral nerves can regenerate back to their targets. For example, postganglionic sympathetic nerves re-innervate denervated target tissues including the iris (Olson and Malmfors, 1970;Lorez et al., 1975), mesenteric arteries (Aguayo et al., 1973;Hill et al., 1985), pineal gland (Bowers et al., 1984), and skin (Gloster and Diamond, 1992). In addition to regeneration following injury, sympathetic nerves innervating the uterus undergo degeneration and regeneration during each estrous cycle (Zoubina and Smith, 2000). The presence of nerve growth factor (NGF) in the target tissue is important for promoting innervation of during development (Glebova and Ginty, 2004) and reinnervation of a tissue after denervation (Aloe et al., 1985;Gloster and Diamond, 1995;Vo and Tomlinson, 1999).

One of the best characterized targets of the sympathetic nervous system, and sympathetic axon regeneration, is the heart. Release of norepinephrine (NE) from sympathetic nerves stimulates heart rate, conduction velocity, and ventricular contractility. Regeneration of sympathetic nerves in the heart has been well characterized in animal models of chronic cardiac ischemia, where high levels of NGF in the infarcted myocardium lead to nerve sprouting and hyperinnervation (Vracko et al., 1990;Zhou et al., 2004;Hasan et al., 2006;El-

Helou et al., 2008). Post-mortem analysis of human hearts following heart failure or cardiomyopathy also revealed sympathetic hyperinnervation (Cao et al., 2000b). The cardiac sympathetic innervation has been examined in vivo by monitoring uptake of the labeled NE transporter substrates C-11 hydroxyephedrine or iodine-123 meta-iodobenzylguanidine (123I-MIBG). These studies reveal denervation after I-R (Stanton et al., 1989) that is followed by reinnervation of peri-infarct myocardium (Hartikainen et al., 1996), and reveal significant reinnervation in transplanted hearts (Bengel et al., 1999;Estorch et al., 1999;Bengel et al., 2001). Imaging studies showing reinnervation of transplanted hearts are complemented by functional responses to exercise (Wilson et al., 2000) and functional responses to drugs that cause NE release or block NE receptors (Bengel et al., 2004). Finally, sympathetic reinnervation of transplants was confirmed post-mortem by tyrosine hydroxylase (TH) staining (Kim et al., 2004).

Since sympathetic nerve regeneration is well documented in the heart, we were surprised to discover that the cardiac infarct was not re-innervated following ischemia-reperfusion injury (I-R)(Li et al., 2004). This was particularly unexpected given infarct reinnervation observed after chronic cardiac ischemia (Vracko et al., 1990;El-Helou et al., 2008;Hasan et al., 2006), and evidence of elevated NGF in the scar after I-R (Zhou et al., 2004;Hiltunen et al., 2001). Cardiac I-R triggers an inflammatory response that initiates fibroblast migration and proliferation (Porter and Turner, 2009). Activation of fibroblasts results in production of a collagen-based infarct, or scar, that contains hyaluronic acid (HA)

and other extracellular matrix components (Dobaczewski et al., 2006) that are present in glial scars after central nervous system injury (Sherman and Back, 2008). Here we investigate the possibility that the lack of sympathetic regeneration into the infarct after cardiac ischemia-reperfusion is due to blockade of axon growth by inhibitory components of extracellular matrix within the cardiac scar.

III. Methods

Animals: C57BL/6J mice were obtained from Jackson Laboratories West (Sacramento, CA), and were used for all experiments except those using PTPσ transgenic mice. *ptprs*+/- transgenic mice (BalbC background) were supplied by Michel Tremblay at McGill University (Elchebly et al., 1999), and were bred as heterozygotes. *ptprs*+/+ and *ptprs*+/- littermates were used as "wild type" controls for *ptprs*-/- studies. All mice were kept on a 12h:12h light-dark cycle with *ad libitum* access to food and water. Age and gender-matched male and female mice 12-18 weeks old were used for surgeries, while ganglia from male and female neonatal mice were used for explants and dissociated cultures. All procedures were approved by the OHSU Institutional Animal Care and Use Committee and comply with the Guide for the Care and Use of Laboratory Animals published by the National Academies Press (8th edition).

Surgery: Myocardial ischemia-reperfusion: Anesthesia was induced with 4% isoflurane and maintained with 2% isoflurane. The left anterior descending coronary artery (LAD) was reversibly ligated for 30 min and then reperfused by

release of the ligature. Occlusion was confirmed by sustained S-T wave elevation and regional cyanosis. Reperfusion was confirmed by the return of color to the ventricle distal to the ligation and reperfusion arrhythmia. Core body temperature was monitored by a rectal probe and maintained at 37°C, and a two-lead electrocardiogram was monitored. *Myocardial ischemia:* Chronic ischemia was done in exactly the same manner as described above, but with permanent occlusion of the LAD using 8-0 gauge suture. *Sham surgery:* Sham animals underwent the procedure described above, except for the LAD ligature.

Dissociated primary cell culture with CSPG (chondroitin sulfate proteoglycan) and HA (hyaluronan) treatment: Cultures of sympathetic neurons were prepared from superior cervical ganglia (SCG) of newborn mice as described (Dziennis and Habecker, 2003). Neurons were plated onto poly-L-lysine (PLL, 0.01%, Sigma-Aldrich) and collagen (10 µg/mL, BD Biosciences) coated plates, and grown in serum free C2 medium (Lein et al., 1995;Pellegrino et al., 2011) supplemented with 50 ng/mL NGF (BD Biosciences), 100 U/mL penicillin G, and 100 µg/mL streptomycin sulfate (Invitrogen). Cells were incubated at 37° C in a humidified 5% CO_2 incubator. Cells were maintained for 48 hrs in the presence of the anti-mitotic agent cytosine arabinoside (Ara C, 1 µM) to reduce the number of non-neuronal cells. CSPG treatments were carried out using soluble or fixed CSPGs (Millipore #CC117; mixture includes neurocan, phosphacan, versican, and aggrecan). HA treatments were similarly carried out, using mixed molecular weight HA (MP biomedicals) for soluble treatments. For fixed treatments, high

molecular weight (HMW) HA (Lifecore Biomedical) was degraded using bovine testes hyaluronidase (Sigma) to produce low molecular weight (LMW) HA (Generously provided by Dr. Stephen Back, OHSU) **1)** Soluble: Neurons were grown in 48-well plates coated with PLL and collagen. Vehicle (media), CSPGs (10 ng/ml-20 µg/ml), or HA (10 ng/ml-100 µg/ml) were added to the cultures 24 hrs after plating, and 24 hours after addition of CSPGs, HA, or vehicle, images were acquired for Sholl analysis. **2)** Fixed: Plates were coated with PLL/collagen, PLL/collagen/CSPGs (100 ng/mL – 1 µg/mL), or PLL/collagen/HA (100 ng/mL – 1 µg/mL; low and high molecular weight) prior to addition of neurons. Images were acquired for Sholl analysis 24 hours after plating.. For CSPG degradation experiments, Chondroitinase ABC (ChABC, 4 µU/mL; Seikagaku Biobusiness Corporation) was added to culture media at the time of plating.

Sholl analysis: To quantify neurite outgrowth in dissociated neurons, the Sholl method was used (SHOLL, 1953). A series of concentric circles were superimposed over the cell body using Image J, and neurite intersections with the circles were counted. The number of intersections provides an estimate of neurite length and/or increased branching.

Compartmentalized cultures. To generate micro-fluidic chambers providing separation of two media compartments (450µm apart), SYLGARD 184 silicone elastomer (Dow Corning) was poured into a pre-cast mold, and heated at 50-60° C for 2 hours. Cleaned chambers were placed in 10 cm culture dishes (Corning)

pre-coated with 0.01% PLL. The axonal compartment was then coated with 10 µg/mL collagen or collagen + 1 µg/mL CSPGs. SCG were placed in reduced growth factor Matrigel (BD Bioscience) within the cell body compartment. C2 media supplemented with 10 ng/mL NGF was added to both compartments, and cultures were maintained at 37° C in a humidified 5% CO_2 incubator. After 24 hrs, or when axons were first visible in the axonal compartment, images were acquired (t=0). Additional images were obtained 3 hours later (t=3), and a growth rate was calculated based on the distance extended during that 3 hour period.

Heart/ganglia co-cultures: Co-culture experiments were carried out in 24 well plates by plating pieces of infarcted left ventricle (LV) or corresponding sham tissue, collected 10 days after surgery, with neonatal SCGs. Tissues were plated in 30 µL of reduced growth factor Matrigel, separated by approximately 1mm, and placed at 37 ºC to solidify the Matrigel before addition of C2 media supplemented with 2 ng/mL NGF. Co-cultures were incubated at 37°C in a humidified 5% CO_2 incubator for 48 hours. Following 48 hours in culture, images of the cultures were acquired using phase contrast microscopy (10X) and axon length was analyzed using Nikon Elements. For ChABC experiments, tissue from a single heart was split between the vehicle and ChABC treatment groups to promote consistency. Co-cultures were treated from the time of plating with ChABC (4 µU/mL) diluted in culture media, or media alone. For co-cultures examining the role of the CSPG receptor PTPσ, SCG were dissected from an

entire litter of neonatal mice containing the range of PTPσ genotypes (*ptprs+/+, ptprs+/-, ptprs-/-*). The two ganglia from an individual mouse were divided so that one SCG was cultured with a sham explant and one with an infarct explant. Following 48 hours in culture, images were acquired using phase contrast microscopy (10X) and axon length was analyzed using Nikon Elements. Genotyping was completed after image acquisition and analysis so that the experiment was blinded.

Co-Culture axon length analysis: Axon length was measured on three cardinal sides of each ganglion (0, 90, and 180 degrees). Growth toward the myocardium was designated 0º, growth perpendicular was 90º and growth away from the myocardium was 180º. In order to normalize for inter-well variability of growth, a ratio of these measures was used (0/90 or 0/180). Values for the 0/90 or 0/180 ratio near 1 indicated growth was similar in all directions. In contrast, ratios significantly less than 1 reflected significantly shorter axons on the side of the ganglion projecting toward the heart explant.

Immunohistochemistry: Hearts were fixed for 1 hr in 4% paraformaldehyde, rinsed in phosphate buffered saline (PBS), cryoprotected in 30% sucrose overnight, and frozen in mounting medium for sectioning. Transverse 10 µm sections were cut on a cryostat and thaw mounted onto charged slides. To reduce fixative-induced autofluorescence, sections were rinsed in 10 mg/mL sodium borohydride 3X10 min and then rinsed in PBS 3X10 min. Sections were

then blocked in 3% B.S.A/ 0.3% Triton X-100 in PBS for 1 hr. Slides were then incubated with rabbit anti-TH (1:1000, Millipore/Chemicon) and mouse anti-chondroitin sulfate (1:300, Sigma CS-56) or sheep anti-fibrinogen (1:500, AbD Serotec) antibodies overnight at 4ºC, rinsed 3x10 min in PBS, and incubated 1.5 hr with the AlexaFluor 488-conjugated rabbit IgG-specific antibody (1:1000; Invitrogen) and AlexaFluor 568-conjugated mouse IgG-specific antibody (1:500) or AlexaFluor 568-conjugated sheep IgG-specific antibody (1:1000). Due to non-specific binding of AlexaFluor 568-conjugated mouse IgG, anti-mouse IgG was added to the blocking solution to prevent non-specific secondary binding. Sections were rinsed 3x10 min in PBS, incubated for 30 min in $CuSO_4$ in 50 mM ammonium acetate to reduce background signal further, rinsed 3x10 min in PBS, coverslipped in a 1:1 PBS:glycerol solution and visualized by fluorescence microscopy.

Co-cultures were fixed for 15 min in 4% paraformaldehyde and rinsed in PBS 3x10 minutes. The tissue was blocked in 3% B.S.A/ 0.3% Triton X-100 in PBS for 1 hr, then incubated with rabbit anti-TH (1:1000) overnight at 4ºC. Tissue was rinsed with PBS and incubated for 1.5 hours with the AlexaFluor 488-conjugated rabbit IgG-specific antibody (1:1000), rinsed again in PBS and imaged using fluorescence microscopy.

Imaging and Threshold Analysis: TH staining was quantified to assess sympathetic innervation density. Images were taken of the infarct and peri-infarct zone of each section, and 3 sections obtained from a similar level of the base to

apex axis were quantified in each heart using threshold discrimination analysis (Image J)(Lorentz et al., 2010).

Statistics: Student's t-test was used for comparisons of just two samples. Data with more than two groups were analyzed by one-way ANOVA using the Tukey post-hoc test to compare all conditions. For experiments comparing different surgical groups and a second variable (±NGF antibody, PTPσ genotype) two-way ANOVA was carried out using the Bonferroni post-hoc test. All statistical analyses were carried out using Prism 5.0.

IV. Results

Sympathetic denervation following ischemia-reperfusion (I-R)

We observed in previous studies that the infarct (scar) and area adjacent to the infarct remained denervated 7 days after I-R in the rat heart, while hyperinnervation was visible farther away from the developing scar (Li et al., 2004). Subsequent studies have shown hyperinnervation within the infarct after chronic ischemia (Hasan et al., 2006). To investigate further neural remodeling after I-R, we moved to the mouse heart where the cardiac infarct is fully formed and stable 10 days after I-R (Dobaczewski et al., 2006). We examined sympathetic nerve density in the left ventricle 10 days after I-R or sham surgery using TH immunohistochemistry. Sympathetic nerve fibers were detected throughout the LV of sham operated animals, but no sympathetic fibers were observed within the infarct 10 after I-R (Figure 1A+B). A follow up experiment

revealed ongoing denervation of the infarct 20 days after I-R (Figure 1D). Sympathetic fiber density outside of the infarct was similar to the innervation density in sham animals 10 and 20 days after surgery (Figure 1C+D). Following 10 days of chronic ischemia (Figure 1E), however, sympathetic innervation density within the infarct was similar to the surrounding peri-infarct (Figure 1F).

Cardiac ischemia increases cardiac NGF and enhances axon outgrowth

The lack of scar-reinnervation 10 and 20 days after I-R in the mouse heart, while the rest of the heart had normal innervation, suggested that axon regeneration was blocked at the edge of the infarct. This presented a striking contrast to the reinnervation observed in the rat heart 10 days after chronic ischemia (Hasan et al., 2006)(Fig 1E, F). Co-culture of ischemic heart tissue with a sympathetic ganglion leads to enhanced axon outgrowth that is blocked by an anti-NGF antibody (Hasan et al., 2006). To determine if this apparent discrepancy was due to differential effects of chronic ischemia vs. ischemia-reperfusion, we carried out explant experiments with tissue from both types of injury. We co-cultured mouse heart tissue taken 10 days after sham, chronic ischemia, or I-R surgery with neonatal sympathetic ganglia, with or without antibodies to NGF, and measured axon outgrowth after 48 hours. Axon length was quantified in three cardinal directions around the ganglion (Figure 2A) to determine if explanted myocardium released factors into the media that stimulated axon growth. Heart explants from both types of myocardial infarction – ischemia and I-R – enhanced axon outgrowth compared to sham explants

(Figure 2B). The increase in axon growth was blocked by anti-NGF antibodies, but anti-NGF had no effect on axon length in sham co-cultures (Figure 2B). Thus, NGF is released from the cardiac scar after both ischemia and ischemia-reperfusion.

Although axon growth was enhanced overall in I-R explant co-cultures, we noted that growth was more variable in those co-cultures compared to sham and chronic ischemia explants. This was due to a consistent asymmetry in axon outgrowth in the I-R-ganglion co-cultures, where axons growing directly toward the heart were consistently shorter than axons growing in other cardinal directions (Figure 2C). Figure 2C shows axon lengths from representative co-cultures. In three independent experiments, symmetrical growth was observed in sham and chronic ischemia co-cultures, while asymmetrical growth was observed in I-R co-cultures, with significantly shorter axons growing directly toward heart explants (Figure 2D). Our anti-NGF data suggested that NGF was elevated in I-R co-cultures, so the consistently shorter axons projecting toward the heart led us to ask if I-R infarcts might be producing inhibitory extracellular matrix that formed a barrier to axon extension.

Chondroitin sulfate proteoglycans (CSPGs) are present in the heart following I-R

Nerve regeneration in the CNS is commonly prevented by inhibitory extra-cellular matrix that includes hyaluronic acid (HA) (Tona and Bignami, 1993) and chondroitin sulfate proteoglycans (CSPGs)(McKeon et al., 1999;Asher et al., 2001;Jones et al., 2002). HA is present in the developing mouse infarct after I-R

and is highest at the border zone of the mature scar (Dobaczewski et al., 2006), but it is not known if CSPGs are present in the heart after I-R. We ask whether CSPGs were present within the I-R infarct by carrying out immunohistochemistry with the pan-CSPG antibody CS-56 (Avnur and Geiger, 1984). This antibody binds to chondroitin sulfate (CS) rather than a specific core protein. CS-56 staining was absent in sham hearts (Figure 3A) and localized to the infarct after I-R (Figure 3B). Interestingly, CSPGs were undetectable in the chronic ischemia infarct (Figure 3C). This suggests that CSPGs and HA are present after I-R and are candidates for inhibiting axon growth into the infarct.

CSPGs inhibit sympathetic axon outgrowth in vitro, but HA does not

CSPGs (McKeon et al., 1991;Davies et al., 1997) and HA (Tona and Bignami, 1993) inhibit axon regeneration in the CNS, but they have not been examined in sympathetic nerve regeneration. To examine sympathetic axon responses to CSPGs, dissociated sympathetic neurons were grown in serum free medium to limit formation of dendrites (Lein et al., 1995), and treated for 24 hrs with increasing concentrations of CSPGs diluted in media. Neurites were analyzed using the Sholl method. Soluble CSPGs inhibited process outgrowth in a dose-dependent manner (Figure 4B). Similar results were obtained when neurons were grown on plates pre-coated with increasing concentrations of CSPGs (Figure 4C). CSPG-induced inhibition of axon outgrowth was prevented by treatment of CSPGs with ChABC (data not shown). While these experiments indicated that CSPGs inhibited axon outgrowth when in contact with the entire

neuron, they don't reveal whether local contact of the growing axon with CSPGs would block extension. To determine if CSPG interaction with axons blunted outgrowth, compartmentalized micro-fluidic chambers were used, and only the axonal compartment was coated with CSPGs. When axons encountered CSPGs, growth slowed significantly, and axon bundles formed that were absent in the control cultures (Figure 4E). Axon growth was restored by degradation of CSPGs by ChABC, indicating that sympathetic axon outgrowth was inhibited by CSPGs in the axonal compartment (Figure 4F). In contrast to the strong inhibition of axon outgrowth by CSPGs, soluble HA had no effect on sympathetic axon outgrowth (Figure 5A). This was also true when both high and low molecular weight forms of HA were pre-coated onto plates (Figure 5B).

Enzymatic degradation of infarct-derived CSPGs restores axon outgrowth

We observed CSPGs in infarcted myocardium after I-R, and found that CSPGs inhibited sympathetic axon outgrowth. To test if infarct-derived CSPGs prevented sympathetic axon extension, we carried out co-culture experiments with or without ChABC to degrade CSPGs. Sham or I-R myocardium was split into two pieces and co-cultured with a sympathetic ganglion in the presence of vehicle or ChABC. In vehicle-treated I-R co-cultures, axons growing directly toward the heart were shorter than axons growing in other directions (Figure 6A). However, in the ChABC-treated I-R co-cultures, axons growing toward the heart were not significantly shorter than axons growing in other directions (Figure 6B). This suggests that I-R explants secreted inhibitory CSPGs into the surrounding

Matrigel and these CSPGs were degraded by ChABC. Treatment with ChABC had no effect on axon growth in sham co-cultures (data not shown). These data can be expressed as a ratio of growth toward the heart/growth away from the heart (0º/90º) to control for different amounts of total growth in each individual co-culture, and data combined across multiple co-cultures (Figure 6C). ChABC consistently increased axon growth toward I-R explants, providing strong evidence that CSPGs produced by infarcted myocardium after I-R inhibit sympathetic regeneration into the infarct.

Absence of PTPσ restores axon outgrowth

Enzymatic degradation of CSPGs proved sufficient to overcome infarct-induced inhibition of sympathetic axon outgrowth *in vitro*. To further test the role of infarct-derived CSPGs, we used mice that lack the CSPG receptor protein tyrosine phosphatase sigma (PTPσ) (Elchebly et al., 1999;Shen et al., 2009). First, we confirmed that CSPGs did not inhibit sympathetic outgrowth in neurons lacking PTPσ. Sympathetic ganglia from *ptprs+/-* and *ptprs-/-* mice were treated with or without (1µg/mL) CSPGs, and the growth rate was quantified. *ptprs+/-* axon growth was inhibited by CSPGs, but *ptprs-/-* axons were not affected (Figure 7A). Sympathetic ganglia from *ptprs+/-* and *ptprs -/-* mice were then cultured with sham or I-R explants to determine if the lack of PTPσ would allow axon growth through the CSPGs release by I-R explants. Figure 7B shows an example of tissue from a single heart co-cultured with *ptprs-/-* and *ptprs+/-* ganglia. Infarcted myocardium inhibited the growth of *ptprs+/+* and *ptprs+/-*

axons but did not inhibit growth of *ptprs-/-* axons (Figure 7C). Similar results were obtained in three independent experiments, averaged in Figure 7D. Together, these *in vitro* experiments strongly support the idea that CSPGs are the primary agents responsible for inhibiting sympathetic axon regeneration in the heart after I-R, and that PTPσ is the major receptor for CSPGs in these neurons.

To test the role of CSPGs *in vivo*, *ptprs-/- and ptprs+/-* mice underwent ischemia-reperfusion or sham procedures. Ten days after surgery, heart sections were double-labeled for TH to identify sympathetic neurons and fibrinogen to identify the infarct. Sham animals showed no significant fibrinogen staining, and TH positive sympathetic fibers were evenly distributed in the sham left ventricles of both genotypes (Figure 8A+C). Likewise, TH-positive fiber densities outside the infarct were similar in both genotypes 10 days after I-R (Figure 8E). However, the infarct was devoid of sympathetic innervation in *ptprs+/-* mice, while *ptprs-/-* hearts exhibited significant hyperinnervation within the infarct (Figure 8B+D). The hyperinnervation is consistent with co-culture experiments indicating high levels of NGF in the scar, and confirms that CSPGs prevent reinnervation of the infarct after cardiac ischemia-reperfusion.

V. Discussion

Sympathetic neurons typically regenerate after injury, in contrast to central neurons whose regeneration is often limited. Reinnervation of the heart after chronic ischemia (Vracko et al., 1990;Zhou et al., 2004;Hasan et al., 2006;El-Helou et al., 2008) or cardiac transplantation (Bengel et al., 1999;Estorch et al.,

1999;Bengel et al., 2001;Bengel et al., 2002) fit this model of robust sympathetic regeneration. However, we found that a common injury affecting over a million people each year in the US (Roger et al., 2012a) – cardiac ischemia-reperfusion – generates a scar that is refractory to reinnervation. In this study, we found that regeneration into the cardiac scar is prevented by CSPGs, which also inhibit axon regeneration in the CNS (McKeon et al., 1991;Davies et al., 1997). We further showed that CSPGs prevent scar reinnervation by acting through PTPσ on sympathetic neurons, and that the absence of PTPσ led to hyperinnervation of the scar *in vivo*. This is the first demonstration of injury-induced CSPGs preventing sympathetic reinnervation of a target innervated by the autonomic nervous system.

We investigated a role for CSPGs in cardiac remodeling after I-R, because the lack of scar reinnervation was reminiscent of the lack of axon regeneration in the CNS after injury. Neurons in the CNS are prevented from regenerating by inhibitory molecules of the extracellular matrix including CSPGs, tenascin C (TnC), and HA (Reviewed by (Properzi et al., 2003;Silver and Miller, 2004;Sherman and Back, 2008;Fitch and Silver, 2008). These inhibitory matrix molecules are generated by reactive astrocytes and are key components of the "glial scar". CSPGs are particularly important for preventing axon regeneration in the CNS, and removal of CS chains from core proteins with the enzyme chondroitinase ABC can restore axon regeneration in culture and *in vivo* (Lin et al., 2008;Massey et al., 2008;Nakamae et al., 2009;Lee et al., 2010;Tom et al., 2009). Formation of a cardiac scar shares some similarities with formation of a

glial scar. Cardiac I-R triggers a significant inflammatory response including production of cytokines and infiltration of neutrophils and monocytes, a process that initiates fibroblast proliferation and migration (Porter and Turner, 2009).

Similar to astrocytes in CNS injury, activation of fibroblasts results in the production of extracellular matrix and maturation of a collagen based scar that contains TnC (Tamaoki et al., 2005) and HA (Dobaczewski et al., 2006). HA inhibits myelination of central axons (Back et al., 2005), but at least some of its effects on axon outgrowth are due to interactions with CSPGs (Sherman and Back, 2008). Our data indicate that low and high molecular weight HA had no effect on sympathetic axon outgrowth, and that CSPGs are the major source of axon inhibition. It is not yet clear if fibroblasts are the source of CSPGs in the I-R infarct, or why CSPGs are not present in the chronic ischemia infarct which is also characterized by fibrosis (Pfeffer and Braunwald, 1990), but future studies can address these issues.

The striking hyperinnervation observed in *ptprs-/-* hearts after I-R confirms the central role for CSPGs inhibiting regeneration, as well as the presence of high NGF in the scar. This hyperinnervation is interesting for several reasons. First, multiple receptors have now been identified for CSPGs (Shen et al., 2009;Fisher et al., 2011;Dickendesher et al., 2012), and our data suggest that PTPσ is the major receptor in sympathetic neurons. Second, removal of CSPGs in the spinal cord is not sufficient to restore growth without also adding neurotrophins (Jones et al., 2003;Garcia-Alias et al., 2011). Our data show that in the heart, simply removing inhibitory CSPG signaling results in

hyperinnervation of the scar, making this an interesting model for testing CSPG-targeted therapeutics. Third, proNGF was recently identified as elevated in the heart after I-R, where it contributes to expansion of the infarct after reperfusion (Siao et al., 2012). ProNGF, which is elevated in the mouse heart 1 and 3 days after I-R (Siao et al., 2012), stimulates axon degeneration rather than outgrowth in adult sympathetic neurons in vivo (Al-Shawi et al., 2008). Given that we carried out the mouse I-R procedure identically in the proNGF study (Siao et al., 2012) and the current study, our data suggest that sometime between days 3 and 10 post-injury, the balance shifts between proNGF and NGF so that NGF effects predominate and hyperinnervation occurs. Finally, high levels of NGF are sufficient to support sensory neuron growth over CSPGs *in vitro* (Zhou et al., 2006), but our data indicate that the amount of NGF in the heart is not sufficient to stimulate sympathetic regeneration through CSPGs and into the cardiac scar.

The functional consequences of reinnervating the infarct are not yet understood. While reinnervation of the infarct and presumptive restoration of NE release following I-R will not enhance contractile function in the scar, it may stimulate contractility of myocytes surrounding the infarct, and thus increase cardiac output in *ptprs-/-* mice. It is likely, however, that reinnervation of the scar will have a greater impact on arrhythmia susceptibility than on contractile function or cardiac output. Heterogeneity of sympathetic transmission after MI, and subsequent electrical remodeling of cardiac myocytes, is a major contributor to the development of arrhythmias and sudden cardiac death in humans (Rubart and Zipes, 2005;Nishisato et al., 2010). Early studies mapping sympathetic

innervation in human hearts after I-R with 123I-MIBG imaging and identified denervation (Stanton et al., 1989) followed by some reinnervation of peri-infarct myocardium (Hartikainen et al., 1996). Recent detailed mapping studies in intact human hearts revealed sympathetic denervation of the normal myocardium directly adjacent to the scar (Vaseghi et al., 2012). Denervation led to electrical remodeling, so that the activation recovery interval at the border zone differed from that of the scar and surrounding viable myocardium. Dispersion of activation recovery interval is indicative of electrical instability in the heart, and significantly increases the probability of arrhythmia (Kuo et al., 1983). Given the secretion of CSPGs from infarct explants, the denervation at the border zone in human hearts may be due to the presence of inhibitory CSPGs. Thus, degrading CSPGs *in vivo* with ChABC might restore innervation to the border zone and decrease arrhythmia susceptibility.

In summary, this study provides the first example of CSPGs preventing sympathetic reinnervation of an autonomic target following injury, despite high levels of NGF in the infarct. We show that CSPGs act through PTPσ to block sympathetic axon outgrowth, and that the absence of PTPσ results in hyperinnervation of the infarct. This may have important consequences for cardiac function and arrhythmia susceptibility for people who suffer a myocardial infarction.

VI. Figures

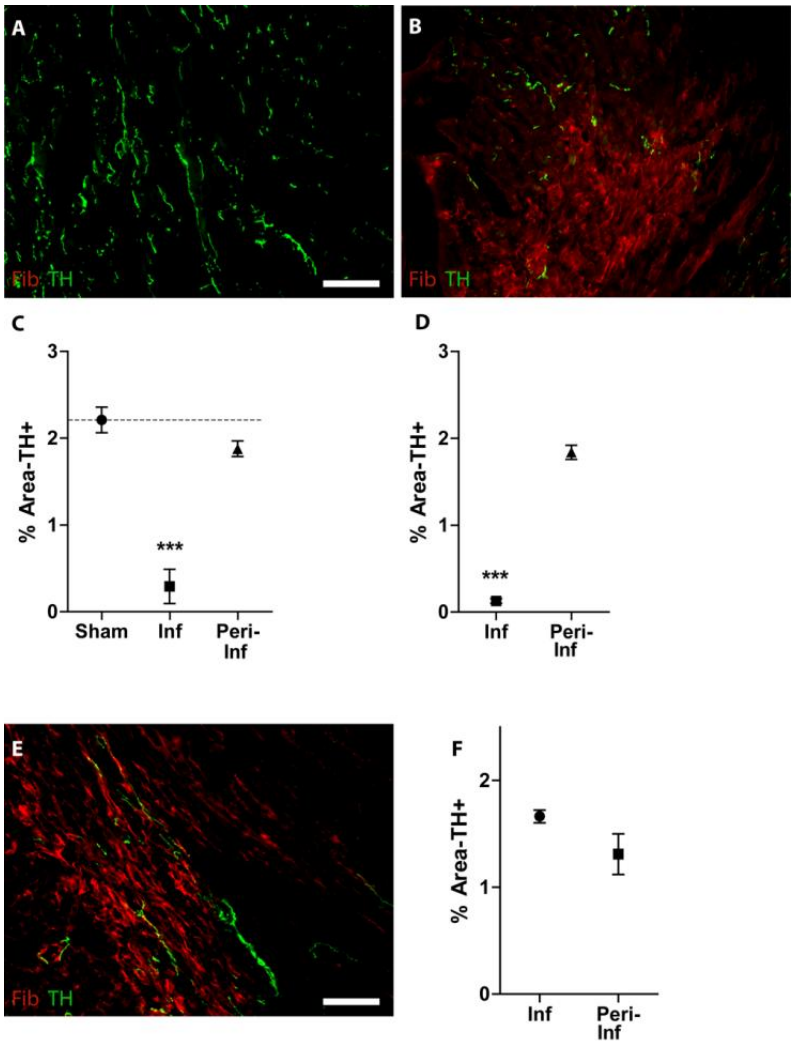

Figure 2.1. Sympathetic denervation after ischemia-reperfusion. Heart sections from Sham **(A),** I-R **(B),** and chronic ischemia **(E)** operated mice were stained for TH (green) to identify sympathetic nerve fibers and fibrinogen (red) to identify the infarct (scale bars=100μm). TH+ fibers were quantified in the infarct and peri-infarct ventricle (or the corresponding area of sham ventricle) 10 days **(C)** or 20 days **(D)** after reperfusion, or after 10 days of chronic ischemia **(F)**. Data are the Mean±SEM, n=4/surgical group; (C) ***p<.001 vs. sham and vs. peri-infarct; (D) ***p<.001 vs. peri-infarct; (F) no significant differences.

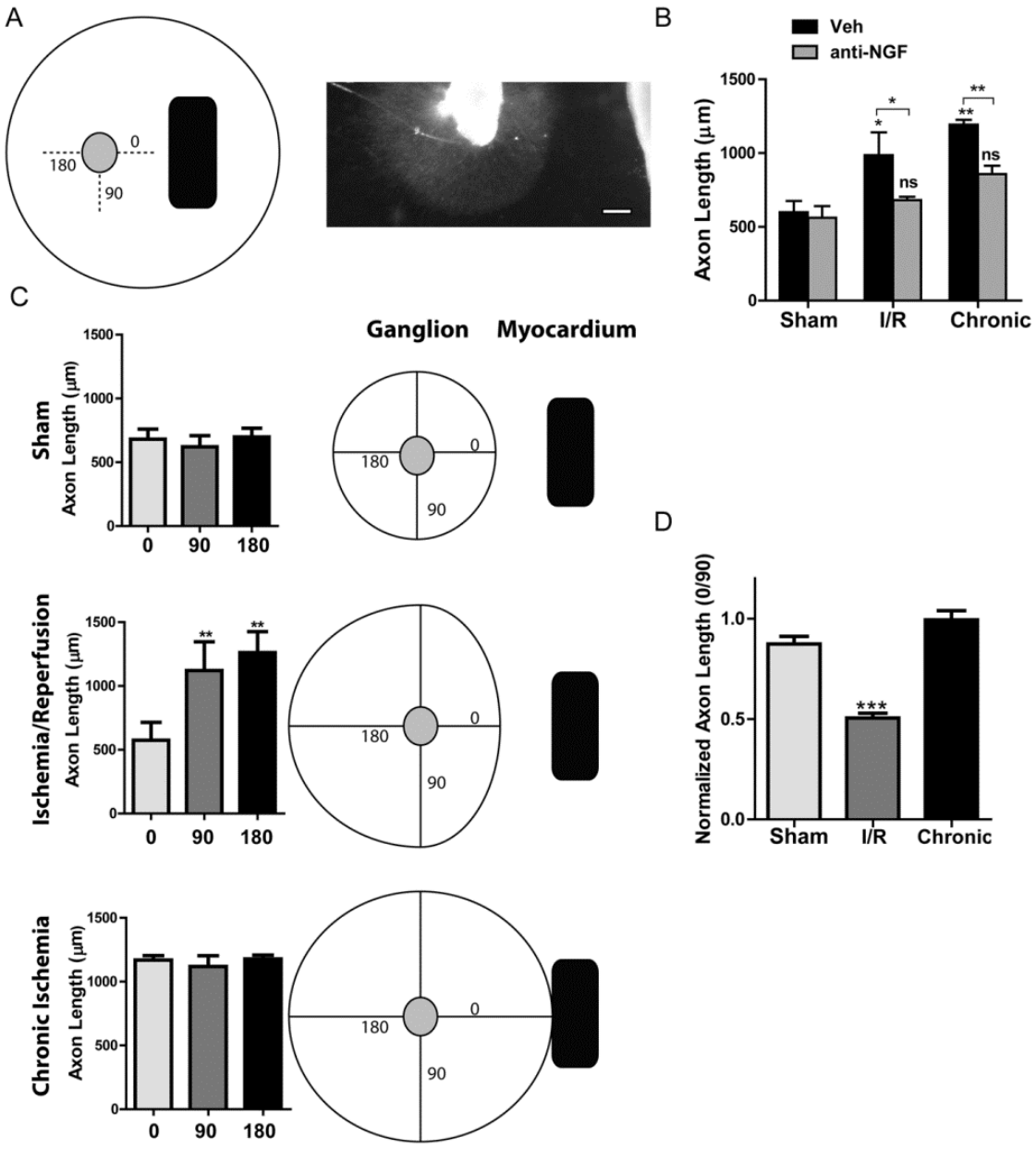
A
0
180
90
B
Veh
anti-NGF
Axon Length (µm)
1500
1000
500
0
*
**
ns
Sham
I/R
Chronic
C
Ganglion
Myocardium
Sham
Axon Length (µm)
0
90
180
Ischemia/Reperfusion
Chronic Ischemia
D
Normalized Axon Length (0/90)
1.0
0.5
0.0
***

Figure 2.2. Infarcted heart explants stimulate axon outgrowth. (A) Left: An illustration of the co-culture method showing three cardinal directions around the ganglion where axon length was quantified (0º, 90º, 180º). Right: photo of a ganglion co-cultured with I-R heart explant (scale bar=200µm). **(B)** SCGs were co-cultured with heart tissue from sham, I-R infarcts, or chronic ischemia infarcts, treated with vehicle or a function blocking anti-NGF antibody, and axon length was quantified. Triplicate co-cultures were assayed for each condition. Data are Mean±SEM; without anti-NGF, *p<.05 and **p<.01 vs. sham; with anti-NGF, *p<.05 and **p<.01 vs. vehicle, not significant (n.s.) vs. sham. **(C)** Directional axon length for the vehicle treated co-cultures quantified in panel B. Axon length at 0º, 90º, and 180º is graphed separately rather than pooled together (triplicate co-cultures, 6 measurements/direction in each co-culture, Mean±SEM, **p<.01 vs. 0º). For illustration purposes, the length measurements at 0º, 90º, and 180º were used to generate a diagram of axon growth in all directions. **(D)** Ratio of growth toward the heart/growth away from the heart (0º length/90º length) averaged across three independent co-culture experiments carried out without NGF antibodies (Mean ±SEM; ***p<.001). A ratio of 1 is similar growth at 0º and 90º, a ratio less than 1 indicates shorter axons at 0º.

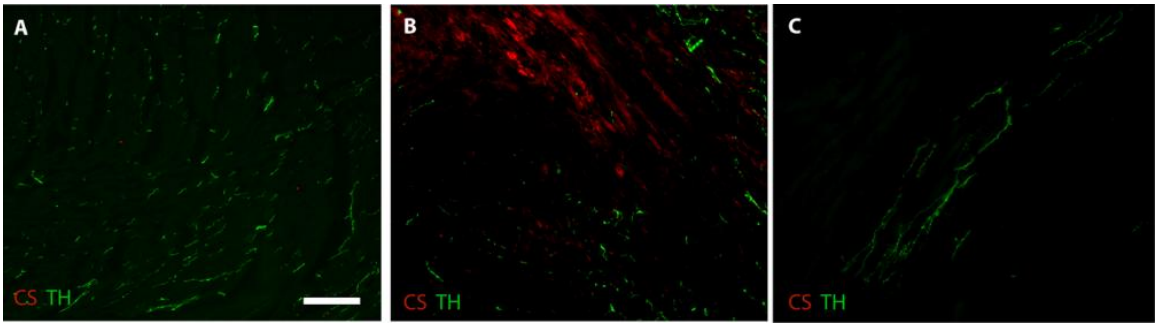

Figure 2.3. Ischemia-reperfusion stimulates CSPG production in the heart. Heart sections from Sham **(A),** I-R **(B),** and chronic ischemia **(C)** operated mice were stained 10 days after surgery for TH (green) to identify sympathetic nerve fibers, and for chondroitin sulfate proteoglycans (CS) using the CS-56 antibody (red) (scale bar=100µm) . Similar results were obtained in sections from 4 hearts in each surgical group.

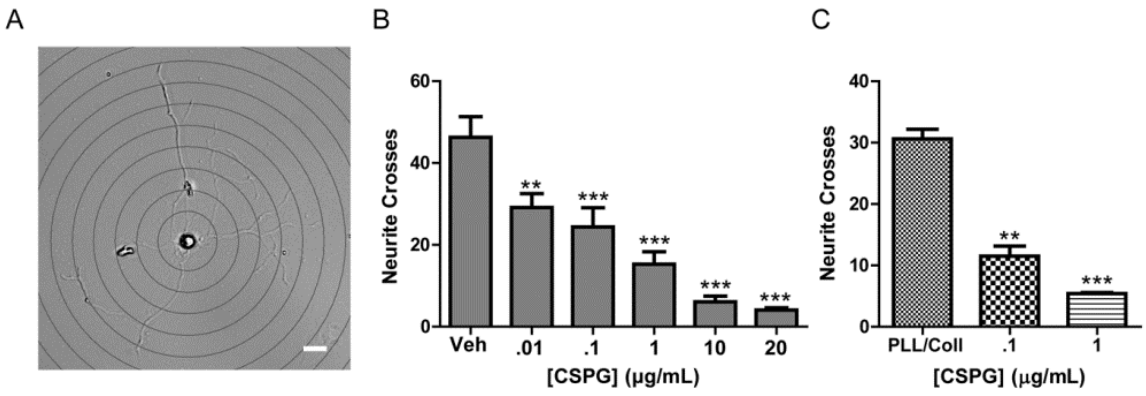

Figure 2.4a. CSPGs inhibit sympathetic axon outgrowth in vitro (A) A representative image of a sympathetic neuron, overlayed with a series of concentric circles for Sholl analysis (scale bar=20µm). Dissociated sympathetic neurons were treated with soluble CSPGs **(B)**, or plated onto dishes pre-coated with CSPGs **(C)**, and neurite crosses were quantified by Sholl analysis. Data are the Mean±SEM of least 10 neurons/condition, **p<.01; ***p<.001. Similar results were obtained in 3 independent experiments.

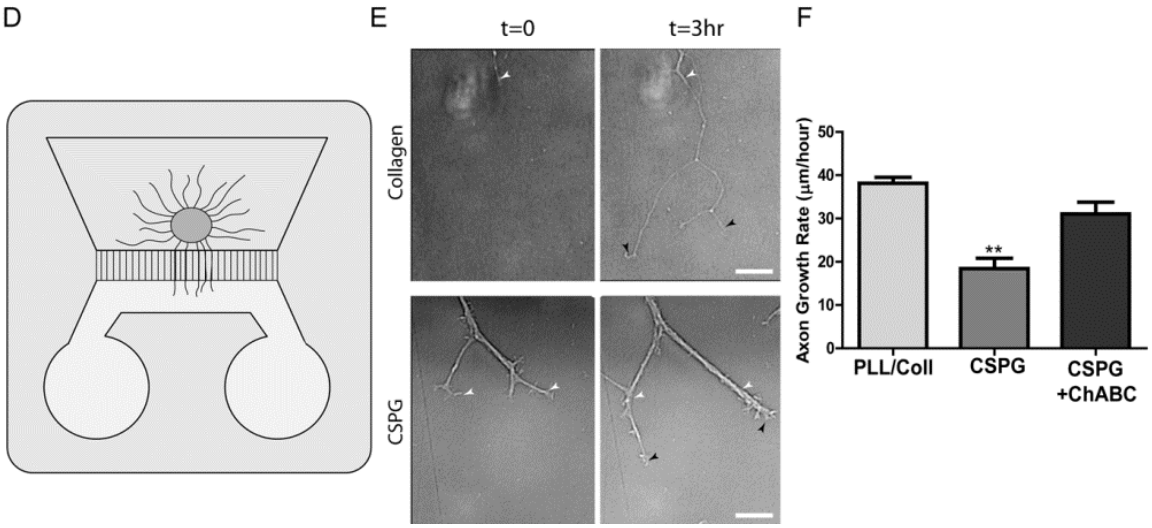

Figure 2.4b. (D) Illustration of a microfluidic chamber with a ganglion explant on one side and axons growing through grooves into a second chamber that was coated with collagen or CSPGs. **(E)** Representative micrographs of axons growing at t=0 and t=3 hr on collagen or CSPGs (1µg/mL). White arrowheads indicate the leading edge of the axon in the t=0 image, while black arrowheads indicate the final point of the axon at t=3hr (scale bar=20µm). Note bundling of the axons growing on CSPGs. **(F)** Quantification of axon growth in microfluidic chambers where the distal compartment was coated with Collagen, Collagen/CSPGs, or Collagen/CSPGs+ChABC. Data are Mean±SEM of at least eight axons per condition, **p<.01, and similar results were obtained in three independent experiments.

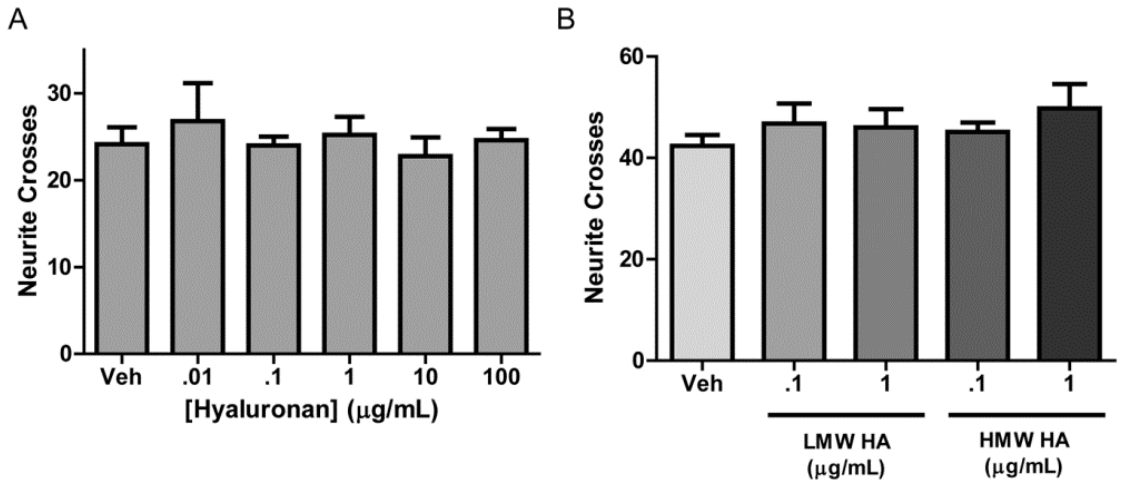

Figure 2.5. Hyaluronan does not inhibit sympathetic axon outgrowth in vitro. Dissociated sympathetic neurons were treated with soluble HA **(A)**, or plated onto dishes pre-coated with low molecular weight (LMW) or high molecular weight (HMW) HA **(B)**, and neurite crosses were quantified by Sholl analysis. Data are the Mean±SEM of least 10 neurons/condition. Similar results were obtained in three independent experiments.

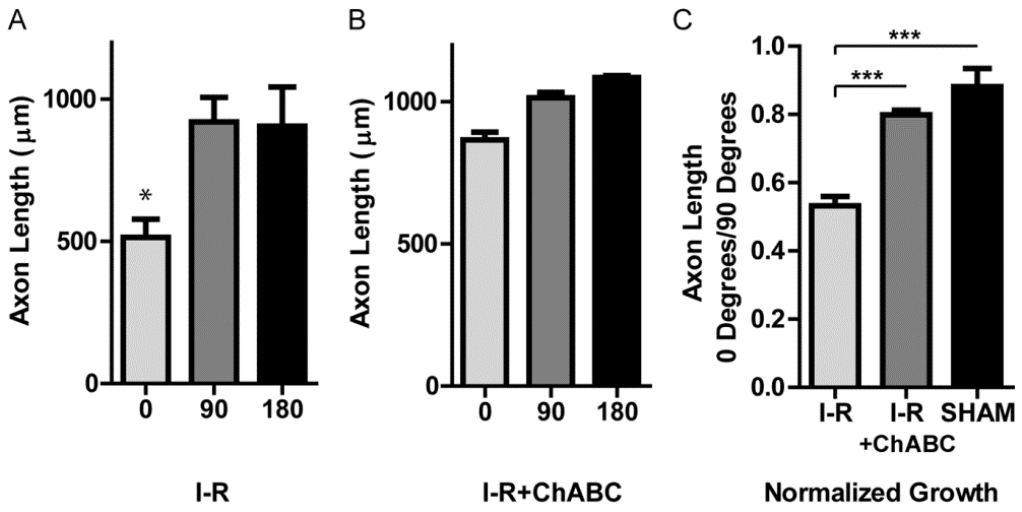

Figure 2.6. Enzymatic degradation of infarct-derived CSPGs restores axon outgrowth. SCGs were co-cultured with heart tissue after sham or I-R surgery, and treated with either vehicle **(A)** or ChABC **(B)**. Tissue from a single heart was split between the vehicle and ChABC groups. Axon length was quantified at 0º, 90º, and 180º (6 measurements/direction) and triplicate co-cultures were averaged (Mean±SEM, *p<.05 vs. 90º and 180º). **(C)** Axon length normalized as the ratio of growth toward the heart/growth away from the heart (0º length/90º length) averaged from three independent experiments, each assayed in triplicate. (Mean ±SEM; ***p<.001).

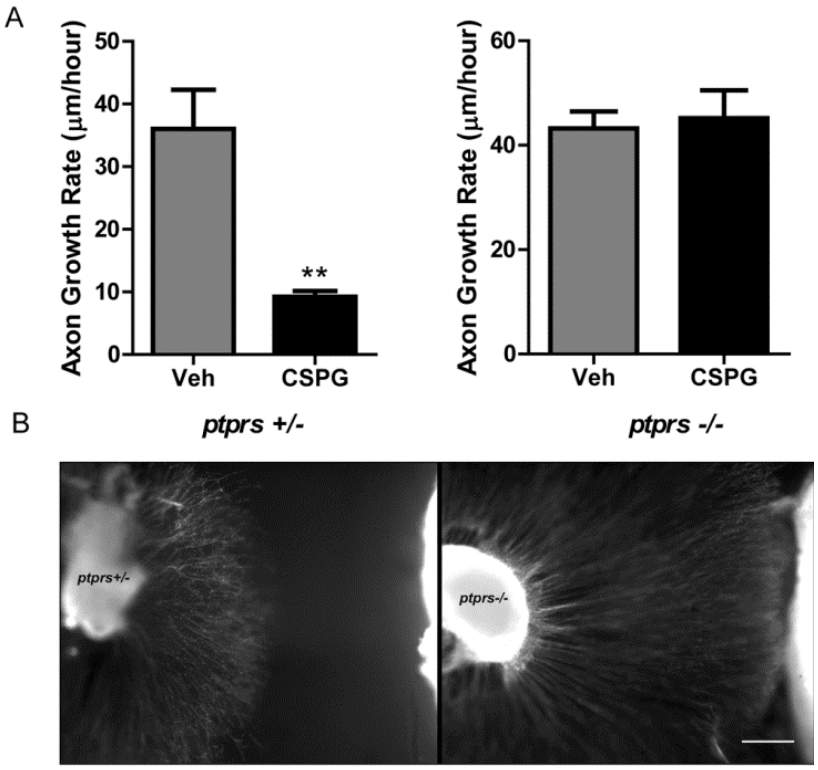

Figure 2.7a. Loss of PTPσ restores axon outgrowth *in vitro* (A) Axon growth rate in *ptprs +/-* and *ptprs -/-* SCG explants treated with 1µg/mL CSPGs. Data are Mean±SEM; n=3, **p<.01, and are representative of 3 independent experiments. **(B)** Micrographs of a *ptprs+/-* and *ptprs-/-* SCG co-cultured with I-R infarct tissue from the same heart. The culture was fixed and stained for TH to highlight axons (scale bar=200µm).

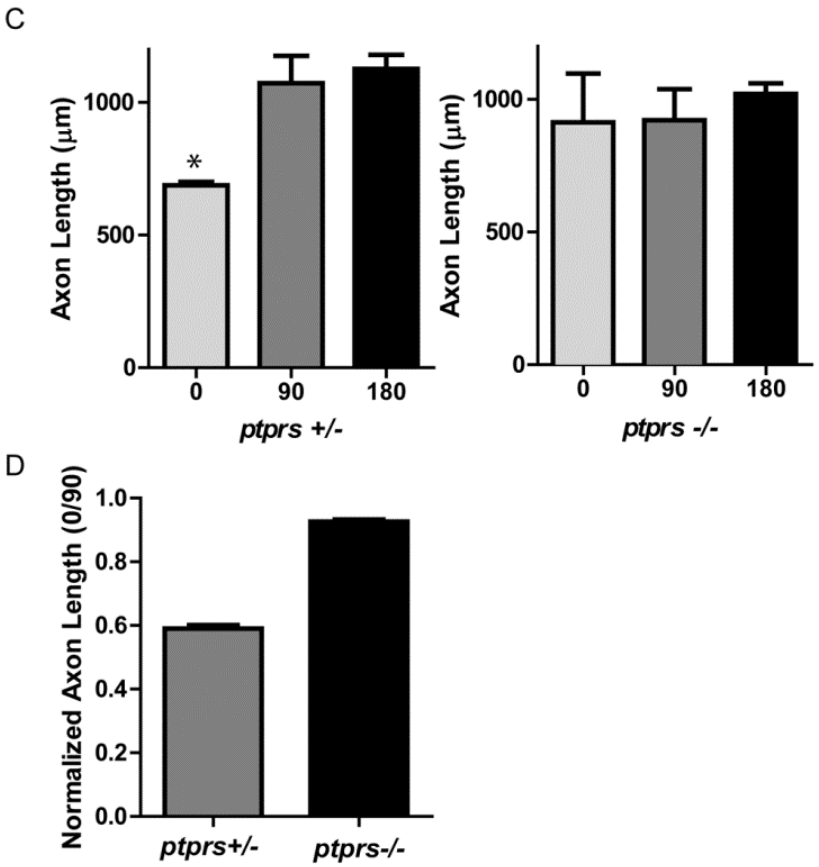

Figure 2.7b. (C) *ptprs* +/- and *ptprs* -/- SCG explants were co-cultured with sham or I-R infarcted heart tissue. Axon length was quantified at 0º, 90º, and 180º (6 measurements/direction) and triplicate co-cultures were averaged (Mean±SEM, *p<.05 vs. 90º and 180º). **(D)** Axon length normalized as the ratio of growth toward the heart/growth away from the heart (0º length/90º length) averaged from three independent experiments, each assayed in triplicate.

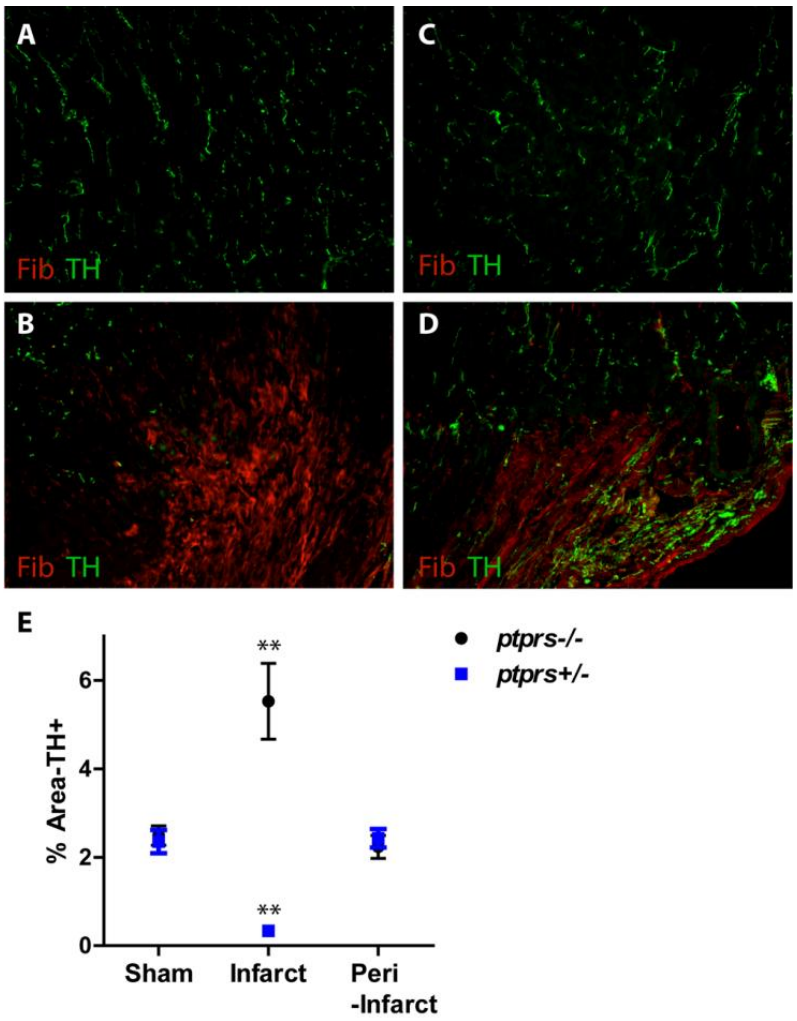

Figure 8. Loss of CSPG receptor PTPσ restores axon outgrowth in vivo. Heart sections from Sham (A,C) or I-R (B,D) operated ptprs +/- (A,B) and ptprs -/- (C,D) mice were stained for TH (green) to identify sympathetic nerve fibers and fibrinogen (red) to identify the infarct (scale bar=100µm). Sham hearts of both genotypes (A,C) exhibit normal innervation. In contrast, the infarct is denervated in ptprs+/- hearts (B), but hyper-innervated in ptprs-/- hearts (D). (E) Quantification of TH-positive fiber density within the left ventricle of sham and I-R operated (infarct and peri-infarct) animals 10 days post surgery (Mean ±SEM, n=5 mice/group; two way ANOVA **p<.01, ***p<.001).

Chapter 3

Targeting protein tyrosine phosphatase σ after myocardial infarction restores cardiac sympathetic innervation and prevents arrhythmias

Gardner RT[1], Wang L[2], Lang BT[3], Dunbar C[1], Woodward WR[4], Silver J[3], Ripplinger CM[2], Habecker BA[1]

[1]Department of Physiology & Pharmacology, Neuroscience Graduate Program, [4]Department of Neurology, Oregon Health and Science University, Portland, OR 97239, USA. [2]Department of Pharmacology, School of Medicine, University of California, Davis, CA 95616, USA. [3]Department of Neurosciences, Case Western Reserve University, Cleveland, Ohio 44106, USA.

Submitted in entirety to *Nature*

Acknowledgments: This work was supported by NHLBI HL093056 & HL068231 (BAH) and HL111600 (CMR); NINDS NS25713 (JS); the American Heart Association 12SDG9010015 (CMR); and an Oregon Brain Institute Neurobiology of Disease Fellowship (RTG).

The authors thank Michel Tremblay (McGill University, Montreal, Canada) for providing the PTPσ transgenic mice.

I. Abstract

Millions of people suffer a myocardial infarction (MI) every year, and those who survive have increased risk of arrhythmias and sudden cardiac death. Recent clinical studies have identified sympathetic denervation as a predictor of increased arrhythmia susceptibility. Chondroitin sulfate proteoglycans present in the cardiac scar after MI prevent sympathetic reinnervation by binding the neuronal protein tyrosine phosphatase receptor σ (PTPσ). We targeted PTPσ in mice to promote sympathetic reinnervation of infarcted and peri-infarct myocardium, and asked if this altered arrhythmia susceptibility. We found that the absence of PTPσ, or pharmacologic modulation of PTPσ by the novel intracellular sigma peptide (ISP) beginning three days after injury, restored sympathetic innervation to the scar and markedly reduced arrhythmia susceptibility. Using optical mapping we observed increased dispersion of action potential duration, super-sensitivity to β-adrenergic receptor stimulation, and Ca^{2+} mishandling following MI. Sympathetic reinnervation prevented these changes and rendered hearts remarkably resistant to induced arrhythmias.

II. Introduction

Survivors of myocardial infarction (MI) remain at high risk for cardiac arrhythmias and sudden cardiac death (Solomon et al., 2005). The infarct, or scar, generates an anatomical substrate that promotes re-entrant arrhythmias (Jalife, 2000), but numerous studies indicate that altered sympathetic neurotransmission in the heart also plays a key role in the onset of post-infarct

cardiac arrhythmias (Nademanee et al., 2000;Basu et al., 1997;Billman et al., 1997;Exner et al., 1999;SCHWARTZ et al., 1992). The transmural (epicardial to endocardial) gradient in action potential duration (APD), which is accompanied by a transmural gradient in sympathetic innervation density, is critical for normal activation and repolarization of the left ventricle (Antzelevitch et al., 1991;Nabauer et al., 1996;Brunet et al., 2004;Kimura et al., 2012). Norepinephrine (NE) released from sympathetic nerves activates cardiac β-adrenergic receptors (β-AR) to modulate myocyte repolarization by altering transmembrane currents and Ca^{2+} homeostasis (Thomas et al., 2004;Cutler et al., 2011;Bers, 2008), and simply disrupting the transmural gradient of sympathetic innervation in an otherwise normal heart is arrhythmogenic (Ieda et al., 2007;Lorentz et al., 2010). Cardiac sympathetic function is altered in a region-specific manner following MI, and studies in animals and humans reveal denervation of the infarct and adjacent, viable (peri-infarct) myocardium (Barber et al., 1983;Dae et al., 1995;Li et al., 2004;Simula et al., 2000;Stanton et al., 1989;Stanton et al., 1989). Three recent studies in patients with implanted cardioverter defibrillators (ICDs) suggest that the amount of sympathetic denervation after MI predicts the probability of serious ventricular arrhythmias (Boogers et al., 2010;Nishisato et al., 2010;Fallavollita et al., 2013). A detailed electrical mapping study in intact human hearts revealed that sympathetic denervation of the normal myocardium adjacent to the scar resulted in β-AR agonist super-sensitivity and increased dispersion of repolarization that was arrhythmogenic (Vaseghi et al., 2012). These studies and others led to the model

that inappropriate heterogeneity of sympathetic transmission across the left ventricle, and subsequent electrical remodeling of cardiac myocytes, is a major contributor to post-infarct arrhythmias in humans (Rubart and Zipes, 2005).

The observation that denervated myocardium adjacent to the infarct contributes to the generation of post-infarct arrhythmias (Vaseghi et al., 2012) was especially interesting to us because chondroitin sulfate proteoglycans (CSPGs) in the cardiac scar prevent re-innervation of the infarct and adjacent myocardium by sympathetic axons (Gardner and Habecker, 2013). Although axons sprout and regenerate toward the scar (Lorentz et al., 2013), they are stopped near the outer edge of the infarct by CSPGs. In the absence of the CSPG receptor, Protein Tyrosine Phosphatase receptor sigma (PTPσ), sympathetic axons fully reinnervate undamaged peri-infarct tissue and hyperinnervate the infarct (Gardner and Habecker, 2013). Given the clinical significance of sympathetic denervation after MI (Boogers et al., 2010;Fallavollita et al., 2013;Nishisato et al., 2010;Vaseghi et al., 2012), we were interested to determine if restoring sympathetic innervation to the infarct and surrounding myocardium altered post-MI arrhythmia susceptibility.

We targeted PTPσ using both genetic and pharmacologic approaches in order to promote reinnervation of the infarct, and used electrocardiogram (ECG) telemetry to examine arrhythmia susceptibility. Transmembrane potential (V_m) and intracellular Ca^{2+} dynamics were assessed using *ex vivo* optical mapping in order to investigate the mechanisms underlying changes in arrhythmia

susceptibility. Restoring sympathetic innervation to the infarct and the surrounding tissue decreased arrhythmia susceptibility and normalized cardiac electrophysiology and Ca^{2+} dynamics, despite the presence of a scar.

III. **Methods** (additional details in the detailed methods chapter)

PTPσ (ptprs) transgenic mice (BalbC) were supplied by Michel Tremblay (McGill University) (Elchebly et al., 1999), and were bred as heterozygotes (Gardner and Habecker, 2013). Age and gender-matched mice 12-18 weeks old were used for all experiments. All procedures were approved by Institutional Animal Care and Use Committees and comply with the Guide for the Care and Use of Laboratory Animals published by the National Academies Press (8^{th} edition).

Myocardial ischemia-reperfusion (I-R) was carried out as described (Gardner and Habecker, 2013;Lorentz et al., 2013). Anesthesia was induced with 4% isoflurane and maintained with 2% isoflurane. The left anterior descending coronary artery (LAD) was reversibly ligated for 30 min (telemetry studies) or 45 min (*ex vivo* mapping) and then reperfused by release of the ligature.

In vivo telemetry devices were implanted 5 days prior to I-R surgery (Lorentz et al., 2010). Arrhythmias were induced by IP injection of 10 µg isoproterenol (ISO) 10 days after I-R. Some mice were given daily IP injections of vehicle (5% DMSO/Saline), IMP (Intracellular Mu Peptide; 10 µmol), or ISP (Intracellular Sigma Peptide,10 µmol) beginning 3 days after I-R.

Immunohistochemistry for tyrosine hydroxylase (TH; sympathetic nerve fibers) and fibrinogen (Fib; infarct/scar) was carried out as described previously (Gardner and Habecker, 2013;Lorentz et al., 2013). Sympathetic nerve density and infarct size were quantified using ImageJ.

NE content was quantified by HPLC as described previously (Lorentz et al., 2013).

Langendorff perfusion and dual optical mapping of V_m and Ca^{2+} were carried out as described previously(Myles et al., 2012), using the fluorescent intracellular Ca^{2+} indicator Rhod-2 AM (Molecular Probes) and the voltage-sensitive dye RH237 (Molecular Probes).

*Statistic*s: Data were analyzed by t-test, one-way ANOVA, or two-way ANOVA depending on the number and size of groups. Analyses were carried out using Prism 5.0.

IV. Results

Targeting PTPσ restores sympathetic innervation after MI and prevents ventricular arrhythmias

We previously observed (Gardner and Habecker, 2013) that CSPGs generated in the cardiac scar after ischemia-reperfusion prevented reinnervation of the infarct (Figure 1A) despite high levels of NGF (Nerve Growth Factor) in the scar. The infarct becomes hyperinnervated in animals lacking the CSPG receptor PTPσ (Gardner and Habecker, 2013) (Figure 1B), confirming the crucial role for

PTPσ in sympathetic denervation after MI. Since cardiac denervation is linked to risk for arrhythmia and cardiac arrest in human studies (Boogers et al., 2010;Nishisato et al., 2010;Fallavollita et al., 2013), we asked if restoring sympathetic innervation to the infarct and surrounding myocardium affected arrhythmia susceptibility. Control mice (ptprs+/-; HET) and mice lacking PTPσ (ptprs-/-; KO) were implanted with ECG telemetry transmitters and then subjected to sham or MI surgery. Ten days after surgery, mice were injected with 10 µg of the beta agonist isoproterenol (ISO) to mimic circulating catecholamines and provoke arrhythmias. ISO stimulated comparable increases in heart rate in all mice (Figure 1C), but the arrhythmia response differed based on the innervation status of the infarct. Isoproterenol stimulated few premature ventricular complexes (PVCs) in sham mice of either genotype, but triggered a significant number of PVCs in HET mice with denervated infarcts (Figure 1E). In contrast, KO mice with innervated infarcts were resistant to ISO-induced arrhythmias, having the same number of PVCs as sham animals (Figure 1E). The infarct size in both genotypes was the same (Figure 1D), indicating the difference in arrhythmia susceptibility could not be explained by scar size.

To confirm that reinnervation of the infarct and surrounding tissue decreased arrhythmia susceptibility, we sought to restore innervation in mice expressing normal levels of PTPσ. In order to promote regeneration of sympathetic axons through the CSPG-rich cardiac scar, we utilized Intracellular Sigma Peptide (ISP), developed by Lang and Silver to target the intracellular dimerization domain of PTPσ (Lang and et al., 2013). ISP restored growth of

CNS axons through CSPGs *in vitro* (Lang and et al., 2013), and systemic injections of ISP enhanced axon sprouting through CSPGs after spinal cord injury *in vivo* (Lang and et al., 2013). We asked if targeting PTPσ with ISP could restore sympathetic axon regeneration into the cardiac scar. Wild type (*ptprs*+/+) mice were implanted with ECG telemetry transmitters, and a week later subjected to ischemia-reperfusion surgery. Beginning three days after MI, when the infarct was fully denervated (Lorentz et al., 2013), mice were injected daily (IP) with vehicle (5% DMSO/Saline), ISP (10 µmol; 44 µg) or IMP (Intracellular Mu Peptide) as a negative control (10 µmol; 42 µg). IMP targets the receptor PTPµ, which is not present in sympathetic neurons. Fourteen days after the MI surgery, mice were treated with ISO to mimic circulating catecholamines and provoke arrhythmias, and hearts were collected for analyses of sympathetic innervation. Animals treated with either vehicle or IMP had denervated infarcts (Figure 2 A,B), whereas animals treated with ISP had normal levels of sympathetic innervation throughout the left ventricle, including the infarct (Figure 2C). Thus, daily ISP injections beginning 3 days after the injury, when denervation was well established, allowed robust regeneration of sympathetic axons into the CSPG-laden cardiac scar.

Several studies indicate that newly regenerating sympathetic axons in the damaged heart have low levels of NE (Parrish et al., 2010;Kimura et al., 2007), likely due to local depletion of TH by inflammatory cytokines (Shi and Habecker, 2011). The cardiac scar in mouse heart is mature by 10-12 days after reperfusion and acute inflammation has resolved (Dobaczewski et al., 2006).

Therefore, we quantified NE levels in the infarct and peri-infarct myocardium 14 days after surgery to determine if the axons that had reinnervated the infarct and surrounding myocardium had normal NE levels. NE content was low in the denervated infarct of vehicle-treated animals, but was normal in the innervated infarct of ISP-treated animals (Figure 2E). NE content in the undamaged portion of the left ventricle was similar in both treatment groups (Figure 2E), consistent with identical innervation densities (Figure 2D). Likewise, NE content in the undamaged right ventricle was similar in both groups (data not shown). These data indicate that restoring innervation to the infarct with ISP normalizes NE levels across the left ventricle by two weeks after MI.

Since regional sympathetic denervation is thought to be an important source of post-MI arrhythmia susceptibility, we quantified ISO-induced arrhythmias 14 days after MI in mice treated with vehicle, IMP, or ISP. Isoproterenol triggered significantly fewer PVCs in ISP- treated mice, which had innervated infarcts and normal NE content, than in the vehicle or IMP treated groups which had denervated infarcts and low NE content (Figure 2F). These data suggest that restoring sympathetic transmission throughout the infarcted left ventricle, even days after denervation is established, is sufficient to decrease arrhythmia susceptibility.

Restoring innervation decreases dispersion of APD_{90} and prevents β-AR super-sensitivity

Activation of cardiac β receptors decreases myocyte action potential duration (APD_{90}) by changing ion channel activity and Ca^{2+} handling to allow for adaptation to fast heart rates (Thomas et al., 2004;Cutler et al., 2011;Bers, 2008). In order to assess directly the impact of infarct reinnervation on cardiac electrophysiology, we used optical mapping to simultaneously image intracellular Ca^{2+} and V_m in Langendorff-perfused isolated hearts. PTP KO mice were used to examine the effect of reinnervation on cardiac electrophysiology, with ptprs+/- (HET) mice serving as denervated controls.

In order to compare baseline electrical properties, a pacing electrode was positioned on the base of the LV epicardium, and APD_{90} was assessed at a pacing interval of 150 ms (400 bpm heart rate). Figure 3B (top) shows a representative sample of action potential propagation across a heart from each group: HET Sham, KO Sham, HET MI, and KO MI. Quantification of mean APD_{90} revealed it was similar across all four groups (Figure 3C). Figure 3B (bottom) shows a representative map of APD_{90} throughout a single heart. Although mean APD_{90} is the same, it is clear that the denervated HET MI heart exhibits greater extremes of APD_{90} than the other hearts. The interquartile range (IQR) is a measure of APD_{90} variability, or dispersion, across an individual heart. IQR was significantly higher in denervated HET MI hearts compared to all other groups (Figure 3D), consistent with increased dispersion of APD after myocardial infarction in human studies (Vaseghi et al., 2012). Surprisingly, sympathetic reinnervation of the infarct prevented an increase in APD dispersion following MI

(Figure 3D), despite the presence of a cardiac scar similar to that in the HET MI group (Figure 3E).

Sudden cardiac death is most common in the morning (Muller et al., 1987), when circulating catecholamines (NE and epinephrine) are rising rapidly (Scheer et al., 2010). Given the protective role of beta blockers in humans, we wanted to examine the role of β-AR and circulating catecholamines in arrhythmia generation in our infarcted mouse hearts. We treated hearts with tyramine to induce release of endogenous NE from sympathetic axons within the heart, and with ISO to mimic circulating catecholamines. Release of endogenous NE with tyramine resulted in similar APD shortening across all groups (% change: HET Sham -0.5±0.6, HET MI -0.8±0.6, KO Sham -0.2±0.2, KO MI -2.1±0.6; n=3-5, mean±sem). In contrast, treatment with ISO, which mimics the effect of circulating catecholamines *in vivo*, stimulated a significantly greater shortening of APD_{90} in denervated HET MI hearts compared to all other groups (Figures 4A, B). This denervation-induced β-AR super-sensitivity is consistent with studies in other animal models and recent human data (Schomig and Richardt, 1990;Vaseghi et al., 2012).

Restoring sympathetic innervation prevents intracellular Ca^{2+} mishandling and PVCs

In order to identify the mechanisms underlying changes in cardiac electrophysiology, we examined intracellular Ca^{2+} handling at various pacing frequencies and after ISO treatment. Disrupted calcium homeostasis can result

in beat-to-beat fluctuations between large and small intracellular calcium transients (CaT) called alternans, which is a sensitive noninvasive marker for risk of sudden cardiac death in humans (Wilson et al., 2006). Intracellular Ca^{2+} handling appeared normal in sham hearts of both genotypes when paced with a 100 ms pulse interval (600 bpm heart rate; Figure 5). However, HET hearts with denervated infarcts (HET MI) exhibited significant intracellular Ca^{2+} alternans at the same pacing frequency (Figure 5). Interestingly, KO hearts with infarcts (KO MI) did not exhibit intracellular Ca^{2+} alternans (Figure 5), suggesting that restoring sympathetic innervation to the infarct and surrounding tissue protects intracellular Ca^{2+} homeostasis.

The notion that sympathetic reinnervation of the peri-infarct border and scar protects intracellular Ca^{2+} handling was confirmed by analyzing intracellular Ca^{2+} after ISO administration. Under baseline conditions, normal excitation-contraction coupling occurred, in which membrane depolarization (V_m; black) preceded the Ca_T upstroke (red) in hearts from both genotypes and surgical groups (Figure 6A). In sham hearts treated with ISO, depolarization continues to precede the Ca_T (data not shown). However, in the infarcted hearts, the response to ISO differed depending on innervation status. Infarcted hearts with sympathetic innervation restored throughout the entire left ventricle (KO-MI) continued to exhibit normal Ca^{2+} handling after ISO treatment, Figure 6A, B), while hearts with sympathetic denervation (HET-MI) exhibited increases in diastolic intracellular [Ca^{2+}] that preceded membrane depolarization (Figure 6A,

B). This Ca^{2+} elevation was prevented by addition of the β-AR blocker propranolol (Figure 6A, B).

We previously showed that strong localized β-AR stimulation can trigger Ca^{2+} release independent of membrane depolarization that is sufficient to cause PVCs (Myles et al., 2012). Therefore, we asked if ISO-stimulated Ca^{2+} mishandling led to the production of PVCs after MI. Quantification of PVCs in HET and KO MI hearts confirmed the striking difference in arrhythmia susceptibility observed during the *in vivo* ECG telemetry studies. ISO triggered significantly more PVCs in HET MI hearts with denervated infarct/peri-infarct myocardium compared to KO hearts with innervated infarct/peri-infarct tissue (Figure 6D). Sham animal of both genotypes, however, had a similar number of PVCs (HET vs. KO; Base: 1.00±.71 vs. 1.33±.88, Iso: 1.75±.48 vs. 1.33±.33). As expected, administration of propranolol prevented ISO-induced PVCs in MI hearts, confirming the role of β-AR (Figure 6D). Importantly, Ca^{2+} mapping revealed that the Ca^{2+} elevation triggered by ISO was associated with PVCs arising from the infarct region (Figure 6C). Thus, denervation induced β-AR super-sensitivity leads to diastolic Ca^{2+} elevation near the infarct that is sufficient to trigger PVCs. Restoration of sympathetic innervation to the infarct and surrounding tissue normalizes Ca^{2+} handling and makes hearts resistant to ISO-induced arrhythmias (Figure 6D).

V. Discussion

Our data provide an important validation of the hypothesis that targeting PTPσ can promote nerve regeneration through CSPG-containing scars *in vivo*, and confirm the efficacy of the therapeutic peptide ISP(Lang and et al., 2013). Myocardial infarction is an ideal system to test therapeutics targeted to PTPσ because the cardiac scar contains high levels of NGF and simply removing PTPσ is sufficient to promote robust regeneration into the scar (Gardner and Habecker, 2013). In complex situations like spinal cord injury where many types of neurons are damaged and growth factor expression is low, it is likely that robust axon regeneration through the scar will require targeting PTPσ and other inhibitors together with the addition of appropriate growth factors or bridging scaffolds (Lu and Tuszynski, 2008). Our data indicate that the peptide ISP is effective in disrupting PTPσ *in vivo* and is able to restore axon regeneration through CSPGs when appropriate growth factors are present. These data have important implications for the treatment of spinal cord injury and other peripheral nerve injuries where CSPG-PTPσ interactions prevent nerve regeneration.

Our data also have implications for patients who survive a myocardial infarction and remain at risk for severe cardiac arrhythmias and sudden cardiac death (Solomon et al., 2005). Those patients who have a left ventricular ejection fraction ≤35% often receive prophylactic implantation of an ICD (Moss et al., 2002), but low ejection fraction has not proven to be a very good predictor of

those truly in need of ICDs. This is illustrated by the 8 year follow-up study from the Multicenter Automatic Defibrillator Implantation Trial II, which found that 8 people must be implanted with ICDs to save 1 life over 8 years (Goldenberg et al., 2010). ICDs are not risk free (Atwater and Daubert, 2012), so substantial effort has gone into identifying parameters that can predict those patients most likely to benefit. Three recent trials found that sympathetic denervation within the heart after MI predicted the incidence of sudden cardiac arrest and arrhythmia independent of infarct size and left ventricular ejection fraction (Boogers et al., 2010;Nishisato et al., 2010;Fallavollita et al., 2013). Thus, testing for sympathetic denervation is now being proposed as a method for identifying patients most likely to need an ICD (Fallavollita et al., 2013).

The observation that local sympathetic denervation in the heart leads to high arrhythmia risk seems to contradict the many clinical studies showing that blocking sympathetic transmission in the heart, either with beta blockers or surgical ganglionectomy, prolongs life after MI (Nademanee et al., 2000;Lopez-Sendon et al., 2004;Exner et al., 1999;SCHWARTZ et al., 1992;Vaseghi et al., 2013). However, a consensus has developed that inappropriate heterogeneity of sympathetic transmission in the heart, and subsequent electrical remodeling of cardiac myocytes, is arrhythmogenic (Rubart and Zipes, 2005). This heterogeneity can be caused by the loss of sympathetic transmission in a portion of the heart (Boogers et al., 2010;Nishisato et al., 2010;Fallavollita et al., 2013;Vaseghi et al., 2012), or it can be caused by regional nerve sprouting and hyperinnervation (Cao et al., 2000a;Cao et al., 2000b;Hasan et al., 2006;Oh et

al., 2006;Zhou et al., 2004). In this context, surgical denervation and administration of beta blockers can be seen as methods for “evening out” sympathetic transmission across the heart by decreasing it everywhere. Our data fully support the model that heterogeneity of sympathetic transmission after MI is pathological, but our approach to correcting that problem was to restore sympathetic transmission throughout the left ventricle by targeting PTPσ. It is especially notable that we were able to restore innervation using a pharmacologic intervention begun several days after injury when the infarct and peri-infarct myocardium was denervated (Lorentz et al., 2013). Daily injections with ISP were sufficient to restore functional sympathetic innervation, and reinnervation rendered hearts surprisingly resistant to arrhythmias. Indeed, infarcted hearts with restored sympathetic innervation were electrically indistinguishable from sham hearts, despite the presence of a scar. These data raise the possibility that targeting PTPσ using a simple systemically deliverable peptide in patients who have survived a myocardial infarction might promote reinnervation of otherwise denervated cardiac tissue, and that normalizing the innervation might decrease arrhythmia risk.

VI. Figures

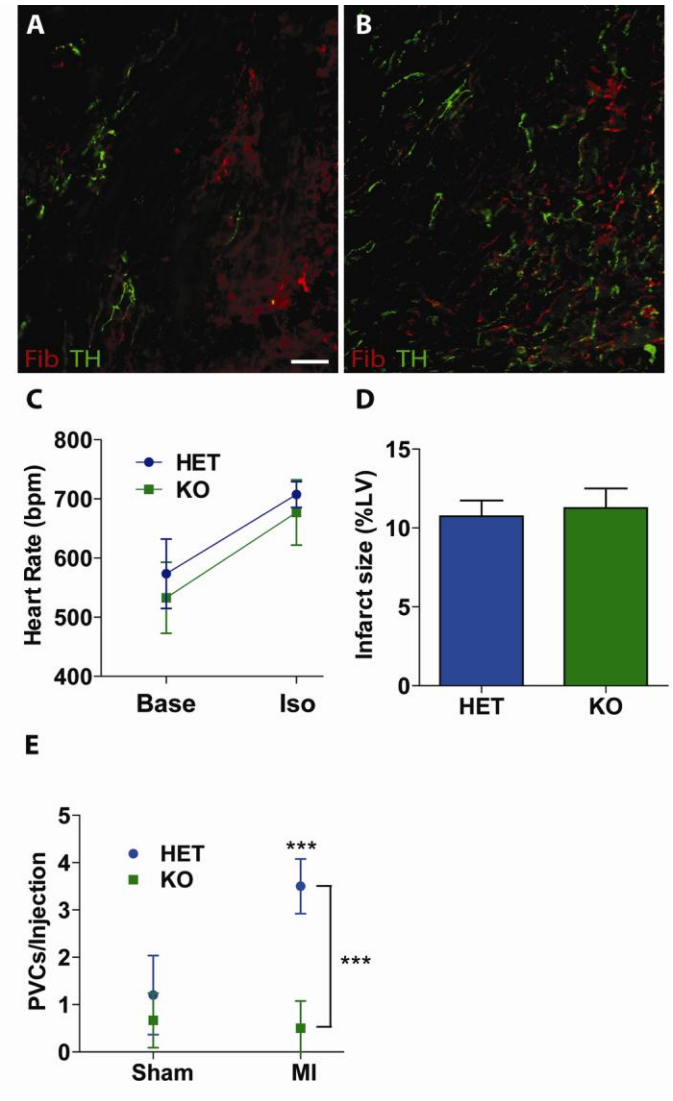

Figure 3.1) Absence of PTPσ restores sympathetic innervation to infarcted myocardium, and prevents ventricular arrhythmias. Heart sections from *ptprs+/-* **(A)** and *ptprs-/-* **(B)** mice were stained for TH (green) to identify sympathetic nerve fibers and fibrinogen (red) to identify the infarct. Scale bar, 100 µm. **(C)** Heart rate was similar in both genotypes before (Base) and after (ISO) 10µg isoproterenol injection (mean ± SEM, n=8/genotype). **(D)** Infarct size in HET and KO hearts following 35 min of occlusion (mean ± SEM, n=4/group). **(E)** Isoproterenol induced comparable levels of PVCs in conscious Sham HET and KO mice; however isoproterenol induced significantly more PVCs in infarcted HET mice compared to KO mice and to Sham HET mice (mean ± SEM, n=4/group, ***p<.001 vs. *ptprs+/-* sham and *ptprs-/-* MI).

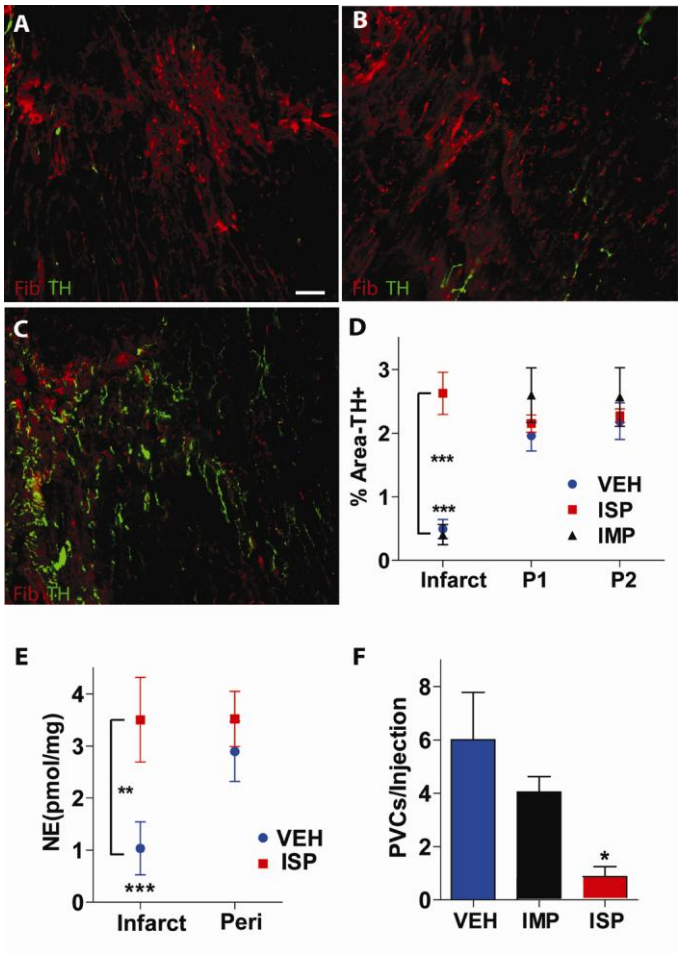

Figure 3.2) ISP injection promotes sympathetic reinnervation of the infarct and decreases arrhythmia. A-C) Representative images of infarcted LV from mice treated with vehicle **(A)**, IMP **(B)**, or ISP **(C)**. Sections were stained for TH (green) to identify sympathetic nerve fibers and fibrinogen (red) to identify the infarct. ISP treatment resulted in extensive sympathetic reinnervation of the infarct. **(D)** Quantification of TH+ fiber density within the infarct, the area immediately adjacent to the infarct (P1), and distal peri-infarct myocardium (P2; 540 □m from infarct) 14 day post-MI (mean ± SEM, n=5/group; ***p<.001). **(E)** Norepinephrine (NE) content in the infarct and peri-infarct LV (P1 and P2 combined) (mean ± SEM; n=5; ** p<.01, ***p<0.001). **(F)** Isoproterenol induced PVCs in conscious mice 14 days after MI (mean ± SEM, n=5-6; * p<.05 vs vehicle and IMP). Vehicle and IMP groups are not significantly different.

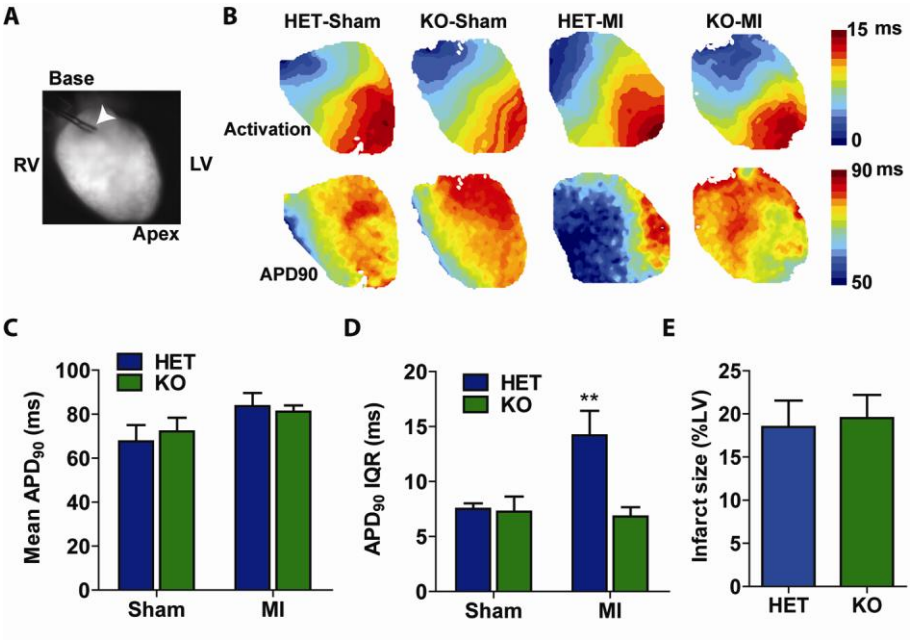

Figure 3.3) Sympathetic innervation of the infarct reduces dispersion of APD. **(A)** Image of a heart prepared for mapping. All maps are represented in this same orientation. White arrow head indicates stimulating electrodes **(B)** Activation maps of transmembrane potential (Vm) show propagation of a stimulus depolarization event spreading from base to apex of the heart (top), and representative maps of APD_{90} (bottom). **(C)** MeanAPD_{90} is similar in all groups (mean ± SEM; n=5-6 hearts/group). **(D)** Interquartile range (IQR) of APD_{90}, a measure of APD dispersion (mean ± SEM; n=5-6, * p<.05). Hearts with denervated infarcts (HET MI) have increased APD dispersion compared to sham hearts, while hearts with innervated infarcts (KO MI) do not. **(E)** Infarct size in HET and KO hearts following 45 min of occlusion (mean ± SEM, n=5/group).

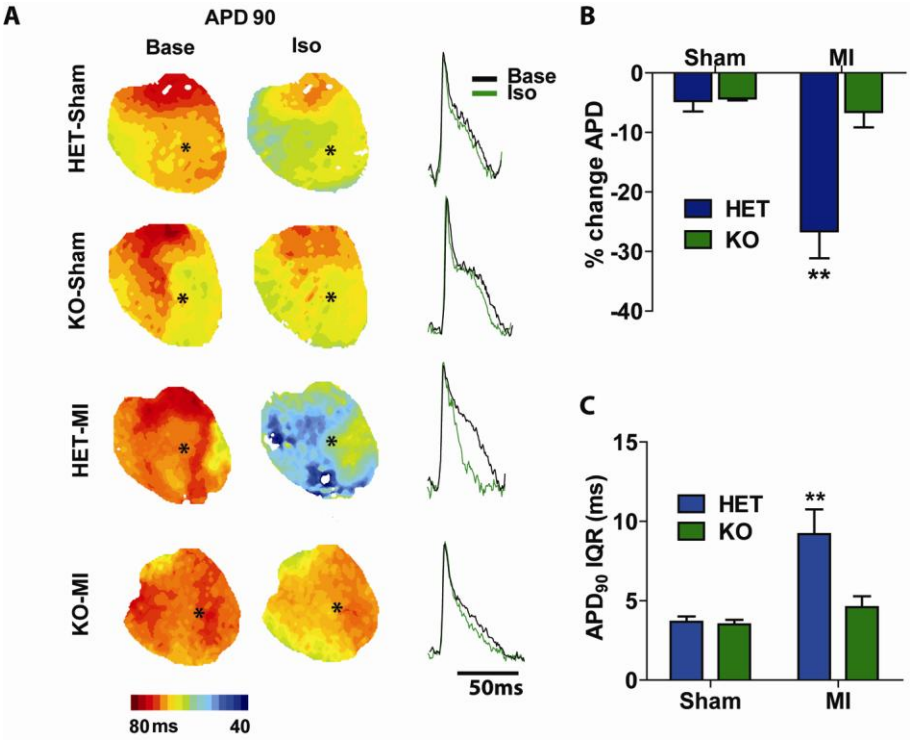

Figure 3.4) Sympathetic innervation of the infarct prevents β-AR super-sensitivity. **(A)** APD_{90} maps before (Baseline) and after 1µM isoproterenol (1µM ISO) (100 ms pacing interval, or 600 bpm heart rate), and representative traces of optical action potentials from sites marked with *. **(B)** Percent change in APD_{90} following isoproterenol (Iso) treatment (mean± SEM; n=5-6 hearts/group; ** p<.01). **(C)** IQR of APD_{90} following isoproterenol treatment (mean± SEM; n=5-6 hearts; ** p<.01).

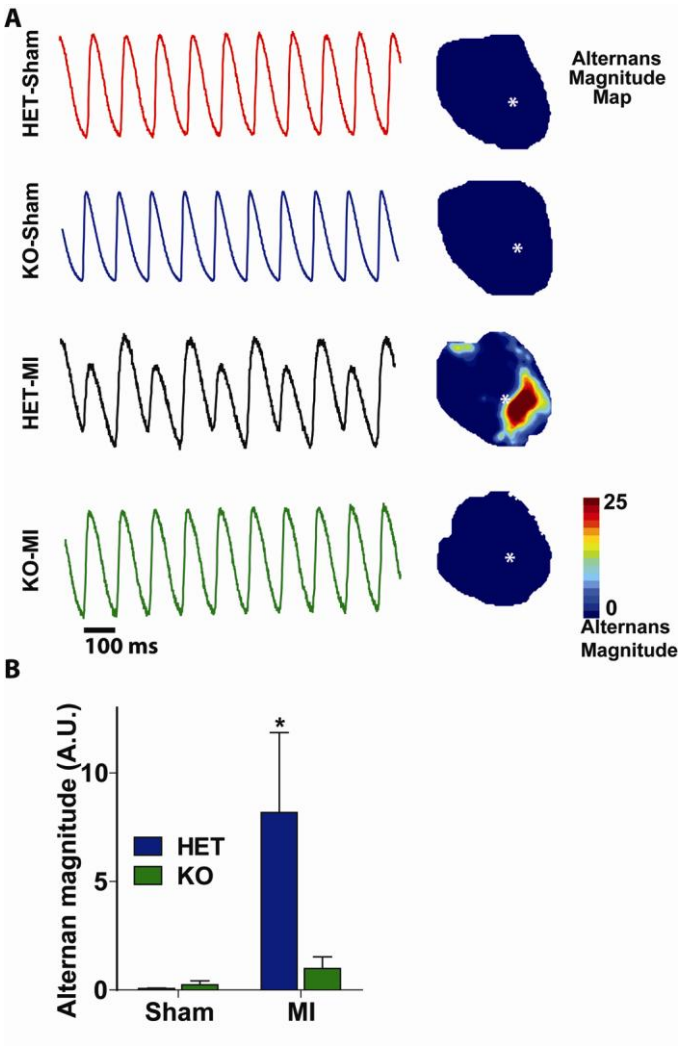

Figure 3.5) Sympathetic innervation of the infarct prevents post-MI Ca^{2+} mishandling. **(A)** Representative optical Ca^{2+} transients and alternans maps from the sites on sham and post-MI hearts marked (*) (100 ms pacing interval, or 600 bpm heart rate). Denervated hearts (HET MI) exhibit Ca^{2+} alternans, while sham hearts and infarcted hearts with sympathetic innervation of the scar (KO MI) do not. **(B)** Alternans magnitude quantified by spectral analysis (mean± SEM; n=5-6 hearts; * p<.05 vs. other groups).

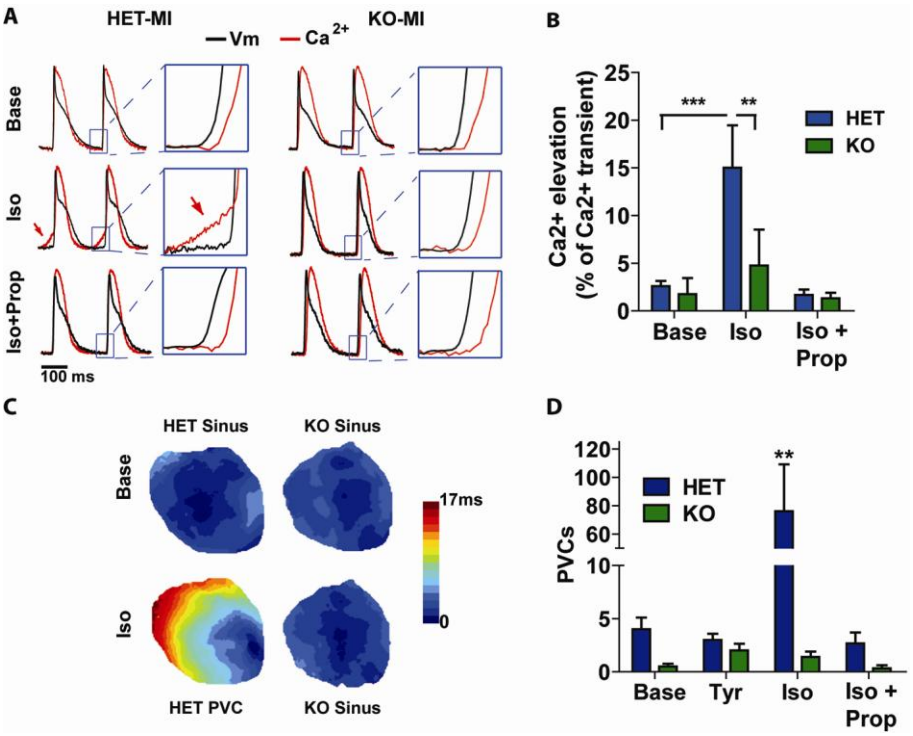

Figure 3.6) Sympathetic reinnervation of the infarct area prevents Ca^{2+} mishandling and ventricular arrhythmias. **(A)** Representative optical Ca^{2+} transients in HET and KO hearts at baseline (Base), with isoproterenol (Iso), and with both isoproterenol and propranolol (Iso+Prop). Red arrows indicate Ca^{2+} elevation prior to V_m depolarization. Insets show an expanded time scale of Vm and Ca^{2+} upstrokes **(B)** Quantification of Ca^{2+} transient that precedes depolarization averaged across the entire surface of the heart (mean± SEM; n=5-6 hearts; two-way ANOVA, ** p<.01, *** p<.001). **(C)** Representative calcium maps in HET and KO hearts depicting Ca^{2+} transients during sinus rhythm (Base) and with isoproterenol treatment (Iso). **(D)** Quantification of PVCs during baseline stimulation and treatment with tyramine (Tyr), isoproterenol (Iso) and isoproterenol plus propranolol (Iso+Prop) (mean± SEM; n=5-6 hearts; two-way ANOVA, **p<.01 vs all other groups).

Chapter 4

Summary of Results and Discussion

I. Summary of Results

Sympathetic denervation and subsequent rhythm instability is a well established consequence of myocardial infarction in humans and animal models. While heterogeneity of sympathetic transmission is thought to be a major contributor, the mechanisms of sympathetic regeneration failure and subsequent increase in arrhythmia susceptibility are largely unknown. This thesis describes the observations that 1) CSPGs are upregulated following I-R and 2) that CSPGs prevent sympathetic axon outgrowth. Additionally, the absence of the CSPG receptor, PTPσ, leads to sympathetic reinnervation of the infarct after MI, which is aided by endogenous production of NGF. Pharmacological modulation of PTPσ also restored sympathetic innervation of the infarct. Using both approaches, we observed a reduction in ventricular arrhythmias *in vivo*. Optical mapping uncovered that denervated hearts had dispersion of repolarization, β-AR super-sensitivity, baseline Ca^{2+} mishandling, and Ca^{2+} elevation in response to β-AR stimulation. These electrophysiological and Ca^{2+} abnormalities were associated with increased arrhythmia susceptibility *ex vivo*. In the absence of PTPσ, hearts were free of these abnormalities and were remarkably similar to sham hearts. This was the first time that simultaneous Ca^{2+} and voltage imaging was performed in mice after MI, and, using this technique along with *in vivo* experiments, we show that sympathetic reinnervation stabilizes injured hearts

and is protective against arrhythmias even in the presence of a scar (summarized in Figure 4.1).

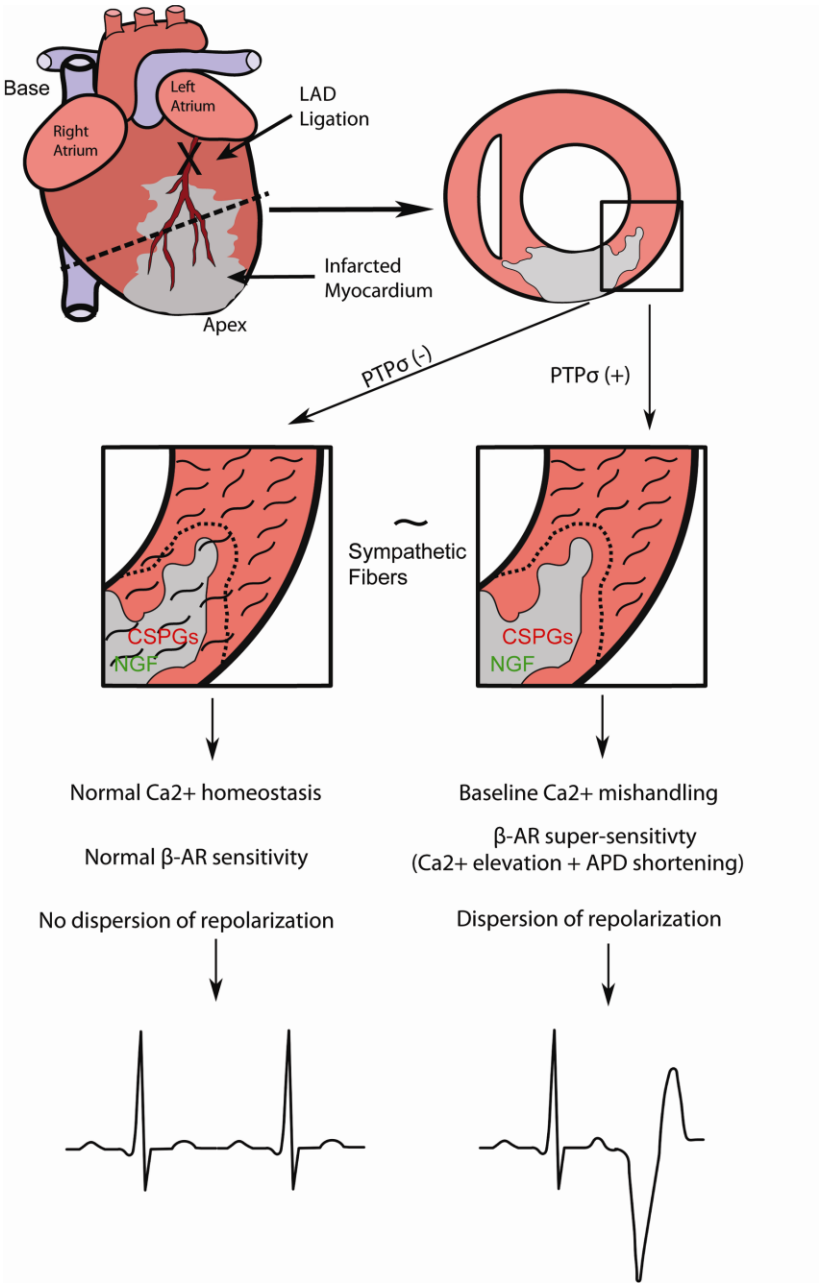

Figure 4.1) Summary of Results. I-R leads to myocardial remodeling and expression of CSPGs within the infarct. In the presence of PTPσ, CSPGs prevent sympathetic reinnervation of the infarct. This sympathetic denervation leads to Baseline Ca2+ handling abnormalities, dispersion of repolarization, and super-sensitivity to β-AR stimulation. The absence of PTPσ allows sympathetic reinnervation, aided by endogenous NGF. Restoration of sympathetic innervation to the infarct normalizes Ca2+ handling and electrophysiology.

II. Discussion

A. Sympathetic nerve regeneration after MI

The absence of sympathetic fibers in the infarct following I-R injury was surprising due to the dynamic capabilities of sympathetic nerves to regenerate, as well as the high levels of endogenous NGF in the scar. The behavior of damaged nerves and the scar were similar to that in the CNS, where production of a glial scar rich in inhibitory HA, tenascins, and CSPGs prevents axon outgrowth (Sherman and Back, 2008). Both HA and tenascin C are known components of the cardiac scar (Dobaczewski et al., 2006), which suggested that regeneration failure in the heart could be due to inhibition by the ECM. This was further supported by our observation that CSPGs were also present at the site of injury. Digestion of CSPGs *in vitro*, and loss of the receptor *in vitro* and *in vivo*, resulted in robust increases in axon extension and innervation of infarcted tissue. At the same time, both low and high molecular weight forms of HA had no effect on sympathetic outgrowth. These findings suggest that CSPGs are the primary inhibitory component of the cardiac scar.

Our data also suggest that CSPG-dependent inhibition is primarily mediated (perhaps exclusively) by PTPσ. *In vitro* outgrowth experiments in the presence of CSPGs exhibit full rescue in the absence of PTPσ. This is also supported by hyperinnervation of the scar in PTPσ KO mice; however, this is at least partially aided by increased expression of NGF. Given the discovery of alternative CSPG receptors NgR1 (Nogo receptor), NgR3 (Dickendesher et al., 2012), and LAR1 (Leukocyte Antigen-Related Tyrosine Phosphatase) (Fisher et

al., 2011), it is surprising that targeting only PTPσ fully rescues growth into the scar. It does, however, establish cardiac I-R as an optimal *in vivo* assay to determine the efficacy of PTPσ targeted therapeutics.

It is still unclear how CSPG-dependent inhibition of growth is mediated by PTPσ. While multiple signaling pathways have been described (Chagnon et al., 2010) (Faux et al., 2007), unpublished work by collaborators suggests an alternative method. Using dorsal root ganglion neurons on a CSPG-rich substrate, they found that growth cones, upon CSPG detection, lose their dynamic filopodia and become immobilized. This immobilization is due to extremely strong adhesion between CSPGs and PTPσ, which can be relieved by ChABC or ISP treatment. These results seem to contrast with the proposed mechanisms of cytoskeletal destabilization and repellant behavior of CSPGs, but do continue support for the importance of CSPG-PTPσ interaction in reduced axon outgrowth.

While CSPGs are an important component of the scar after I-R, it is still unknown what produces them. Resident cardiac fibroblasts play a critical role in tissue remodeling, as they are responsible for both break down of existing ECM and production of the scar (Porter and Turner, 2009). Fibroblasts behave similarly to reactive astrocytes of the CNS, which are responsible for producing CSPGs (Sofroniew, 2005). This similarity suggests that fibroblasts are the most likely source of CSPGs. In addition to fibroblasts, however, infiltrating monocytes express elevated mRNA for Versican (one member of the CSPG family) after MI (Toeda et al., 2005), although it is not established whether Versican is translated

or acts as an inhibitor in this context. As the remodeling process is complex and involves several cell types, it remains a possibility that the source of CSPGs is not a single cell type.

No matter the source, CSPGs are potent regulators of axon extension and guidance in both developing and adult animals (Davies et al., 1997) (Landolt et al., 1995) (McKeon et al., 1995). This suggests that CSPGs in the heart prevent sympathetic nerve regeneration after injury, rather than promoting initial denervation. However, the first observation of sympathetic fibers present in the infarct (using *ptprs-/-* mice) did not address whether these nerves were regenerating fibers or whether they were original fibers that failed to degenerate as remodeling took place. Using germ line knock outs also raised the possibility that the regenerative capabilities of nerves that developed in the absence of PTPσ were different than those from heterozygous and wild type littermates. Using a pharmacological modulator of PTPσ, we were able to address these concerns. As previously described, sympathetic denervation of the infarct is complete three days after I-R(Lorentz et al., 2013); therefore, using only wild type littermates, ISP administration began at this time. The presence of sympathetic fibers in the infarct following 10 days of ISP treatment demonstrated the ability of these fibers to regenerate and also suggested that the regeneration observed in *ptprs-/-* mice was not due to developmental compensation.

While the ability to regenerate, and the degree to which regeneration occurred by targeting only PTPσ was promising, it was not clear whether these nerves were functional. Injury and the subsequent inflammatory reaction alter the

intrinsic functional capabilities of neurons. As discussed previously, injured neurons switch roles from transmission to regeneration (Costigan et al., 2002) (Hoffman and Cleveland, 1988). This switch results in down-regulation of ion channels and enzymes involved in neurotransmitter synthesis and up-regulation of cytoskeletal machinery. For example, gp130 activation by CNTF or LIF reduces TH expression by targeting the enzyme for degradation (Shi and Habecker, 2011). Additionally, inflammation related to heart failure causes neuronal transdifferentiation, where once sympathetic fibers become biochemically parasympathetic (Kanazawa et al., 2010). With that in mind, it was unclear whether these regenerating nerves would produce normal levels of NE. However, HPLC analysis revealed that sympathetic regeneration promoted by ISP treatment restored NE content within the infarct. The innervation state of the infarct was also inversely correlated to the susceptibility of arrhythmias. In the absence of other notable anatomical or functional differences, including infarct size, the prevention of arrhythmias would suggest that these nerve fibers are functional and electrophysiologically stabilizing to their target myocytes.

B. *Sympathetic heterogeneity and arrhythmias*

Sympathetic input to the heart is a significant modulator of cardiac function. Much of this ability to control cardiac output is through modulation of ion channels involved in the cardiac AP and excitation contraction coupling. β -AR activation by NE (or epinephrine) leads to several downstream effects, including phosphorylation and enhanced activity of Na^+ (Matsuda et al., 1992), K^+ (Yue et al., 1999), and Ca^{2+} channels (Kamp and Hell, 2000) (Valdivia et al.,

1995) by PKA. α1-AR activation also leads to phosphorylation of Ca^{2+} channels by PKC (Uchi et al., 2005) (Jhun et al., 2012). Activity of these channels directly modulates excitability of cardiomyocytes and APD. Not surprisingly, alterations in sympathetic input have long been thought to play a role in the susceptibility of arrhythmias.

1. Clinical evidence and gross observations

Numerous studies in humans support the link between sympathetic input and arrhythmia risk. For example, β-AR antagonism and ganglionic blockade significantly reduces mortality in humans after MI (Nademanee et al., 2000). More recently, rhythm instability was linked specifically to heterogeneous sympathetic input (Boogers et al., 2010;Fallavollita et al., 2013;Nishisato et al., 2010), which 123I-MIBG imaging studies reveal occurs by sympathetic denervation of infarcted myocardium (Stanton et al., 1989). More detailed mapping suggests that not only is the infarct denervated, but the viable myocardium located within the border zone adjacent to the infarct is denervated as well (Vaseghi et al., 2012). The degree of overall denervation is directly correlated to the risk of developing arrhythmias and is a more sensitive predictor than infarct size or ejection fraction (Boogers et al., 2010;Fallavollita et al., 2013;Nishisato et al., 2010). While these studies identified an important clinical link between sympathetic heterogeneity and arrhythmia susceptibility they do not address the underlying mechanism.

More recent detailed electrophysiological mapping in human hearts after MI identified regional variation in repolarization that is exacerbated by adrenergic stimulation and suggests that these regional differences are tied to sympathetic innervation state (Vaseghi et al., 2012). Specifically, there is a gradient of repolarization between the infarct/border zone and innervated, viable, myocardium. This dispersion of repolarization provides a substrate that is susceptible to arrhythmias (Vaseghi et al., 2012). Our data in post-MI mice also identify baseline dispersion of APD in denervated hearts and that with sympathetic reinnervation of infarcted myocardium dispersion of APD is abolished. In addition to baseline dispersion of APD, we also identified continued dispersion with adrenergic stimulation, which is also prevented with sympathetic reinnervation of the scar. The protective effect of reinnervation is probably due to abolishing the repolarization gradient of the border zone between the scar and normal, un-injured myocardium.

2. Molecular Mechanisms

A major mediator of sympathetic input and myocardial response is activation of β-ARs by NE or epinephrine. The primary source of NE is local sympathetic neurotransmission, whereas epinephrine is produced in the adrenal medulla and released into the blood (along with a small fraction of NE). We mimicked cardiac β-AR activation by both sources using tyramine (sympathetic neurotransmission) and isoproterenol (circulating catecholamines). The striking difference in APD shortening by tyramine versus isoproterenol may highlight two subsets of β-ARs and their importance in arrhythmogenesis. Release of

endogenous NE by tyramine activates only β-ARs in proximity of sympathetic nerves. The limited but consistent response to tyramine suggests that innervated receptors, and activation of those receptors by release of NE, play a minimal role in arrhythmia susceptibility. In contrast, the large response to isoproterenol in only denervated hearts illustrates the super-sensitivity of denervated β-ARs. This suggests that stimulation of β-ARs by sympathetic nerve activity is probably not a major concern but rather activation of denervated β-ARs by circulating catecholamines is the major contributor to arrhythmogenesis. Additionally, these experiments indicate heterogeneous regulation of β-ARs or downstream β-AR effectors, which are governed directly by sympathetic innervation state (will be discussed in more detail later).

The Ca^{2+} dynamics of excitation-contraction coupling are an important effector of β-AR activation, of which we observed significant variation based on sympathetic innervation state. We observed both basal Ca^{2+} mishandling, manifested in Ca^{2+} alternans, and β-AR induced Ca^{2+} mishandling which lead to triggered ventricular activity (PVCs). The presence of Ca^{2+} alternans indicates general rhythm instability and propensity for arrhythmias (similar to dispersion of repolarization). In fact, the presence of alternans in people is a very sensitive predictor of future arrhythmias and SCD (Wita et al., 2012). Studies examining the molecular basis of Ca^{2+} alternans have identified both SERCA and RyR as major contributors. Specifically, SERCA and RyR are both reduced in alternan prone cardiomyocytes, and pharmacological inhibition of either protein is

sufficient to produce alternans in normal cells (Diaz et al., 2004;Huser et al., 2000;Wan et al., 2005).

In addition to basal Ca^{2+} alternans, we observed Ca^{2+} elevation in response to β-AR stimulation. Previous work has shown that localized NE is sufficient to cause PVCs in healthy hearts by increasing Ca^{2+} leak from intracellular stores (Myles et al., 2012). On its own, this suggests that heterogeneous sympathetic innervation and neurotransmission is sufficient to trigger ectopic, Ca^{2+}-dependent activity in the absence of any remodeling. However, we observed β-AR super-sensitivity in denervated receptors corresponding to the site of PVC origin. This suggests that sympathetic denervation induces myocyte Ca^{2+} handling changes that increase the likelihood of Ca^{2+} elevation and PVC production in response to circulating catecholamines. It is unclear what denervation-induced molecular changes underlie these changes in Ca^{2+} handling, or if they are the same changes that contribute to dispersion of repolarization. However, prior work characterizing electrical remodeling of border zone myocardium may provide clues.

While the infarct itself is the most notable region of denervation, the viable myocardium of the border zone is also denervated (Barber et al., 1983;Inoue and Zipes, 1987), and seems to play an important role in generating arrhythmias (Kramer et al., 1997;Saeki et al., 1993;Vaseghi et al., 2012). Studies of the border zone identify several changes in ion channel activity, including K^+ currents (Lue and Boyden, 1992;Jiang et al., 2000), Na+ currents (Pu and Boyden, 1997), and Ca^{2+} handling (Pu et al., 2000). Together these changes lead to APD

elongation similar to what would be expected in the absence of adrenergic stimulation. Additionally, reduced Connexin-43 expression in the border zone limits current conduction via gap junctions (Peters et al., 1997;Yao et al., 2003). Regional changes in both APD and Connexin-43 would increase the susceptibility to arrhythmias. While the border zone exhibits sympathetic denervation (Barber et al., 1983;Inoue and Zipes, 1987), these studies involve an injury paradigm that may induce electrical remodeling independent of sympathetic innervation. On the other hand, studies that manipulate sympathetic input in healthy myocardium identify similar changes in ion dynamics.

Due to the importance of sympathetic heterogeneity and arrhythmia susceptibility, several studies have attempted to characterize the electrophysiological changes brought upon by sympathetic denervation. One of the better characterized changes occurs in the transient outward K^+ current, I_{to}. I_{to} is an outward K^+ current responsible for the initial repolarization seen in phase 1 of the AP. Reduction in I_{to} is observed following ablation of neuronal catecholamine production in reserpine treated rats, which corresponded to down regulation of Kv4.2 and K4.3, two major subunits responsible for I_{to} (Bru-Mercier et al., 2003). The suppression of I_{to} has also been observed following chemical sympathetic denervation by 6-OH-dopamine (Bai et al., 2008) and during disease states where sympathetic denervation occurs, including Changes disease (Pacioretty et al., 1995) and diabetic neuropathy (Jourdon and Feuvray, 1993).

Heterogeneous reduction in I_{to} may be the link between sympathetic denervation and dispersion of APD. However, the consequences of sympathetic

denervation are not limited to I_{to}. β-AR activation of PKA and α-AR activation of PKC enhance the delayed rectifier K^+ channel subunit Kv 1.5 via phosphorylation (Yue et al., 1999), which is important for phase 3 repolarization to resting potential. In addition to K^+ channels, β-AR activation also regulates voltage gated Na+ activity and localization (Ono et al., 1993;Yarbrough et al., 2002). Phosphorylation of Nav 1.5 by PKA enhances excitability and current amplitude (Ono et al., 1993), while the α-subunit of Gs is responsible for channel localization (Yarbrough et al., 2002). Absence of adrenergic stimulation in the border zone and scar could reduce activity of both Kv 1.5 and Nav 1.5, both of which would elongate APD in denervated myocytes and create spatial heterogeneity in repolarization.

While heterogeneous voltage gated Na^+ and K^+ channel activity can result is dispersion of repolarization, we also observed significant basal and β-AR-dependent Ca^{2+} mishandling associated with increased susceptibility to arrhythmias. Interestingly, regulation of Ca^{2+} handling proteins can be directly affected by sympathetic activity. These changes include increased activity and expression of L-type Ca^{2+} channels by PKA and PKC resulting from β-AR and α-AR activation (Uchi et al., 2005;Jhun et al., 2012). Similarly, cultured cardiomyocytes lacking sympathetic innervation exhibit reduced L-type Ca^{2+} channel expression compared to innervated cells (Ogawa et al., 1992). RyR activity is also enhanced by β-AR stimulation (Valdivia et al., 1995). Heterogeneously innervated tissue could result in regional variation in these Ca^{2+} handling proteins. Regional variation in the proteins would result not only in

dispersion of repolarization, but could also explain Ca^{2+} leak due to β-AR stimulation. Alternatively, denervation-dependent electrical remodeling may not rely solely on ion channel expression.

An important regulator of β-AR activity is the G-protein receptor kinase 2 (GRK2). GRK2 is activated by PKA and acts to inhibit β-AR activity (Rockman et al., 2002). Expression and activity of GRK2 is tightly regulated by β-AR activation (Iaccarino et al., 1998), and GRK2 is down-regulated following sympathetic denervation (Yatani et al., 2006). In GRK2 KO hearts, Ca^{2+} homeostasis is significantly altered, namely by a reduction in SERCA activity and increased Na^{+}/Ca^{2+} exchange at the membrane (Raake et al., 2012). Overall, this leads to reduced sarcoplasmic Ca^{2+} load and increased cytosolic Ca^{2+} levels. Reduced sequestration of Ca^{2+} into the sarcoplasmic reticulum then increases activity of the electrogenic Na^{+}/Ca^{2+} exchanger. Increased Na^{+}/Ca^{2+} exchange, as a result of reduced GRK2, would initiate DADs and potentially trigger PVCs. GRK2 KO hearts also exhibit super-sensitivity to β-AR agonists (Raake et al., 2012), very similar to denervated hearts after MI. Overall, the electrophysiological effects associated with reduction of GRK2 are very similar to what we observe in denervated myocardium and establish it as a primary candidate for future studies.

While reduction in GRK2 appears to be a likely consequence of sympathetic denervation, perhaps the simplest explanation for denervation induced changes in AP and Ca^{2+} handling lies with altered expression of β-AR by the cardiomyocyte. Receptor expression itself is regulated by sympathetic

activity (Bahouth, 1992;Bristow et al., 1986), and could be an explanation for β-AR super-sensitivity. Specifically, β1-AR decreases during heart failure as a response to chronically elevated sympathetic nerve activity (Bristow et al., 1986), and expression increases in response to sympathetic denervation (Bahouth, 1992). Although altered β-AR expression would explain much of the denervation induced changes in cardiac AP and Ca^{2+} handling, given the broad regulation by AR activity, it remains likely that several components of ion handling and regulation are responsible for these effects. The studies described above present numerous potential targets for future characterization of electrical remodeling after MI (summarized in Table 4.1 and illustrated in Figure 4.1).

Ion Channel or Other Effector	Current or Handling Process	Increased Sympathetic Activity	Decreased Sympathetic Activity	Reference
Na_v 1.5	I_{Na}	↑ activity		Matsuda, 1992
K_v 1.5	I_{kur}		↑ expression	Mercier, 2003
		↑ activity		Yue, 1999
K_v 4.2 and 4.3	I_{to}		↓ expression	Mercier, 2003
K_v 11.1	I_{kr}	↑ activity		Heath, 2000
Ca_v 1.2	$I_{Ca,\ L}$	↑ activity		Kamp, 2000
	(L-type)		↓ expression	Ogawa, 1992
			↓ activity	Ogawa, 1992
RyR	SR Ca2+ Release	↑ activity		Valdivia, 1995
Cx43	Gap Junctions	↑ expression		Darrow, 1996
		↑ activity		Salameh, 2006
GRK2	βAR Inhibition	↑ expression		Iaccarino, 1998
			↓ expression	Yatani, 2006
β1AR			↑ expression	Bahouth, 1992
		↓ expression		Bristow, 1986

Table 4.1) Selected AP and excitation contraction components that experience regulation by altered sympathetic activity. If tied to sympathetic innervation state after MI, these changes would occur in a regionally heterogeneous pattern and could be the basis for dispersion of repolarization and βAR super-sensitivity that leads to triggered ventricular activity.

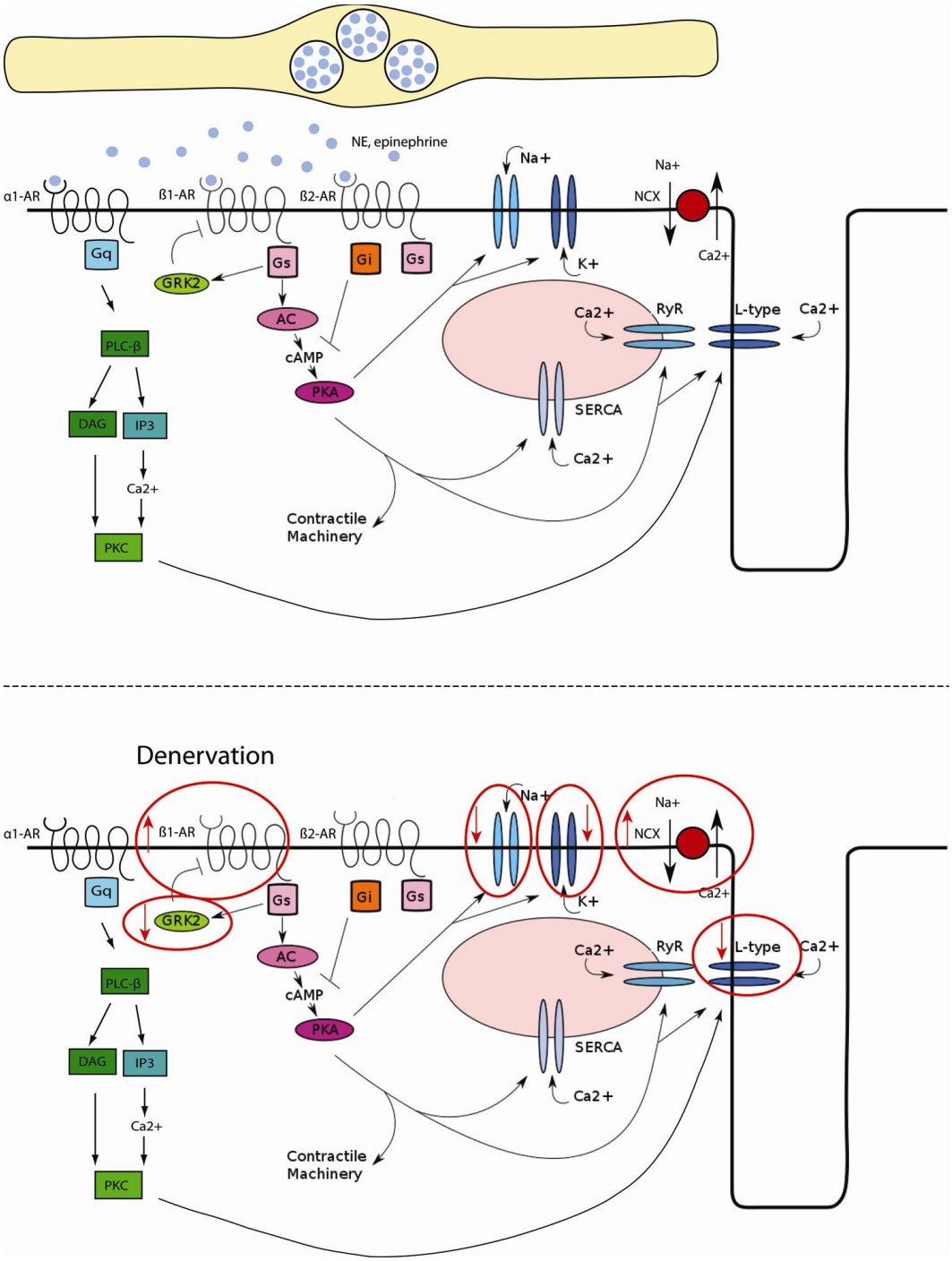

Figure 4.2) Potential denervation induced changes in excitation contraction coupling and AP regulation and how they may account for the electrophysiological remodeling we observed after MI. With the importance of βAR activity in regulation of these downstream effectors, it is not surprising that sympathetic reinnervation appears to reverse these changes.

C. Clinical considerations

1. Cardiac applications

Myocardial infarction is a common pathology in the United States (Roger et al., 2012a) and, if survived, leads to increased risk of ventricular arrhythmias and SCD (Solomon et al., 2005). The data in this thesis further support the link that sympathetic denervation after MI is a major contributor to these risks and that Ca^{2+} mishandling underlies this rhythm instability. This was the first work to show that targeting PTPσ restored sympathetic reinnervation to the scar and border zone and that this prevented abnormal heart rhythms. We also identify ISP, a novel modulator of PTPσ, to be extraordinarily effective in restoring sympathetic reinnervation.

Current treatment to prevent arrhythmias after MI often involves β-blockers and may also include placement of an ICD. Unfortunately, current risk-stratification for ICD is ineffective and is associated with incredible costs and significant side effects (Atwater and Daubert, 2012;Goldenberg et al., 2010). The development of ISP for therapeutic use in humans could transform how patients are treated after heart attacks. Restoration of sympathetic nerves could negate any reason for long term β-blocker use and could limit the use of ICDs to only extreme cases. The result could be an electrically stable heart that, following acute treatment with ISP, needs no constant medical intervention.

While rhythm instability and SCD are common secondary pathologies to I-R injury, they are not alone. The loss of functional myocytes and the production

of a non-contractile scar limit the ability of the heart to effectively eject blood (Pfeffer and Braunwald, 1990). Progressive compensatory remodeling and fibrosis cause further degeneration of cardiac function until heart failure occurs. Large animal studies (Guccione et al., 2001;Jackson et al., 2002;Wenk et al., 2011), as well as recent human studies (Wenk et al., 2012), have identified depressed contractility in the viable myocardium of the border zone as an important pathophysiological feature of this progressive remodeling into heart failure. As sympathetic activity is an important driver of cardiac contractility, restoring sympathetic innervation may protect cardiac function by maintaining high contractility at the border zone and limit the progression into heart failure.

2. Non-cardiac clinical applications

Modulation of PTPσ by genetic and pharmacological approaches has proven to be a promising therapeutic approach to restore sympathetic innervation and prevent arrhythmias. However, PTPσ is not limited to cardiac pathologies. This thesis is based upon studies of CNS injury and remodeling and subsequent axon regeneration failure. ISP itself was designed to be a therapeutic for spinal cord injury, where it has also been effective in allowing axon regeneration and restoring function in rats. Injury due to stroke may be another potential application for ISP, where much like cardiac I-R, axons are limited to the lesion penumbra by CSPGs (Leonardo et al., 2008;Soleman et al., 2012). Additionally, PTPσ has been identified in limiting oligodendrocyte differentiation and migration in MS models (Pendleton et al., 2013). With further characterization, ISP may

prove to be an effective, non-invasive therapeutic for several neuronal pathologies.

III. Limitations and Future directions

The work in this thesis supports the current hypothesis that sympathetic heterogeneity leads to ventricular arrhythmias following MI. This work also advances our understanding of the electrophysiological and Ca^{2+} homeostatic changes that underlie the increased arrhythmia susceptibility and demonstrates that these changes can be reversed by restoring sympathetic innervation. However, the work done in this thesis leaves several questions unanswered and also uncovers many more.

One of the more basic unanswered questions is what cell type produces CSPGs. The primary candidates include resident fibroblasts and infiltrating monocytes. To determine the cell type, an immunohistochemical screen could be performed by double-labeling for CSPGs and various cell type markers. An initial screen could include the pan-macrophage marker CD68 and the cardiac fibroblast marker discoidin domain receptor 2. After determining a general cell type, more specific markers can be examined. Uncovering the specific cell type could provide alternative pharmacological targets to prevent CSPG synthesis.

While the work in this thesis strongly supports CSPG-dependent axon regeneration failure, it was not tested directly *in vivo.* The presence of CSPGs within the infarct, combined with the robust increase in innervation in the absence of the CSPG receptor PTPσ, strongly indicates CSPG-dependent inhibition.

However, as noted previously, PTPσ is a known inhibitor of TrkA (Faux et al., 2007). Given the high levels of NGF in the infarct, the absence or inhibition of PTPσ could result in increased NGF/TrkA dependent axon outgrowth, completely independent of CSPG signaling. If this were the case, however, we would expect to see heightened axon extension in PTPσ KO neurons compared to wild-type neurons *in vitro*. In those experiments, we observe equal growth rates across genotype in NGF supplemented media while only neurons with PTPσ are inhibited by CSPGs (Figure 2.7). Although this suggests that reinnervation *in vivo* is independent of enhanced TrkA signaling, the question still remains untested. Viral expression of ChABC following MI in wild type animals could be used to address this directly. Any sympathetic regeneration into the infarct using this technique would be attributed to the degradation of CSPGs and would confirm their role in preventing sympathetic regeneration. Additionally, while the use of ChABC would directly assess the role of CSPGs in nerve remodeling, it may also alter myocardial remodeling and scar production. CS has been implicated as modulator of neuroinflammation and can directly inhibit cytokine production (Rolls et al., 2006). Elevated CS via CSPG degradation may dampen the inflammatory response and subsequent activation of fibroblasts and overall scar production.

The presence of sympathetic fibers with normal NE levels, in combination with electrophysiological stabilization of the heart, suggested that the regenerated fibers present in the infarct were functional. This, however, was also not directly tested. Electron microscopy could be used to assess functional

morphology, specifically whether sympathetic nerves in the infarct properly package NE. Actual NE release can be assessed by myocardial explant stimulation followed by HPLC (Hasan et al., 2012). If nerve fibers are functional, PTPσ KO infarct explants would release elevated levels of NE compared to wild type controls.

While targeting PTPσ results in clear sympathetic regeneration into border zone and infarcted myocardium, a major remaining question is how nerve fibers electrically remodel their target cardiomyocytes. There have been several studies examining the effect of sympathetic denervation on ion dynamics, including K^+, Na^+, and Ca^{2+} channel expression (Bai et al., 2008;Bru-Mercier et al., 2003;Ogawa et al., 1992). These studies, however, have only been performed in healthy hearts. In addition, there has been some characterization of electrical remodeling at the border zone in dogs, but it is unclear that these changes result from denervation. In order to understand the electrical remodeling at the border zone, further investigation is needed. Fortunately, we can now compare two distinct sympathetic innervation states to assess the role of innervation in electrical remodeling after MI.

Unfortunately, the border zone is a thin strip of myocardium located between the infarct and more distal, innervated myocardium, leaving limited tissue for analysis. Laser capture micro-dissection would allow precise collection of microscopic areas of myocardium. The limited amount of captured tissue would then be analyzed by small sample profiling RT-PCR, which requires as little as 500 pg of template. Targets of an initial RT-PCR screen would include

genes identified by denervation studies, including Kv 4.2, Kv 4.3, SERCA, RyR, L-type Ca^{2+} channels, Na+/Ca^{2+} exchanger, and Connexin-43, and would be compared to expression in PTPσ KO border zones. Following PCR analysis, notably altered targets would be assessed by IHC.

Finally, the data in this thesis describe a common injury paradigm that is remarkably protected by simply targeting PTPσ. A systemically deliverable PTPσ targeted therapeutic could change the way some spinal cord and cardiac injuries are treated. ISP has already proven to be effective *in vivo* in mice, and, while our small molecule inhibitors show potential *in vitro,* they need to be examined *in vivo.* As sympathetic nerve regeneration failure seems to require only PTPσ, I-R injury is an ideal system to test the efficacy of these drugs. Both ISP and potential small molecule inhibitors also require thorough pharmacokinetic characterization and use in larger animals.

IV. Concluding Remarks

Cumulatively, the data in this thesis contribute to our understanding of myocardial and sympathetic remodeling and the role of CSPGs in sustained sympathetic denervation following I-R injury. This work also establishes PTPσ as an important mediator of this process and a significant therapeutic target as a potential clinical approach to preventing long term sympathetic denervation. While several studies have addressed the link between this sustained denervation and arrhythmia susceptibility, the work in this thesis uncovers Ca^{2+} mishandling as an important component of this instability. This work is the first to

show that sympathetic reinnervation is protective against electrophysiological remodeling and ventricular arrhythmias even in the presence of a scar.

Chapter 5

Detailed Methods

Animals: C57BL/6J mice were obtained from Jackson Laboratories West (Sacramento, CA), and were used for all experiments except those using *ptprs* transgenic mice. *ptprs*+/- transgenic mice (BalbC background) were supplied by Michel Tremblay at McGill University (Elchebly et al., 1999), and were bred as heterozygotes. *ptprs*+/+ and *ptprs*+/- littermates were used as "wild type" controls for *ptprs*-/- studies. All mice were kept on a 12h:12h light-dark cycle with *ad libitum* access to food and water. Age and gender-matched male and female mice 12-18 weeks old were used for surgeries, while ganglia from male and female neonatal mice were used for explants and dissociated cultures. All procedures were approved by the OHSU Institutional Animal Care and Use Committee and comply with the Guide for the Care and Use of Laboratory Animals published by the National Academies Press (8th edition).

Dissociated primary sympathetic neuron culture with CSPG (chondroitin sulfate proteoglycan) and HA (hyaluronan) treatment: Cultures of sympathetic neurons were prepared from superior cervical ganglia (SCG) of newborn mice as described (Dziennis and Habecker, 2003). Neurons were plated onto poly-L-lysine (PLL, 0.01%, Sigma-Aldrich) and collagen (10 µg/mL, BD Biosciences) coated plates, and grown in serum free C2 medium (Lein et al., 1995;Pellegrino et al., 2011) supplemented with 50 ng/mL NGF (BD Biosciences), 100 U/mL penicillin G, and 100 µg/mL streptomycin sulfate (Invitrogen). Cells were

incubated at 37° C in a humidified 5% CO_2 incubator. Cells were maintained for 48 hrs in the presence of the anti-mitotic agent cytosine arabinoside (Ara C, 1 μM) to reduce the number of non-neuronal cells. CSPG treatments were carried out using soluble or fixed CSPGs (Millipore #CC117; mixture includes neurocan, phosphacan, versican, and aggrecan). HA treatments were similarly carried out, using mixed molecular weight HA (MP biomedicals) for soluble treatments. For fixed treatments, high molecular weight (HMW) HA (Lifecore Biomedical) was degraded using bovine testes hyaluronidase (Sigma) to produce low molecular weight (LMW) HA (Generously provided by Dr. Stephen Back, OHSU) 1) Soluble: Neurons were grown in 48-well plates coated with PLL and collagen. Vehicle (media), CSPGs (10 ng/ml-20 μg/ml), or HA (10 ng/ml-100 μg/ml) were added to the cultures 24 hrs after plating, and 24 hours after addition of CSPGs, HA, or vehicle, images were acquired for Sholl analysis. 2) Fixed: Plates were coated with PLL/collagen, PLL/collagen/CSPGs (100 ng/mL – 1 μg/mL), or PLL/collagen/HA (100 ng/mL – 1 μg/mL; low and high molecular weight) prior to addition of neurons. Images were acquired for Sholl analysis 24 hours after plating. For CSPG degradation experiments, Chondroitinase ABC (ChABC, 4 μU/mL; Seikagaku Biobusiness Corporation) was added to culture media at the time of plating.

Sholl analysis: To quantify neurite outgrowth in dissociated neurons, the Sholl method was used (SHOLL, 1953). A series of concentric circles were superimposed over the cell body using Image J, and neurite intersections with

the circles were counted. The number of intersections provides an estimate of neurite length and/or increased branching.

Compartmentalized cultures. To generate micro-fluidic chambers providing separation of two media compartments (450µm apart), SYLGARD 184 silicone elastomer (Dow Corning) was poured into a pre-cast mold, and heated at 50-60° C for 2 hours. Cleaned chambers were placed in 10 cm culture dishes (Corning) pre-coated with 0.01% PLL. The axonal compartment was then coated with 10 µg/mL collagen or collagen + 1 µg/mL CSPGs. SCG were placed in reduced growth factor Matrigel (BD Bioscience) within the cell body compartment. C2 media supplemented with 10 ng/mL NGF was added to both compartments, and cultures were maintained at 37° C in a humidified 5% CO_2 incubator. After 24 hrs, or when axons were first visible in the axonal compartment, images were acquired (t=0). Additional images were obtained 3 hours later (t=3), and a growth rate was calculated based on the distance extended during that 3 hour period.

Small molecule PTPσ inhibitor tests: Novel small molecule PTPσ inhibitors were generated by Dr. Michael Cohen (OHSU), and were tested using two methods: **1)** dissociated SCG neurons, and **2)** whole SCGs in microfluidic chambers. **1)** Neonatal SCGs were dissociated as described above, plated at low density in 48 well plates coated with either PLL/collagen or CSPGs (1 µg/mL), and grown in serum free C2 medium containing 10 ng/mL NGF. At the time of plating, media

contained either vehicle, or one of three prospective small molecule PTPσ inhibitors, and a negative control to which the experimenter was blinded, all of which were tested at three concentrations (100nM, 1µM, or 10 µM). Following 48 hours in culture, images were taken and axon outgrowth was assessed by measuring axon length. **2)** Compartmentalized microfluidic chambers were prepared as described above. The SCG was plated in the cell body compartment using matrigel, and the axonal compartment was coated with either PLL/collagen, or CSPGs (1 µg/mL). Both compartments were then bathed in C2 media containing 10ng/mL NGF. The axonal compartment media also contained either vehicle or prospective inhibitor MC-78. After 24 hrs, or when axons were first visible in the axonal compartment, images were acquired. Additional images were obtained 3 hours later, and a growth rate was calculated based on the distance extended during that 3 hour period.

Dissociated primary cerebellar neurons for Click Chemistry: Identification of MC-78 target by click chemistry was done using cerebellar granule neurons. Cerebella were dissected from isoflurane anesthetized mice following decapitation. Tissue was minced and added to an HBSS-CM solution (1 mM Na^+ pyruvate, 10mM HEPES, 3mg/mL BSA, and 1.2mM $MgSO_4$) supplemented with Trypsin (0.2%) and DNAse I (80 µg/ml) and stirred for 15 mins at 37°C. Fresh HBSS-CM supplemented with SBTI (.1%) and DNAse 1 (80 µg/ml) was added to the trypsinized tissue and centrifuged at a low speed for approximately 1 min to pellet tissue. Supernatant was removed and replaced with fresh HBSS-

CM/SBTI/DNAse 1 solution then passed through a 22 gauge needle 10x. The homogenate was then centrifuged at 1000 x g for 5 mins. The supernatant was removed and replaced with plating media (Neurobasal, B27 supplement, 25.4 mM KCl, 0.5 mM L-Glutamine, 0.1% Gentamicin, 10% FBS, and 10% horse serum). Cells were counted using a hemocytometer, and 1,000,000 cells were added to each well.

Click reaction: The prospective inhibitor MC-78 was modified to contain a "clickable" alkyne group (MC-78*). Dissociated cerebellar granule neurons were plated as described above in a 12 well plate coated with PLL/collagen and cultured for 48 hours, then treated with either vehicle (DMSO) or 100nM MC-78* for 1 hr. Neurons were then lysed in .1% SDS/PBS containing a protease inhibitor cocktail (Roche). Lysate was added to click reagents (final concentration) biotin-azide (100 µM), tris[(1-benzyl-1*H*-1,2,3-triazol-4-yl)methyl]amine (TBTA; 100 µM), $CuSO_4$ (1 mM), and tris(2-carboxyethyl)phosphine (TCEP; 1mM), and rotated at room temperature for 1 hr. The presence of biotinylated protein was then assessed by western blot.

Western Blot Analysis: Neuronal lysates were collected as described above. Lysate was added to 4x XT Sample Buffer and 20x XT Reducing Agent (Biorad) and let sit at room temperature for 10 min. Samples were then size fractionated using 4-12% bis-tris gels (Biorad) and transferred to nitrocellulose membranes. Membranes were blocked in 5% milk/ TBST for 1 hr at room temperature, followed by the addition of streptavidin-horseradish peroxidase (1:5000) for 1 hr at room temperature. Membranes were subsequently washed in TBST 3x10

min. Biotin-streptavidin interaction was visualized by chemiluminescence (Super Signal Dura, Pierce) and imaged using a Biorad ChemiDoc system.

Myocardial infarction surgery: *Myocardial ischemia-reperfusion:* Anesthesia was induced with 4% isoflurane and maintained with 2% isoflurane. The left anterior descending coronary artery (LAD) was reversibly ligated for 30 min and then reperfused by release of the ligature. Occlusion was confirmed by sustained S-T wave elevation and regional cyanosis. Reperfusion was confirmed by the return of color to the ventricle distal to the ligation and reperfusion arrhythmia. Core body temperature was monitored by a rectal probe and maintained at 37°C, and a two-lead electrocardiogram was monitored. *Myocardial ischemia:* Chronic ischemia was done in exactly the same manner as described above, but with permanent occlusion of the LAD using 8-0 gauge suture. *Sham surgery:* Sham animals underwent the procedure described above, except for the LAD ligature.

Heart/ganglia co-cultures: Co-culture experiments were carried out in 24 well plates by plating pieces of infarcted left ventricle (LV) or corresponding sham tissue, collected 10 days after surgery, with neonatal SCGs. Tissues were plated in 30 µL of reduced growth factor Matrigel, separated by approximately 1mm, and placed at 37 ºC to solidify the Matrigel before addition of C2 media supplemented with 2 ng/mL NGF. Co-cultures were incubated at 37°C in a humidified 5% CO_2 incubator for 48 hours. Following 48 hours in culture, images of the cultures were acquired using phase contrast microscopy (10X) and axon

length was analyzed using Nikon Elements. For ChABC experiments, tissue from a single heart was split between the vehicle and ChABC treatment groups to promote consistency. Co-cultures were treated from the time of plating with ChABC (4 µU/mL) diluted in culture media, or media alone. For co-cultures examining the role of the CSPG receptor PTPRS, SCG were dissected from an entire litter of neonatal mice containing the range of PTPRS genotypes (*ptprs+/+, ptprs+/-, ptprs-/-*). The two ganglia from an individual mouse were divided so that one SCG was cultured with a sham explant and one with an infarct explant. Following 48 hours in culture, images were acquired using phase contrast microscopy (10X) and axon length was analyzed using Nikon Elements. Genotyping was completed after image acquisition and analysis so that the experiment was blinded.

Co-Culture axon length analysis: Axon length was measured on three cardinal sides of each ganglion (0, 90, and 180 degrees). Growth toward the myocardium was designated 0º, growth perpendicular was 90º and growth away from the myocardium was 180º. In order to normalize for inter-well variability of growth, a ratio of these measures was used (0/90 or 0/180). Values for the 0/90 or 0/180 ratio near 1 indicated growth was similar in all directions. In contrast, ratios significantly less than 1 reflected significantly shorter axons on the side of the ganglion projecting toward the heart explant.

Immunohistochemistry: Hearts were fixed for 1 hr in 4% paraformaldehyde, rinsed in phosphate buffered saline (PBS), cryoprotected in 30% sucrose overnight, and frozen in mounting medium for sectioning. Transverse 10 µm sections were cut on a cryostat and thaw mounted onto charged slides. To reduce fixative-induced autofluorescence, sections were rinsed in 10 mg/mL sodium borohydride 3X10 min and then rinsed in PBS 3X10 min. Sections were then blocked in 3% B.S.A/ 0.3% Triton X-100 in PBS for 1 hr. Slides were then incubated with rabbit anti-TH (1:1000, Millipore/Chemicon) and mouse anti-chondroitin sulfate (1:300, Sigma CS-56) or sheep anti-fibrinogen (1:500, AbD Serotec) antibodies overnight at 4ºC, rinsed 3x10 min in PBS, and incubated 1.5 hr with the AlexaFluor 488-conjugated rabbit IgG-specific antibody (1:1000; Invitrogen) and AlexaFluor 568-conjugated mouse IgG-specific antibody (1:500) or AlexaFluor 568-conjugated sheep IgG-specific antibody (1:1000). Due to non-specific binding of AlexaFluor 568-conjugated mouse IgG, anti-mouse IgG was added to the blocking solution to prevent non-specific secondary binding. Sections were rinsed 3x10 min in PBS, incubated for 30 min in $CuSO_4$ in 50 mM ammonium acetate to reduce background signal further, rinsed 3x10 min in PBS, coverslipped in a 1:1 PBS:glycerol solution and visualized by fluorescence microscopy.

Co-cultures were fixed for 15 min in 4% paraformaldehyde and rinsed in PBS 3x10 minutes. The tissue was blocked in 3% B.S.A/ 0.3% Triton X-100 in PBS for 1 hr, then incubated with rabbit anti-TH (1:1000) overnight at 4ºC. Tissue was rinsed with PBS and incubated for 1.5 hours with the AlexaFluor 488-conjugated

rabbit IgG-specific antibody (1:1000), rinsed again in PBS and imaged using fluorescence microscopy.

Imaging and Threshold Analysis: TH staining was quantified to assess sympathetic innervation density. Images were taken with a 20x objective using a Zeiss Axiophot II fluorescent microscope. The infarct was identified by positive fibrinogen immunostaining, and peri-infarct was defined as the area adjacent to fibrinogen-positive tissue within one field of view (710 µm x 530 µm). Images of the infarct and peri-infarct were acquired from 3 level-matched sections ranging from the base to apex of each heart. Black and white images were adjusted using the brightness/contrast tool in Image J to set the minimum brightness at the left side of the histogram. The threshold tool was then used to identify TH-positive nerve fibers. The threshold was manually adjusted so that only nerve fibers were identified, and innervation density was calculated based on the percent field of view above the threshold (Lorentz et al., 2010).

Infarct size: Infarct size was quantified in three 10 µm sections from each heart. Images were taken of the entire section, and the LV and infarct areas were measured by outlining the respective regions using the freehand selection tool in ImageJ. Infarct size was then calculated as a percentage of LV area [(infarct area/LV area) x100]. Sections were obtained from the upper, middle, and lower regions of the infarct in each heart.

ECG Telemetry Recordings and Analysis: ECGs were obtained from conscious adult mice using ETA-F10 (Data Sciences International [DSI]) telemetry implants, and were analyzed with Dataquest ART software (DSI). Mice were anaesthetized with 4% inhaled isoflurane and maintained on 2% inhaled isoflurane. A transmitter was implanted subcutaneously in a lead II configuration, with the negative lead placed in the right pectoral muscle and the positive lead to the left of the xyphoid process. Animals were allowed to recover for a week before undergoing MI or sham procedures. ECG recordings were obtained 10 (PTPσ transgenic studies) or 14 (ISP studies) days after sham or MI surgery. The number of premature ventricular complexes (PVCs) was quantified 60 min prior to intraperitoneal (IP) injection of the β-AR agonist isoproterenol (ISO; 10 µg) as a baseline, and then for 60 min after injection to identify isoproterenol-induced PVCs. PVCs were defined as a single premature QRS complex in the absence of a P-wave. Heart rate was also analyzed to confirm that the SA node response to isoproterenol was similar between groups.

NE analysis by HPLC: Frozen, pulverized tissue was weighed, then homogenized in 0.2 M perchloric acid (PCA) containing 0.5 µM dihydroxybenzylamine (DHBA) to correct for sample recovery. The tissue was refrigerated for 1 hour and centrifuged at 14,000 rpm for 4 min. Supernatant was adsorbed onto alumina, followed by 15 min of tumbling. The alumina was washed twice with 1.0 mL of H_2O with centrifugations in between. The NE was desorbed from the alumina with 150 µL of 0.1 M PCA. Aliquots (70 µL) analyzed

by HPLC for NE and DHBA levels. NE standards (0.5 µM) were processed in parallel with tissue samples and interspersed throughout the HPLC run. Retention time for NE was 5.0 min and for DHBA was 8.5 min. To calculate NE content, the area under the NE and DHBA curves was measured using LCsolution post-run analysis software. A ratio of NE area/DHBA area was calculated for each sample and standard trace, which corrects for sample recovery. The sample ratio was then divided by the standard ratio to determine the relative sample amplitude. The relative value was then multiplied by a correction factor that includes the weight of tissue, the fraction of the homogenate used in the assay, and the amount of NE in the standard [(Total homogenate vol / assayed vol) x Amount of NE in standard / starting weight of tissue] to obtain NE content/mg tissue.

Langendorff Perfusion for Optical Mapping: Mice were anesthetized with pentobarbital sodium (150 mg/kg, IP) containing 500 IU/kg of heparin. Following a midsternal incision, hearts were rapidly excised and Langendorff perfused at 37ºC with oxygenated (95% O_2, 5% CO_2) modified Tyrode's solution of the following composition (in mmol/L): NaCl 128.2, $CaCl_2$ 1.3, KCl 4.7, $MgCl_2$ 1.05, NaH_2PO_4 1.19, $NaHCO_3$ 20 and glucose 11.1 (pH 7.4). Flow rate (1.5-3.5 mL/min) was adjusted to maintain a perfusion pressure of 60-80mmHg. One leaflet of the mitral valve was carefully damaged with sharp forceps inserted through the pulmonary vein to prevent solution congestion in the left ventricular (LV) cavity after suppression of ventricular contraction. Two Ag/AgCl disc

electrodes were positioned in the bath to record an ECG analogous to a lead I configuration. ECG was continuously recorded throughout the duration of the experiment. A bipolar electrode was positioned on the base of the LV epicardium for pacing, which was performed at a basic cycle length (BCL) of 150 ms using a 2 ms pulse width at twice the diastolic threshold.

Dual optical mapping of V_m and Ca^{2+}: Hearts were loaded with the fluorescent intracellular Ca^{2+} indicator Rhod-2 AM (Molecular Probes, Eugene, OR; 50 µL of 1 mg/mL in dimethyl sulfoxide [DMSO] containing 10% pluronic acid) and were subsequently stained with the voltage-sensitive dye RH237 (Molecular Probes; 10 µL of 1 mg/mL in DMSO). Blebbistatin (Tocris Bioscience, Ellisville, MO; 10-20 µM) was added to the perfusate to eliminate motion artifact during optical recordings. The anterior epicardial surface was excited using LED light sources centered at 530 nm and bandpass filtered from 511-551 nm (LEX-2, SciMedia, Costa Mesa, CA) and focused directly on the surface of the preparation. The emitted fluorescence was collected through a 50mm objective (Nikon, Japan) and split with a dichroic mirror at 630nm (Omega, Brattleboro, VT). The longer wavelength moiety, containing the V_m signal, was longpass filtered at 700 nm and the shorter wavelength moiety, containing the Ca^{2+} signal, was bandpass filtered between 574-606nm. The emitted fluorescence signals were recorded using two CMOS cameras (MiCam Ultima-L, SciMedia, Costa Mesa, CA) with a sampling rate of 1 kHz and 100x100 pixels with a 10x10 mm field of view.

Experimental protocol: Following dye loading, baseline electrophysiological parameters were recorded during normal sinus rhythm as well as LV epicardial pacing at BCL of 150, 100 and 90 ms. Hearts were subjected to tyramine infusion (20 μM) followed by a washout period. Hearts were then subjected to acute β-AR stimulation with ISO (1 μM). Optical recordings were taken every 5 min following treatment and ECG was continuously recorded. Following 15 min of ISO treatment, the β-AR blocker propranolol (10 μM), was added to the perfusate. Optical recordings were repeated every 5 min for 15 min.

Optical mapping data analysis: Optical mapping data analysis was performed using two commercially available analysis programs (BV_Analyze, Brainvision, Tokyo, Japan; and Optiq, Cairn, UK). V_m and Ca^{2+} datasets were spatially aligned and processed with a Gaussian spatial filter (radius 3 pixels). For both action potentials (AP) and Ca^{2+} transients (Ca_T), activation time was determined as the time at 50% of the maximal amplitude. For APs, repolarization time at 90% return to baseline was used to calculate action potential duration (APD_{90}). Diastolic Ca^{2+} elevation was measured as the percentage of diastolic Ca^{2+} increase relative to the following Ca_T amplitude at baseline and 15 min post-treatment. The average diastolic Ca^{2+} elevation was calculated for each heart by averaging all Ca^{2+} signals from the entire anterior surface of the heart within the optical mapping field of view. PVC incidence was determined from the continuous ECG recording as the number of PVCs that occurred during a 15 min

period of baseline activity (before initiation of treatment) and during the 15 min of treatment.

The spectral method, which has been used clinically for detecting micro-volt T-wave alternans (Verrier et al., 2011), was used to detect the presence of Ca_T alternans as previously described (Myles et al., 2011). The spectral method was chosen due to its high sensitivity and relative immunity to noise. This approach allowed us to determine if an area within the mapping field of view was experiencing significant APD or Ca_T alternans (greater than the background noise levels) as well as the spatial extent of significant alternans. A spectral magnitude of ≥ 2 was used as the minimum threshold for significant Ca_T alternans, corresponding to a beat-to-beat change in Ca_T amplitude ≥5%, respectively.

Statistics: Student's t-test was used for comparisons of just two samples. Data with more than two groups were analyzed by one-way ANOVA using the Tukey post-hoc test to compare all conditions. For experiments comparing different surgical groups and a second variable (±NGF antibody, PTPRS genotype) two-way ANOVA was carried out using the Bonferroni post-hoc test. All statistical analyses were carried out using Prism 5.0.

Chapter 6: Appendices

Appendix A:

Small molecule PTPσ inhibitor tests: Novel small molecule PTPσ inhibitors were generated by Dr. Michael Cohen (OHSU), and were tested using two methods: **1)** dissociated SCG neurons, and **2)** whole SCGs in microfluidic chambers. **1)** Neonatal SCGs were dissociated as described in the methods chapter, plated at low density in 48 well plates coated with either PLL/collagen or CSPGs (1 µg/mL), and grown in serum free C2 medium containing 10 ng/mL NGF. At the time of plating, media contained either vehicle, or one of three prospective small molecule PTPσ inhibitors (01-78, 02-113, 03-02), and a negative control to which the experimenter was blinded, all of which were tested at three concentrations (100nM, 1µM, or 10 µM). Following 48 hours in culture, images were taken and axon outgrowth was assessed by measuring axon length. **2)** Compartmentalized microfluidic chambers were prepared as described in the methods chapter. The SCG was plated in the cell body compartment using matrigel, and the axonal compartment was coated with either PLL/collagen, or CSPGs (1 µg/mL). Both compartments were then bathed in C2 media containing 10ng/mL NGF. The axonal compartment media also contained either vehicle or prospective inhibitor 01-78 or 02-113. After 24 hrs, or when axons were first visible in the axonal compartment, images were acquired. Additional images were obtained 3 hours later, and a growth rate was calculated based on the distance extended during that 3 hour period.

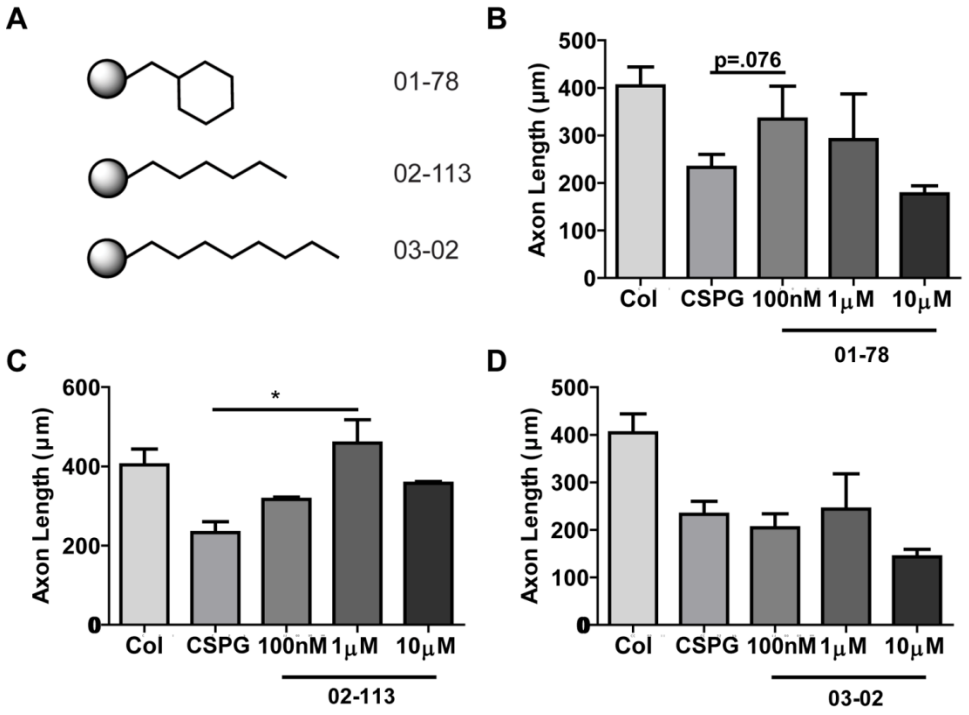

Figure A.1: Novel small molecules inhibitors of PTPσ overcome CSPG-dependent inhibition of dissociated sympathetic neurons (A) Representations of the prospective small molecule PTPσ inhibitors. The grey circle represents a conserved core motif. Quantification of dissociated sympathetic axon length in wells coated with collagen (Col), CSPGs, or CSPGs + 01-78 (B), 02-113 (C), or 03-02 (D) at either 100nM, 1µM, or 10µM . Mean±SEM (n=10-15 neurons), *p<0.05. Representative of 3 experiments.

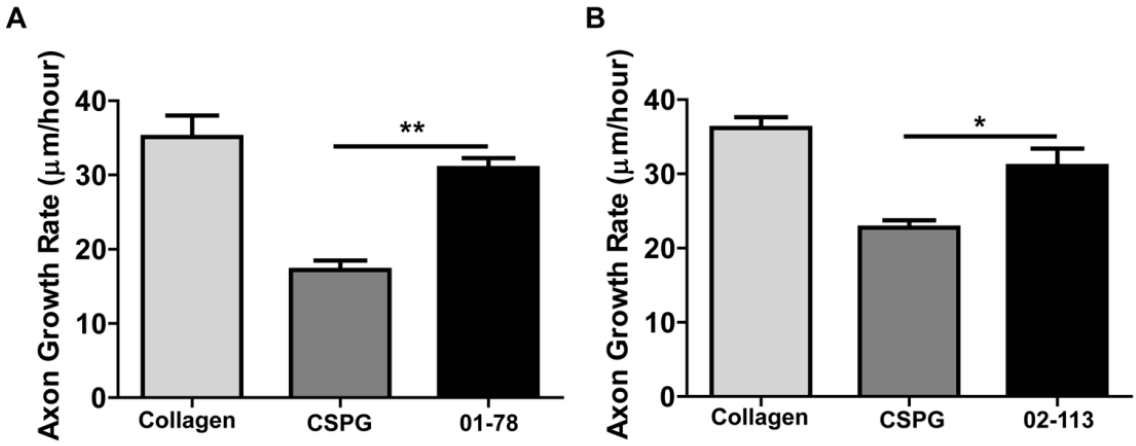

Figure A.2. Novel small molecules inhibitors of PTPσ overcome CSPG-dependent inhibition of sympathetic neurons in microfluidic chambers. Quantification of sympathetic axon growth in microfluidic chambers coated with collagen (Col), CSPGs, or CSPGs + 1 µM 01-78 (A) or 02-113 (B). Mean±SEM (n=3-4 explants; 6-8 axons/explant), *p<0.05, **p<.01. Representative of 3 experiments.

Appendix B:

Dissociated primary cerebellar neurons for Click Chemistry: Identification of the 01-78 target by click chemistry was done using cerebellar granule neurons. Cerebella were dissected from isoflurane anesthetized mice following decapitation. Tissue was minced and added to an HBSS-CM solution (1 mM Na^+ pyruvate, 10mM HEPES, 3mg/mL BSA, and 1.2mM $MgSO_4$) supplemented with Trypsin (0.2%) and DNAse I (80 µg/ml) and stirred for 15 mins at 37°C. Fresh HBSS-CM supplemented with SBTI (.1%) and DNAse 1 (80 µg/ml) was added to the trypsinized tissue and centrifuged at a low speed for approximately 1 min to pellet tissue. Supernatant was removed and replaced with fresh HBSS-CM/SBTI/DNAse 1 solution then passed through a 22 gauge needle 10x. The homogenate was then centrifuged at 1000 x g for 5 mins. The supernatant was removed and replaced with plating media (Neurobasal, B27 supplement, 25.4 mM KCl, 0.5 mM L-Glutamine, 0.1% Gentamicin, 10% FBS, and 10% horse serum). Cells were counted using a hemocytometer, and 1,000,000 cells were added to each well.

Click reaction: The prospective inhibitor 01-78 was modified to contain a "clickable" alkyne group (01-78*). Dissociated cerebellar granule neurons were plated as described above in a 12 well plate coated with PLL/collagen and cultured for 48 hours, then treated with either vehicle (DMSO) or 100nM MC-78* for 1 hr. Neurons were then lysed in .1% SDS/PBS containing a protease inhibitor cocktail (Roche). Lysate was added to click reagents (final concentration) biotin-azide (100 µM), tris[(1-benzyl-1*H*-1,2,3-triazol-4-

yl)methyl]amine (TBTA; 100 µM), $CuSO_4$ (1 mM), and tris(2-carboxyethyl)phosphine (TCEP; 1mM), and rotated at room temperature for 1 hr. The presence of biotinylated protein was then assessed by western blot.

Western Blot Analysis: Neuronal lysates were collected as described above. Lysate was added to 4x XT Sample Buffer and 20x XT Reducing Agent (Biorad) and let sit at room temperature for 10 min. Samples were then size fractionated using 4-12% bis-tris gels (Biorad) and transferred to nitrocellulose membranes. Membranes were blocked in 5% milk/ TBST for 1 hr at room temperature, followed by the addition of streptavidin-horseradish peroxidase (1:5000) for 1 hr at room temperature. Membranes were subsequently washed in TBST 3x10 min. Biotin-streptavidin interaction was visualized by chemiluminescence (Super Signal Dura, Pierce) and imaged using a Biorad ChemiDoc system.

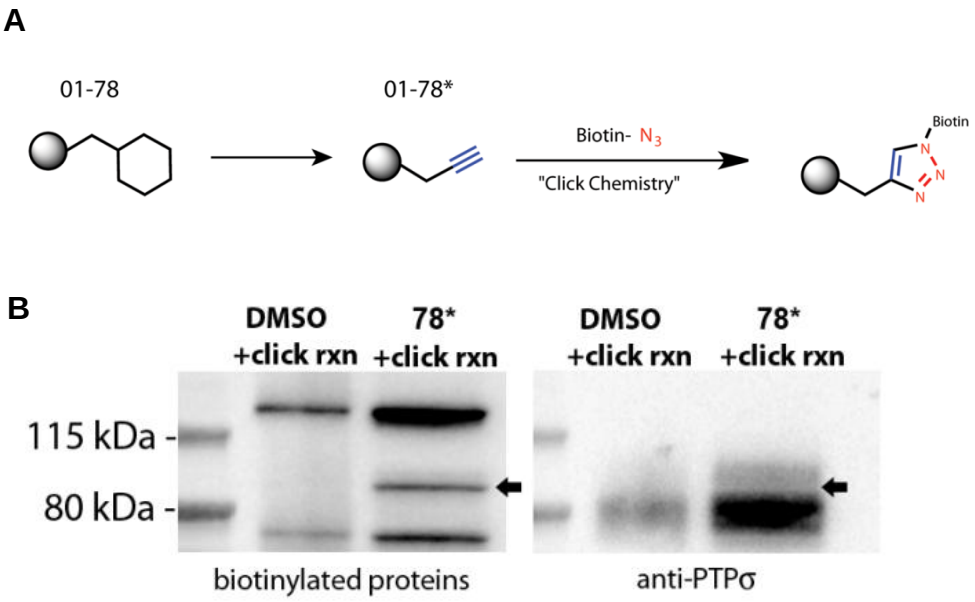

Figure A.3. Novel small molecule inhibitor 01-78 binds PTPσ (A) Depiction of the modification to 01-78 into a clickable compound and modification following click reaction. The final biotinylated compound can be detected using streptavidin. (B) Click chemistry followed by western blotting revealed that 78* binds to PTPσ in cerebellar granule cells. 78* covalently binds to a protein the same size as PTPσ (black arrow). As expected, PTPσ covalently modified by 78* and biotin results in an upward band shift (black arrow).

Appendix C:

Arrhythmia severity score: ECGs from isoproterenol treatment during optical mapping experiments were assessed for arrhythmia severity. Each heart was individually assessed using a scale that was defined as follows: 0=no arrhythmias, 1=individual PVCs, 2=bigeminy or salvos, 3=ventricular tachycardia, 4=ventricular fibrillation. Ventricular tachycardia was defined by three or more consecutive PVCs. Each heart was given a score based on the most severe arrhythmia identified.

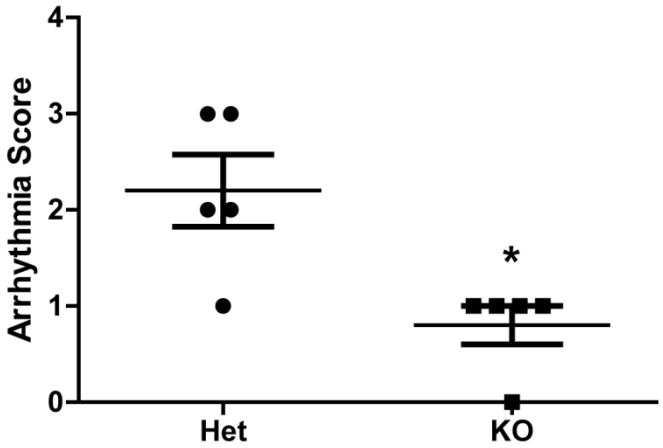

Figure A.4 Sympathetic reinnervation reduces arrhythmia severity. Het and KO MI hearts were assessed for arrhythmia severity during isoproterenol treatment. Each heart was given a score based on the most severe arrhythmia identified. Mean±SEM (n=5 hearts); *p<.05.

Appendix D:

APD_{50} restitution: Het and KO PTPσ hearts after either sham or MI were prepared and perfused for optical mapping as described in the methods. Restitution was assessed by the delivery of a single extrastimulus (S2) after a train of stimuli at a fixed cycle length (S1; 150 ms). S2 cycle length ranged from 60-250 ms. To determine S2 APD, repolarization time at 50% return to baseline was used to calculate action potential duration (APD_{50}). Data analysis was performed using the commercially available analysis program Optiq (Cairn, UK).

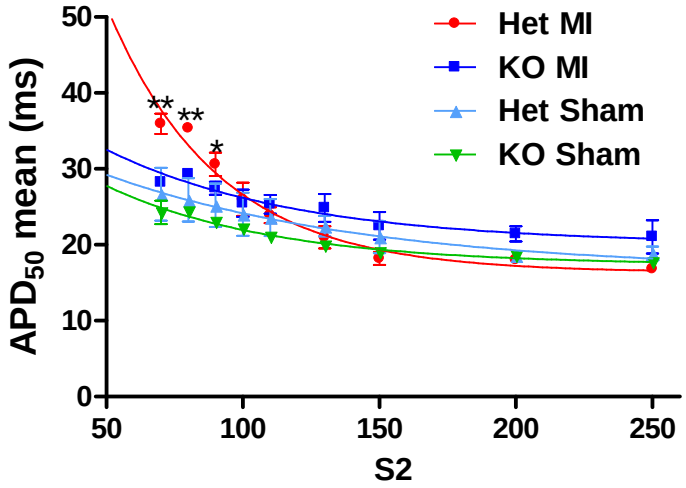

Figure A.5 Sympathetic reinnervation normalizes APD_{50} restitution. APD_{50} was assessed for Het and KO hearts after either sham or MI at several extrastimuli cycle lengths (S2). Mean±SEM (n=3-5 hearts); *p<.05, Het MI vs. both sham groups; **p<.01, Het MI vs. all groups.

Reference List

Adler R (1993) Ciliary neurotrophic factor as an injury factor. Curr Opin Neurobiol 3:785-789.

Aguayo AJ, Peyronnard JM, Bray GM (1973) A quantitative ultrastructural study of regeneration from isolated proximal stumps of transected unmyelinated nerves. J Neuropathol Exp Neurol 32:256-270.

Al-Shawi R, Hafner A, Olsen J, Chun S, Raza S, Thrasivoulou C, Lovestone S, Killick R, Simons P, Cowen T (2008) Neurotoxic and neurotrophic roles of proNGF and the receptor sortilin in the adult and ageing nervous system. Eur J Neurosci 27:2103-2114.

Aloe L, Cozzari C, Levi-Montalcini R (1985) Cyclocytidine-induced release of nerve growth factor from mouse submandibular glands enhances regeneration of sympathetic fibers in adult mice. Brain Res 332:259-265.

Anderson RH, Yanni J, Boyett MR, Chandler NJ, Dobrzynski H (2009) The anatomy of the cardiac conduction system. Clin Anat 22:99-113.

Antzelevitch C, Sicouri S, Litovsky SH, Lukas A, Krishnan SC, Di Diego JM, Gintant GA, Liu DW (1991) Heterogeneity within the ventricular wall. Electrophysiology and pharmacology of epicardial, endocardial, and M cells. Circ Res 69:1427-1449.

Aricescu AR, McKinnell IW, Halfter W, Stoker AW (2002) Heparan sulfate proteoglycans are ligands for receptor protein tyrosine phosphatase sigma. Mol Cell Biol 22:1881-1892.

Arimura A, Somogyvari-Vigh A, Weill C, Fiore RC, Tatsuno I, Bay V, Brenneman DE (1994) PACAP functions as a neurotrophic factor. Ann N Y Acad Sci 739:228-243.

Asher RA, Morgenstern DA, Moon LD, Fawcett JW (2001) Chondroitin sulphate proteoglycans: inhibitory components of the glial scar. Prog Brain Res 132:611-619.

Atwater BD, Daubert JP (2012) Implantable cardioverter defibrillators: risks accompany the life-saving benefits. Heart 98:764-772.

Avnur Z, Geiger B (1984) Immunocytochemical localization of native chondroitin-sulfate in tissues and cultured cells using specific monoclonal antibody. Cell 38:811-822.

Babington EJ, Vatanparast J, Verrall J, Blackshaw SE (2005) Three-dimensional culture of leech and snail ganglia for studies of neural repair. Invert Neurosci 5:173-182.

Back SA, Tuohy TM, Chen H, Wallingford N, Craig A, Struve J, Luo NL, Banine F, Liu Y, Chang A, Trapp BD, Bebo BF, Jr., Rao MS, Sherman LS (2005) Hyaluronan accumulates in demyelinated lesions and inhibits oligodendrocyte progenitor maturation. Nat Med 11:966-972.

Bahouth SW (1992) Effects of chemical and surgical sympathectomy on expression of beta-adrenergic receptors and guanine nucleotide-binding proteins in rat submandibular glands. Mol Pharmacol 42:971-981.

Bai J, Ren C, Hao W, Wang R, Cao JM (2008) Chemical sympathetic denervation, suppression of myocardial transient outward potassium current, and ventricular fibrillation in the rat. Can J Physiol Pharmacol 86:700-709.

Bandtlow CE, Zimmermann DR (2000) Proteoglycans in the developing brain: new conceptual insights for old proteins. Physiol Rev 80:1267-1290.

Barber MJ, Mueller TM, Henry DP, Felten SY, Zipes DP (1983) Transmural myocardial infarction in the dog produces sympathectomy in noninfarcted myocardium. Circulation 67:787-796.

Barczyk M, Carracedo S, Gullberg D (2010) Integrins. Cell Tissue Res 339:269-280.

Barde YA, Edgar D, Thoenen H (1982) Purification of a new neurotrophic factor from mammalian brain. EMBO J 1:549-553.

Basu S, Senior R, Raval U, van der Does R, Bruckner T, Lahiri A (1997) Beneficial effects of intravenous and oral carvedilol treatment in acute myocardial infarction. A placebo-controlled, randomized trial. Circulation 96:183-191.

Bengel FM, Ueberfuhr P, Hesse T, Schiepel N, Ziegler SI, Scholz S, Nekolla SG, Reichart B, Schwaiger M (2002) Clinical determinants of ventricular sympathetic reinnervation after orthotopic heart transplantation. Circulation 106:831-835.

Bengel FM, Ueberfuhr P, Karja J, Schreiber K, Nekolla SG, Reichart B, Schwaiger M (2004) Sympathetic reinnervation, exercise performance and effects of beta-adrenergic blockade in cardiac transplant recipients. Eur Heart J 25:1726-1733.

Bengel FM, Ueberfuhr P, Schiepel N, Nekolla SG, Reichart B, Schwaiger M (2001) Effect of sympathetic reinnervation on cardiac performance after heart transplantation. N Engl J Med 345:731-738.

Bengel FM, Ueberfuhr P, Ziegler SI, Nekolla S, Reichart B, Schwaiger M (1999) Serial assessment of sympathetic reinnervation after orthotopic heart transplantation. A longitudinal study using PET and C-11 hydroxyephedrine. Circulation 99:1866-1871.

Berkemeier LR, Winslow JW, Kaplan DR, Nikolics K, Goeddel DV, Rosenthal A (1991) Neurotrophin-5: a novel neurotrophic factor that activates trk and trkB. Neuron 7:857-866.

Bernstein SA, Morley GE (2006) Gap junctions and propagation of the cardiac action potential. Adv Cardiol 42:71-85.

Bers DM (2002) Cardiac excitation-contraction coupling. Nature 415:198-205.

Bers DM (2008) Calcium Cycling and Signaling in Cardiac Myocytes. Annual Review of Physiology 70:23-49.

Beyer EC, Paul DL, Goodenough DA (1987) Connexin43: a protein from rat heart homologous to a gap junction protein from liver. J Cell Biol 105:2621-2629.

Billman GE, Castillo LC, Hensley J, Hohl CM, Altschuld RA (1997) Beta2-adrenergic receptor antagonists protect against ventricular fibrillation: in vivo and in vitro evidence for enhanced sensitivity to beta2-adrenergic stimulation in animals susceptible to sudden death. Circulation 96:1914-1922.

Boogers MJ, Borleffs CJ, Henneman MM, van Bommel RJ, van RJ, Boersma E, Dibbets-Schneider P, Stokkel MP, van der Wall EE, Schalij MJ, Bax JJ (2010) Cardiac sympathetic denervation assessed with 123-iodine metaiodobenzylguanidine imaging predicts ventricular arrhythmias in implantable cardioverter-defibrillator patients. J Am Coll Cardiol 55:2769-2777.

Bowers CW, Baldwin C, Zigmond RE (1984) Sympathetic reinnervation of the pineal gland after postganglionic nerve lesion does not restore normal pineal function. J Neurosci 4:2010-2015.

Bozler E (1943) The initiation of impulses in cardiac muscle. Am J Physiol 138:273-282.

Bradbury EJ, Carter LM (2011) Manipulating the glial scar: chondroitinase ABC as a therapy for spinal cord injury. Brain Res Bull 84:306-316.

Bradbury EJ, Moon LD, Popat RJ, King VR, Bennett GS, Patel PN, Fawcett JW, McMahon SB (2002) Chondroitinase ABC promotes functional recovery after spinal cord injury. Nature 416:636-640.

Bristow MR, Ginsburg R, Umans V, Fowler M, Minobe W, Rasmussen R, Zera P, Menlove R, Shah P, Jamieson S, . (1986) Beta 1- and beta 2-adrenergic-receptor subpopulations in nonfailing and failing human ventricular myocardium: coupling of both receptor subtypes to muscle contraction and selective beta 1-receptor down-regulation in heart failure. Circ Res 59:297-309.

Brown MC, Perry VH, Lunn ER, Gordon S, Heumann R (1991) Macrophage dependence of peripheral sensory nerve regeneration: possible involvement of nerve growth factor. Neuron 6:359-370.

Bru-Mercier G, Deroubaix E, Capuano V, Ruchon Y, Rucker-Martin C, Coulombe A, Renaud JF (2003) Expression of heart K+ channels in adrenalectomized and catecholamine-depleted reserpine-treated rats. J Mol Cell Cardiol 35:153-163.

Brunet S, Aimond F, Li H, Guo W, Eldstrom J, Fedida D, Yamada KA, Nerbonne JM (2004) Heterogeneous expression of repolarizing, voltage-gated K+ currents in adult mouse ventricles. J Physiol 559:103-120.

Cafferty WB, Gardiner NJ, Gavazzi I, Powell J, McMahon SB, Heath JK, Munson J, Cohen J, Thompson SW (2001) Leukemia inhibitory factor determines the growth status of injured adult sensory neurons. J Neurosci 21:7161-7170.

Cane KN, Anderson CR (2009) Generating diversity: Mechanisms regulating the differentiation of autonomic neuron phenotypes. Auton Neurosci 151:17-29.

Cao JM, Chen LS, KenKnight BH, Ohara T, Lee MH, Tsai J, Lai WW, Karagueuzian HS, Wolf PL, Fishbein MC, Chen PS (2000a) Nerve sprouting and sudden cardiac death. Circ Res 86:816-821.

Cao JM, Fishbein MC, Han JB, Lai WW, Lai AC, Wu TJ, Czer L, Wolf PL, Denton TA, Shintaku IP, Chen PS, Chen LS (2000b) Relationship between regional cardiac hyperinnervation and ventricular arrhythmia. Circulation 101:1960-1969.

Carulli D, Rhodes KE, Brown DJ, Bonnert TP, Pollack SJ, Oliver K, Strata P, Fawcett JW (2006) Composition of perineuronal nets in the adult rat cerebellum and the cellular origin of their components. J Comp Neurol 494:559-577.

Celio MR, Blumcke I (1994) Perineuronal nets--a specialized form of extracellular matrix in the adult nervous system. Brain Res Brain Res Rev 19:128-145.

Celio MR, Spreafico R, De BS, Vitellaro-Zuccarello L (1998) Perineuronal nets: past and present. Trends Neurosci 21:510-515.

Chagnon MJ, Wu CL, Nakazawa T, Yamamoto T, Noda M, Blanchetot C, Tremblay ML (2010) Receptor tyrosine phosphatase sigma (RPTPsigma) regulates, p250GAP, a novel substrate that attenuates Rac signaling. Cell Signal 22:1626-1633.

Chao MV (2003) Neurotrophins and their receptors: a convergence point for many signalling pathways. Nat Rev Neurosci 4:299-309.

Coles CH, Shen Y, Tenney AP, Siebold C, Sutton GC, Lu W, Gallagher JT, Jones EY, Flanagan JG, Aricescu AR (2011) Proteoglycan-specific molecular switch for RPTPsigma clustering and neuronal extension. Science 332:484-488.

Colyer J (1998) Phosphorylation states of phospholamban. Ann N Y Acad Sci 853:79-91.

Costigan M, Befort K, Karchewski L, Griffin RS, D'Urso D, Allchorne A, Sitarski J, Mannion JW, Pratt RE, Woolf CJ (2002) Replicate high-density rat genome oligonucleotide microarrays reveal hundreds of regulated genes in the dorsal root ganglion after peripheral nerve injury. BMC Neurosci 3:16.

Crick SJ, Wharton J, Sheppard MN, Royston D, Yacoub MH, Anderson RH, Polak JM (1994) Innervation of the human cardiac conduction system. A quantitative immunohistochemical and histochemical study. Circulation 89:1697-1708.

Crowley C, Spencer SD, Nishimura MC, Chen KS, Pitts-Meek S, Armanini MP, Ling LH, McMahon SB, Shelton DL, Levinson AD, . (1994) Mice lacking nerve growth factor display perinatal loss of sensory and sympathetic neurons yet develop basal forebrain cholinergic neurons. Cell 76:1001-1011.

Cunningham ME, Greene LA (1998) A function-structure model for NGF-activated TRK. EMBO J 17:7282-7293.

Cutler MJ, Jeyaraj D, Rosenbaum DS (2011) Cardiac electrical remodeling in health and disease. Trends Pharmacol Sci 32:174-180.

Dae MW, O'Connell JW, Botvinick EH, Chin MC (1995) Acute and chronic effects of transient myocardial ischemia on sympathetic nerve activity, density, and norepinephrine content. Cardiovasc Res 30:270-280.

Dailey AT, Avellino AM, Benthem L, Silver J, Kliot M (1998) Complement depletion reduces macrophage infiltration and activation during Wallerian degeneration and axonal regeneration. J Neurosci 18:6713-6722.

Davies SJ, Fitch MT, Memberg SP, Hall AK, Raisman G, Silver J (1997) Regeneration of adult axons in white matter tracts of the central nervous system. Nature 390:680-683.

Desai CJ, Gindhart JG, Jr., Goldstein LS, Zinn K (1996) Receptor tyrosine phosphatases are required for motor axon guidance in the Drosophila embryo. Cell 84:599-609.

Diaz ME, O'Neill SC, Eisner DA (2004) Sarcoplasmic reticulum calcium content fluctuation is the key to cardiac alternans. Circ Res 94:650-656.

Dickendesher TL, Baldwin KT, Mironova YA, Koriyama Y, Raiker SJ, Askew KL, Wood A, Geoffroy CG, Zheng B, Liepmann CD, Katagiri Y, Benowitz LI, Geller HM, Giger RJ (2012) NgR1 and NgR3 are receptors for chondroitin sulfate proteoglycans. Nat Neurosci 15:703-712.

Dobaczewski M, Bujak M, Zymek P, Ren G, Entman ML, Frangogiannis NG (2006) Extracellular matrix remodeling in canine and mouse myocardial infarcts. Cell Tissue Res 324:475-488.

Duffy P, Schmandke A, Schmandke A, Sigworth J, Narumiya S, Cafferty WB, Strittmatter SM (2009) Rho-associated kinase II (ROCKII) limits axonal growth after trauma within the adult mouse spinal cord. J Neurosci 29:15266-15276.

Dziennis S, Habecker BA (2003) Cytokine suppression of dopamine-beta-hydroxylase by extracellular signal-regulated kinase-dependent and -independent pathways. J Biol Chem 278:15897-15904.

Ekstrom PA, Kerekes N, Hokfelt T (2000) Leukemia inhibitory factor null mice: unhampered in vitro outgrowth of sensory axons but reduced stimulatory potential by nerve segments. Neurosci Lett 281:107-110.

El-Helou V, Proulx C, Gosselin H, Clement R, Mimee A, Villeneuve L, Calderone A (2008) Dexamethasone treatment of post-MI rats attenuates sympathetic innervation of the infarct region. J Appl Physiol 104:150-156.

Elchebly M, Wagner J, Kennedy TE, Lanctot C, Michaliszyn E, Itie A, Drouin J, Tremblay ML (1999) Neuroendocrine dysplasia in mice lacking protein tyrosine phosphatase sigma. Nat Genet 21:330-333.

Estorch M, Camprecios M, Flotats A, Mari C, Berna L, Catafau AM, Ballester M, Narula J, Carrio I (1999) Sympathetic reinnervation of cardiac allografts evaluated by 123I-MIBG imaging. J Nucl Med 40:911-916.

Estrach S, Schmidt S, Diriong S, Penna A, Blangy A, Fort P, Debant A (2002) The Human Rho-GEF trio and its target GTPase RhoG are involved in the NGF pathway, leading to neurite outgrowth. Curr Biol 12:307-312.

Exner DV, Reiffel JA, Epstein AE, Ledingham R, Reiter MJ, Yao Q, Duff HJ, Follmann D, Schron E, Greene HL, Carlson MD, Brodsky MA, Akiyama T, Baessler C, Anderson JL (1999) Beta-blocker use and survival in patients with ventricular fibrillation or symptomatic ventricular tachycardia: the Antiarrhythmics Versus Implantable Defibrillators (AVID) trial. J Am Coll Cardiol 34:325-333.

Fabiato A (1985) Simulated calcium current can both cause calcium loading in and trigger calcium release from the sarcoplasmic reticulum of a skinned canine cardiac Purkinje cell. J Gen Physiol 85:291-320.

Fallavollita JA, Heavey BM, Luisi AJ, Jr., Michalek SM, Baldwa S, Mashtare TL, Jr., Hutson AD, Dekemp RA, Haka MS, Sajjad M, Cimato TR, Curtis AB, Cain ME, Canty JM, Jr. (2013) Regional Myocardial Sympathetic Denervation Predicts the Risk of Sudden Cardiac Arrest in Ischemic Cardiomyopathy. J Am Coll Cardiol.

Faux C, Hawadle M, Nixon J, Wallace A, Lee S, Murray S, Stoker A (2007) PTPsigma binds and dephosphorylates neurotrophin receptors and can suppress NGF-dependent neurite outgrowth from sensory neurons. Biochim Biophys Acta 1773:1689-1700.

Ferguson TA, Muir D (2000) MMP-2 and MMP-9 increase the neurite-promoting potential of schwann cell basal laminae and are upregulated in degenerated nerve. Mol Cell Neurosci 16:157-167.

Fisher D, Xing B, Dill J, Li H, Hoang HH, Zhao Z, Yang XL, Bachoo R, Cannon S, Longo FM, Sheng M, Silver J, Li S (2011) Leukocyte Common Antigen-Related Phosphatase Is a Functional Receptor for Chondroitin Sulfate Proteoglycan Axon Growth Inhibitors. J Neurosci 31:14051-14066.

Fitch MT, Silver J (2008) CNS injury, glial scars, and inflammation: Inhibitory extracellular matrices and regeneration failure. Exp Neurol 209:294-301.

Fournier AE, Takizawa BT, Strittmatter SM (2003) Rho kinase inhibition enhances axonal regeneration in the injured CNS. J Neurosci 23:1416-1423.

Francis N, Farinas I, Brennan C, Rivas-Plata K, Backus C, Reichardt L, Landis S (1999) NT-3, like NGF, is required for survival of sympathetic neurons, but not their precursors. Dev Biol 210:411-427.

Friedlander DR, Milev P, Karthikeyan L, Margolis RK, Margolis RU, Grumet M (1994) The neuronal chondroitin sulfate proteoglycan neurocan binds to the neural cell adhesion molecules Ng-CAM/L1/NILE and N-CAM, and inhibits neuronal adhesion and neurite outgrowth. J Cell Biol 125:669-680.

Galtrey CM, Fawcett JW (2007) The role of chondroitin sulfate proteoglycans in regeneration and plasticity in the central nervous system. Brain Res Rev 54:1-18.

Garcia-Alias G, Petrosyan HA, Schnell L, Horner PJ, Bowers WJ, Mendell LM, Fawcett JW, Arvanian VL (2011) Chondroitinase ABC combined with neurotrophin NT-3 secretion and NR2D expression promotes axonal plasticity and functional recovery in rats with lateral hemisection of the spinal cord. J Neurosci 31:17788-17799.

Gardiner NJ, Moffatt S, Fernyhough P, Humphries MJ, Streuli CH, Tomlinson DR (2007) Preconditioning injury-induced neurite outgrowth of adult rat sensory neurons on fibronectin is mediated by mobilisation of axonal alpha5 integrin. Mol Cell Neurosci 35:249-260.

Gardner RT, Habecker BA (2013) Infarct-derived chondroitin sulfate proteoglycans prevent sympathetic reinnervation after cardiac ischemia-reperfusion injury. J Neurosci 33:7175-7183.

Gates MA, Thomas LB, Howard EM, Laywell ED, Sajin B, Faissner A, Gotz B, Silver J, Steindler DA (1995) Cell and molecular analysis of the developing and adult mouse subventricular zone of the cerebral hemispheres. J Comp Neurol 361:249-266.

Ghilardi JR, Freeman KT, Jimenez-Andrade JM, Coughlin KA, Kaczmarska MJ, Castaneda-Corral G, Bloom AP, Kuskowski MA, Mantyh PW (2012) Neuroplasticity of sensory and sympathetic nerve fibers in a mouse model of a painful arthritic joint. Arthritis Rheum 64:2223-2232.

Glebova NO, Ginty DD (2004) Heterogeneous requirement of NGF for sympathetic target innervation in vivo. J Neurosci 24:743-751.

Glebova NO, Ginty DD (2005) Growth and survival signals controlling sympathetic nervous system development. Annu Rev Neurosci 28:191-222.

Gloster A, Diamond J (1992) Sympathetic nerves in adult rats regenerate normally and restore pilomotor function during an anti-NGF treatment that prevents their collateral sprouting. J Comp Neurol 326:363-374.

Gloster A, Diamond J (1995) NGF-dependent and NGF-independent recovery of sympathetic function after chemical sympathectomy with 6-hydroxydopamine. J Comp Neurol 359:586-594.

Goldenberg I, Gillespie J, Moss AJ, Hall WJ, Klein H, McNitt S, Brown MW, Cygankiewicz I, Zareba W (2010) Long-term benefit of primary prevention with an implantable cardioverter-defibrillator: an extended 8-year follow-up study of the Multicenter Automatic Defibrillator Implantation Trial II. Circulation 122:1265-1271.

Grill R, Murai K, Blesch A, Gage FH, Tuszynski MH (1997a) Cellular delivery of neurotrophin-3 promotes corticospinal axonal growth and partial functional recovery after spinal cord injury. J Neurosci 17:5560-5572.

Grill RJ, Blesch A, Tuszynski MH (1997b) Robust growth of chronically injured spinal cord axons induced by grafts of genetically modified NGF-secreting cells. Exp Neurol 148:444-452.

Grumet M, Milev P, Sakurai T, Karthikeyan L, Bourdon M, Margolis RK, Margolis RU (1994) Interactions with tenascin and differential effects on cell adhesion of neurocan and phosphacan, two major chondroitin sulfate proteoglycans of nervous tissue. J Biol Chem 269:12142-12146.

Guccione JM, Moonly SM, Moustakidis P, Costa KD, Moulton MJ, Ratcliffe MB, Pasque MK (2001) Mechanism underlying mechanical dysfunction in the border zone of left ventricular aneurysm: a finite element model study. Ann Thorac Surg 71:654-662.

Habecker BA, Sachs HH, Rohrer H, Zigmond RE (2009) The dependence on gp130 cytokines of axotomy induced neuropeptide expression in adult sympathetic neurons. Dev Neurobiol 69:392-400.

Hallbook F, Ibanez CF, Persson H (1991) Evolutionary studies of the nerve growth factor family reveal a novel member abundantly expressed in Xenopus ovary. Neuron 6:845-858.

Hamel MG, Ajmo JM, Leonardo CC, Zuo F, Sandy JD, Gottschall PE (2008) Multimodal signaling by the ADAMTSs (a disintegrin and metalloproteinase with thrombospondin motifs) promotes neurite extension. Exp Neurol 210:428-440.

Hartikainen J, Kuikka J, Mantysaari M, Lansimies E, Pyorala K (1996) Sympathetic reinnervation after acute myocardial infarction. Am J Cardiol 77:5-9.

Hasan W, Jama A, Donohue T, Wernli G, Onyszchuk G, Al-Hafez B, Bilgen M, Smith PG (2006) Sympathetic hyperinnervation and inflammatory cell NGF synthesis following myocardial infarction in rats. Brain Res 1124:142-154.

Hasan W, Woodward WR, Habecker BA (2012) Altered atrial neurotransmitter release in transgenic p75(-/-) and gp130 KO mice. Neurosci Lett 529:55-59.

Hempstead BL (2002) The many faces of p75NTR. Curr Opin Neurobiol 12:260-267.

Hempstead BL, Martin-Zanca D, Kaplan DR, Parada LF, Chao MV (1991) High-affinity NGF binding requires coexpression of the trk proto-oncogene and the low-affinity NGF receptor. Nature 350:678-683.

Herring N, Cranley J, Lokale MN, Li D, Shanks J, Alston EN, Girard BM, Carter E, Parsons RL, Habecker BA, Paterson DJ (2012) The cardiac sympathetic co-transmitter galanin reduces acetylcholine release and vagal bradycardia: implications for neural control of cardiac excitability. J Mol Cell Cardiol 52:667-676.

Herring N, Lokale MN, Danson EJ, Heaton DA, Paterson DJ (2008) Neuropeptide Y reduces acetylcholine release and vagal bradycardia via a Y2 receptor-mediated, protein kinase C-dependent pathway. J Mol Cell Cardiol 44:477-485.

Hill CE, Hirst GD, Ngu MC, van Helden DF (1985) Sympathetic postganglionic reinnervation of mesenteric arteries and enteric neurones of the ileum of the rat. J Auton Nerv Syst 14:317-334.

Hiltunen JO, Laurikainen A, Vakeva A, Meri S, Saarma M (2001) Nerve growth factor and brain-derived neurotrophic factor mRNAs are regulated in distinct cell populations of rat heart after ischaemia and reperfusion. J Pathol 194:247-253.

Hoffman PN, Cleveland DW (1988) Neurofilament and tubulin expression recapitulates the developmental program during axonal regeneration: induction of a specific beta-tubulin isotype. Proc Natl Acad Sci U S A 85:4530-4533.

Hohn A, Leibrock J, Bailey K, Barde YA (1990) Identification and characterization of a novel member of the nerve growth factor/brain-derived neurotrophic factor family. Nature 344:339-341.

Huser J, Wang YG, Sheehan KA, Cifuentes F, Lipsius SL, Blatter LA (2000) Functional coupling between glycolysis and excitation-contraction coupling underlies alternans in cat heart cells. J Physiol 524 Pt 3:795-806.

Iaccarino G, Tomhave ED, Lefkowitz RJ, Koch WJ (1998) Reciprocal in vivo regulation of myocardial G protein-coupled receptor kinase expression by beta-adrenergic receptor stimulation and blockade. Circulation 98:1783-1789.

Ieda M, Fukuda K, Hisaka Y, Kimura K, Kawaguchi H, Fujita J, Shimoda K, Takeshita E, Okano H, Kurihara Y, Kurihara H, Ishida J, Fukamizu A, Federoff HJ, Ogawa S (2004) Endothelin-1 regulates cardiac sympathetic innervation in the rodent heart by controlling nerve growth factor expression. J Clin Invest 113:876-884.

Ieda M, Kanazawa H, Kimura K, Hattori F, Ieda Y, Taniguchi M, Lee JK, Matsumura K, Tomita Y, Miyoshi S, Shimoda K, Makino S, Sano M, Kodama I, Ogawa S, Fukuda K (2007) Sema3a maintains normal heart rhythm through sympathetic innervation patterning. Nat Med 13:604-612.

Inoue H, Zipes DP (1987) Results of sympathetic denervation in the canine heart: supersensitivity that may be arrhythmogenic. Circulation 75:877-887.

Inoue H, Zipes DP (1988) Time course of denervation of efferent sympathetic and vagal nerves after occlusion of the coronary artery in the canine heart. Circ Res 62:1111-1120.

Ip NY, Nye SH, Boulton TG, Davis S, Taga T, Li Y, Birren SJ, Yasukawa K, Kishimoto T, Anderson DJ, . (1992) CNTF and LIF act on neuronal cells via shared signaling pathways that involve the IL-6 signal transducing receptor component gp130. Cell 69:1121-1132.

Jackson BM, Gorman JH, Moainie SL, Guy TS, Narula N, Narula J, John-Sutton MG, Edmunds LH, Jr., Gorman RC (2002) Extension of borderzone myocardium in postinfarction dilated cardiomyopathy. J Am Coll Cardiol 40:1160-1167.

Jalife J (2000) Ventricular fibrillation: mechanisms of initiation and maintenance. Annu Rev Physiol 62:25-50.

Jhun BS, Uchi J, Wang W, Ha CH, Zhao J, Kim JY, Wong C, Dirksen RT, Lopes CM, Jin ZG (2012) Adrenergic signaling controls RGK-dependent trafficking of cardiac voltage-gated L-type Ca2+ channels through PKD1. Circ Res 110:59-70.

Jiang M, Cabo C, Yao J, Boyden PA, Tseng G (2000) Delayed rectifier K currents have reduced amplitudes and altered kinetics in myocytes from infarcted canine ventricle. Cardiovasc Res 48:34-43.

Jing S, Tapley P, Barbacid M (1992) Nerve growth factor mediates signal transduction through trk homodimer receptors. Neuron 9:1067-1079.

Johnson D, Lanahan A, Buck CR, Sehgal A, Morgan C, Mercer E, Bothwell M, Chao M (1986) Expression and structure of the human NGF receptor. Cell 47:545-554.

Johnson KG, McKinnell IW, Stoker AW, Holt CE (2001) Receptor protein tyrosine phosphatases regulate retinal ganglion cell axon outgrowth in the developing Xenopus visual system. J Neurobiol 49:99-117.

Jones LL, Sajed D, Tuszynski MH (2003) Axonal regeneration through regions of chondroitin sulfate proteoglycan deposition after spinal cord injury: a balance of permissiveness and inhibition. J Neurosci 23:9276-9288.

Jones LL, Yamaguchi Y, Stallcup WB, Tuszynski MH (2002) NG2 is a major chondroitin sulfate proteoglycan produced after spinal cord injury and is expressed by macrophages and oligodendrocyte progenitors. J Neurosci 22:2792-2803.

Jourdon P, Feuvray D (1993) Calcium and potassium currents in ventricular myocytes isolated from diabetic rats. J Physiol 470:411-429.

Kamp TJ, Hell JW (2000) Regulation of cardiac L-type calcium channels by protein kinase A and protein kinase C. Circ Res 87:1095-1102.

Kanazawa H, Ieda M, Kimura K, Arai T, Kawaguchi-Manabe H, Matsuhashi T, Endo J, Sano M, Kawakami T, Kimura T, Monkawa T, Hayashi M, Iwanami A, Okano H,

Okada Y, Ishibashi-Ueda H, Ogawa S, Fukuda K (2010) Heart failure causes cholinergic transdifferentiation of cardiac sympathetic nerves via gp130-signaling cytokines in rodents. J Clin Invest 120:408-421.

Kandel E.R., Schwartz J.H., Jessell T.M. (2000) Principles of Neural Science. Appleton and Lange.

Kaplan DR, Miller FD (2000) Neurotrophin signal transduction in the nervous system. Curr Opin Neurobiol 10:381-391.

Kaprielian R, Sah R, Nguyen T, Wickenden AD, Backx PH (2002) Myocardial infarction in rat eliminates regional heterogeneity of AP profiles, I(to) K(+) currents, and [Ca(2+)](i) transients. Am J Physiol Heart Circ Physiol 283:H1157-H1168.

Kass RS, Lederer WJ, Tsien RW, Weingart R (1978) Role of calcium ions in transient inward currents and aftercontractions induced by strophanthidin in cardiac Purkinje fibres. J Physiol 281:187-208.

Kerr RS, Newgreen DF (1997) Isolation and characterization of chondroitin sulfate proteoglycans from embryonic quail that influence neural crest cell behavior. Dev Biol 192:108-124.

Killeen MJ, Sabir IN, Grace AA, Huang CL (2008) Dispersions of repolarization and ventricular arrhythmogenesis: lessons from animal models. Prog Biophys Mol Biol 98:219-229.

Kim DT, Luthringer DJ, Lai AC, Suh G, Czer L, Chen LS, Chen PS, Fishbein MC (2004) Sympathetic nerve sprouting after orthotopic heart transplantation. J Heart Lung Transplant 23:1349-1358.

Kimura K, Ieda M, Fukuda K (2012) Development, maturation, and transdifferentiation of cardiac sympathetic nerves. Circ Res 110:325-336.

Kimura K, Ieda M, Kanazawa H, Yagi T, Tsunoda M, Ninomiya S, Kurosawa H, Yoshimi K, Mochizuki H, Yamazaki K, Ogawa S, Fukuda K (2007) Cardiac sympathetic rejuvenation: a link between nerve function and cardiac hypertrophy. Circ Res 100:1755-1764.

Kjellen L, Lindahl U (1991) Proteoglycans: structures and interactions. Annu Rev Biochem 60:443-475.

Klimaschewski L, Hauser C, Heym C (1996) PACAP immunoreactivity in the rat superior cervical ganglion in comparison to VIP. Neuroreport 7:2797-2801.

Klimaschewski L, Tran TD, Nobiling R, Heym C (1994) Plasticity of postganglionic sympathetic neurons in the rat superior cervical ganglion after axotomy. Microsc Res Tech 29:120-130.

Kobayashi NR, Bedard AM, Hincke MT, Tetzlaff W (1996) Increased expression of BDNF and trkB mRNA in rat facial motoneurons after axotomy. Eur J Neurosci 8:1018-1029.

Kramer CM, Nicol PD, Rogers WJ, Suzuki MM, Shaffer A, Theobald TM, Reichek N (1997) Reduced sympathetic innervation underlies adjacent noninfarcted region dysfunction during left ventricular remodeling. J Am Coll Cardiol 30:1079-1085.

Krueger NX, Van VD, Wan HI, Gelbart WM, Goodman CS, Saito H (1996) The transmembrane tyrosine phosphatase DLAR controls motor axon guidance in Drosophila. Cell 84:611-622.

Kummer W (1987) Galanin- and neuropeptide Y-like immunoreactivities coexist in paravertebral sympathetic neurones of the cat. Neurosci Lett 78:127-131.

Kuo CS, Munakata K, Reddy CP, Surawicz B (1983) Characteristics and possible mechanism of ventricular arrhythmia dependent on the dispersion of action potential durations. Circulation 67:1356-1367.

Landolt RM, Vaughan L, Winterhalter KH, Zimmermann DR (1995) Versican is selectively expressed in embryonic tissues that act as barriers to neural crest cell migration and axon outgrowth. Development 121:2303-2312.

Lang B, et al. (2013) Companion ISP manuscript. Nature Submission.

Ledig MM, McKinnell IW, Mrsic-Flogel T, Wang J, Alvares C, Mason I, Bixby JL, Mueller BK, Stoker AW (1999) Expression of receptor tyrosine phosphatases during development of the retinotectal projection of the chick. J Neurobiol 39:81-96.

Lee H, McKeon RJ, Bellamkonda RV (2010) Sustained delivery of thermostabilized chABC enhances axonal sprouting and functional recovery after spinal cord injury. Proc Natl Acad Sci U S A 107:3340-3345.

Leibinger M, Muller A, Andreadaki A, Hauk TG, Kirsch M, Fischer D (2009) Neuroprotective and axon growth-promoting effects following inflammatory stimulation on mature retinal ganglion cells in mice depend on ciliary neurotrophic factor and leukemia inhibitory factor. J Neurosci 29:14334-14341.

Lein P, Johnson M, Guo X, Rueger D, Higgins D (1995) Osteogenic protein-1 induces dendritic growth in rat sympathetic neurons. Neuron 15:597-605.

Leonardo CC, Eakin AK, Ajmo JM, Gottschall PE (2008) Versican and brevican are expressed with distinct pathology in neonatal hypoxic-ischemic injury. J Neurosci Res 86:1106-1114.

Li W, Knowlton D, Van Winkle DM, Habecker BA (2004) Infarction alters both the distribution and noradrenergic properties of cardiac sympathetic neurons. Am J Physiol Heart Circ Physiol 286:H2229-H2236.

Lin R, Kwok JC, Crespo D, Fawcett JW (2008) Chondroitinase ABC has a long-lasting effect on chondroitin sulphate glycosaminoglycan content in the injured rat brain. J Neurochem 104:400-408.

Lindh B, Lundberg JM, Hokfelt T (1989) NPY-, galanin-, VIP/PHI-. Cell Tissue Res 256:259-273.

Lindwall C, Kanje M (2005) Retrograde axonal transport of JNK signaling molecules influence injury induced nuclear changes in p-c-Jun and ATF3 in adult rat sensory neurons. Mol Cell Neurosci 29:269-282.

Liu RY, Snider WD (2001) Different signaling pathways mediate regenerative versus developmental sensory axon growth. J Neurosci 21:RC164.

Lopez-Sendon J, Swedberg K, McMurray J, Tamargo J, Maggioni AP, Dargie H, Tendera M, Waagstein F, Kjekshus J, Lechat P, Torp-Pedersen C (2004) Expert consensus document on beta-adrenergic receptor blockers. Eur Heart J 25:1341-1362.

Lorentz CU, Alston EN, Belcik T, Lindner JR, Giraud GD, Habecker BA (2010) Heterogeneous ventricular sympathetic innervation, altered beta-adrenergic receptor expression, and rhythm instability in mice lacking the p75 neurotrophin receptor. Am J Physiol Heart Circ Physiol 298:H1652-H1660.

Lorentz CU, Parrish DC, Alston EN, Pellegrino MJ, Woodward WR, Hempstead BL, Habecker BA (2013) Sympathetic denervation of peri-infarct myocardium requires the p75 neurotrophin receptor. Exp Neurol 249:111-119.

Lorez HP, Kuhn H, Bartholini G (1975) Degeneration and regeneration of adrenergic nerves in mesenteric blood vessels, iris and atrium of the rat after 6-hydroxydopamine injection. J Neurocytol 4:157-176.

Lu B, Pang PT, Woo NH (2005) The yin and yang of neurotrophin action. Nat Rev Neurosci 6:603-614.

Lu P, Tuszynski MH (2008) Growth factors and combinatorial therapies for CNS regeneration. Exp Neurol 209:313-320.

Lue WM, Boyden PA (1992) Abnormal electrical properties of myocytes from chronically infarcted canine heart. Alterations in Vmax and the transient outward current. Circulation 85:1175-1188.

Lukas A, Antzelevitch C (1993) Differences in the electrophysiological response of canine ventricular epicardium and endocardium to ischemia. Role of the transient outward current. Circulation 88:2903-2915.

Lundberg JM, Hua XY, Franco-Cereceda A (1984) Effects of neuropeptide Y (NPY) on mechanical activity and neurotransmission in the heart, vas deferens and urinary bladder of the guinea-pig. Acta Physiol Scand 121:325-332.

Lundby A, Andersen MN, Steffensen AB, Horn H, Kelstrup CD, Francavilla C, Jensen LJ, Schmitt N, Thomsen MB, Olsen JV (2013) In vivo phosphoproteomics analysis reveals the cardiac targets of beta-adrenergic receptor signaling. Sci Signal 6:rs11.

Maisonpierre PC, Belluscio L, Friedman B, Alderson RF, Wiegand SJ, Furth ME, Lindsay RM, Yancopoulos GD (1990) NT-3, BDNF, and NGF in the developing rat nervous system: parallel as well as reciprocal patterns of expression. Neuron 5:501-509.

Mandolesi G, Madeddu F, Bozzi Y, Maffei L, Ratto GM (2004) Acute physiological response of mammalian central neurons to axotomy: ionic regulation and electrical activity. FASEB J 18:1934-1936.

Martin J.H. (1996) Neuroanatomy. Appleton and Lange.

Massey JM, Amps J, Viapiano MS, Matthews RT, Wagoner MR, Whitaker CM, Alilain W, Yonkof AL, Khalyfa A, Cooper NG, Silver J, Onifer SM (2008) Increased chondroitin sulfate proteoglycan expression in denervated brainstem targets following spinal cord injury creates a barrier to axonal regeneration overcome by chondroitinase ABC and neurotrophin-3. Exp Neurol 209:426-445.

Matsuda JJ, Lee H, Shibata EF (1992) Enhancement of rabbit cardiac sodium channels by beta-adrenergic stimulation. Circ Res 70:199-207.

Matsumoto K, Shionyu M, Go M, Shimizu K, Shinomura T, Kimata K, Watanabe H (2003) Distinct interaction of versican/PG-M with hyaluronan and link protein. J Biol Chem 278:41205-41212.

McKeon RJ, Hoke A, Silver J (1995) Injury-induced proteoglycans inhibit the potential for laminin-mediated axon growth on astrocytic scars. Exp Neurol 136:32-43.

McKeon RJ, Jurynec MJ, Buck CR (1999) The chondroitin sulfate proteoglycans neurocan and phosphacan are expressed by reactive astrocytes in the chronic CNS glial scar. J Neurosci 19:10778-10788.

McKeon RJ, Schreiber RC, Rudge JS, Silver J (1991) Reduction of neurite outgrowth in a model of glial scarring following CNS injury is correlated with the expression of inhibitory molecules on reactive astrocytes. J Neurosci 11:3398-3411.

McLean J, Batt J, Doering LC, Rotin D, Bain JR (2002) Enhanced rate of nerve regeneration and directional errors after sciatic nerve injury in receptor protein tyrosine phosphatase sigma knock-out mice. J Neurosci 22:5481-5491.

McQuarrie IG, Grafstein B (1973) Axon outgrowth enhanced by a previous nerve injury. Arch Neurol 29:53-55.

Mohney RP, Siegel RE, Zigmond RE (1994) Galanin and vasoactive intestinal peptide messenger RNAs increase following axotomy of adult sympathetic neurons. J Neurobiol 25:108-118.

Mohrman DE, Heller LJ (2013) Cardiovascular Physiology. New York: Lange Medical Books/McGraw Hill.

Moller K, Reimer M, Ekblad E, Hannibal J, Fahrenkrug J, Kanje M, Sundler F (1997) The effects of axotomy and preganglionic denervation on the expression of pituitary adenylate cyclase activating peptide (PACAP), galanin and PACAP type 1 receptors in the rat superior cervical ganglion. Brain Res 775:166-182.

Monnier PP, Sierra A, Schwab JM, Henke-Fahle S, Mueller BK (2003) The Rho/ROCK pathway mediates neurite growth-inhibitory activity associated with the chondroitin sulfate proteoglycans of the CNS glial scar. Mol Cell Neurosci 22:319-330.

Moon LD, Asher RA, Rhodes KE, Fawcett JW (2001) Regeneration of CNS axons back to their target following treatment of adult rat brain with chondroitinase ABC. Nat Neurosci 4:465-466.

Moon SY, Zang H, Zheng Y (2003) Characterization of a brain-specific Rho GTPase-activating protein, p200RhoGAP. J Biol Chem 278:4151-4159.

Moss AJ, Zareba W, Hall WJ, Klein H, Wilber DJ, Cannom DS, Daubert JP, Higgins SL, Brown MW, Andrews ML (2002) Prophylactic implantation of a defibrillator in patients with myocardial infarction and reduced ejection fraction. N Engl J Med 346:877-883.

Muller JE, Ludmer PL, Willich SN, Tofler GH, Aylmer G, Klangos I, Stone PH (1987) Circadian variation in the frequency of sudden cardiac death. Circulation 75:131-138.

Myer DJ, Gurkoff GG, Lee SM, Hovda DA, Sofroniew MV (2006) Essential protective roles of reactive astrocytes in traumatic brain injury. Brain 129:2761-2772.

Myles RC, Burton FL, Cobbe SM, Smith GL (2011) Alternans of action potential duration and amplitude in rabbits with left ventricular dysfunction following myocardial infarction. J Mol Cell Cardiol 50:510-521.

Myles RC, Wang L, Kang C, Bers DM, Ripplinger CM (2012) Local beta-adrenergic stimulation overcomes source-sink mismatch to generate focal arrhythmia. Circ Res 110:1454-1464.

Nabauer M, Beuckelmann DJ, Uberfuhr P, Steinbeck G (1996) Regional differences in current density and rate-dependent properties of the transient outward current in subepicardial and subendocardial myocytes of human left ventricle. Circulation 93:168-177.

Nademanee K, Taylor R, Bailey WE, Rieders DE, Kosar EM (2000) Treating electrical storm : sympathetic blockade versus advanced cardiac life support-guided therapy. Circulation 102:742-747.

Nakamae T, Tanaka N, Nakanishi K, Kamei N, Sasaki H, Hamasaki T, Yamada K, Yamamoto R, Mochizuki Y, Ochi M (2009) Chondroitinase ABC promotes corticospinal axon growth in organotypic cocultures. Spinal Cord 47:161-165.

Nakamura T, Komiya M, Sone K, Hirose E, Gotoh N, Morii H, Ohta Y, Mori N (2002) Grit, a GTPase-activating protein for the Rho family, regulates neurite extension through association with the TrkA receptor and N-Shc and CrkL/Crk adapter molecules. Mol Cell Biol 22:8721-8734.

Nian M, Lee P, Khaper N, Liu P (2004) Inflammatory cytokines and postmyocardial infarction remodeling. Circ Res 94:1543-1553.

Niemi JP, DeFrancesco-Lisowitz A, Roldan-Hernandez L, Lindborg JA, Mandell D, Zigmond RE (2013) A critical role for macrophages near axotomized neuronal cell bodies in stimulating nerve regeneration. J Neurosci 33:16236-16248.

Nishisato K, Hashimoto A, Nakata T, Doi T, Yamamoto H, Nagahara D, Shimoshige S, Yuda S, Tsuchihashi K, Shimamoto K (2010) Impaired cardiac sympathetic innervation and myocardial perfusion are related to lethal arrhythmia: quantification of cardiac tracers in patients with ICDs. J Nucl Med 51:1241-1249.

Oakley RA, Tosney KW (1991) Peanut agglutinin and chondroitin-6-sulfate are molecular markers for tissues that act as barriers to axon advance in the avian embryo. Dev Biol 147:187-206.

Ogawa S, Barnett JV, Sen L, Galper JB, Smith TW, Marsh JD (1992) Direct contact between sympathetic neurons and rat cardiac myocytes in vitro increases expression of functional calcium channels. J Clin Invest 89:1085-1093.

Oh YS, Jong AY, Kim DT, Li H, Wang C, Zemljic-Harpf A, Ross RS, Fishbein MC, Chen PS, Chen LS (2006) Spatial distribution of nerve sprouting after myocardial infarction in mice. Heart Rhythm 3:728-736.

Okabe T, Nakamura T, Nishimura YN, Kohu K, Ohwada S, Morishita Y, Akiyama T (2003) RICS, a novel GTPase-activating protein for Cdc42 and Rac1, is involved in the beta-catenin-N-cadherin and N-methyl-D-aspartate receptor signaling. J Biol Chem 278:9920-9927.

Olson L, Malmfors T (1970) Growth characteristics of adrenergic nerves in the adult rat. Fluorescence histochemical and 3H-noradrenaline uptake studies using tissue transplantations to the anterior chamber of the eye. Acta Physiol Scand Suppl 348:1-112.

Ono K, Fozzard HA, Hanck DA (1993) Mechanism of cAMP-dependent modulation of cardiac sodium channel current kinetics. Circ Res 72:807-815.

Pacioretty LM, Barr SC, Han WP, Gilmour RF, Jr. (1995) Reduction of the transient outward potassium current in a canine model of Chagas' disease. Am J Physiol 268:H1258-H1264.

Pardini BJ, Lund DD, Schmid PG (1989) Organization of the sympathetic postganglionic innervation of the rat heart. J Auton Nerv Syst 28:193-201.

Parrish DC, Alston EN, Rohrer H, Nkadi P, Woodward WR, Schutz G, Habecker BA (2010) Infarction-induced cytokines cause local depletion of tyrosine hydroxylase in cardiac sympathetic nerves. Exp Physiol 95:304-314.

Pellegrino MJ, Habecker BA (2013) STAT3 integrates cytokine and neurotrophin signals to promote sympathetic axon regeneration. Mol Cell Neurosci 56:272-282.

Pellegrino MJ, Parrish DC, Zigmond RE, Habecker BA (2011) Cytokines inhibit norepinephrine transporter expression by decreasing Hand2. Mol Cell Neurosci 46:671-680.

Pendleton JC, Shamblott MJ, Gary DS, Belegu V, Hurtado A, Malone ML, McDonald JW (2013) Chondroitin sulfate proteoglycans inhibit oligodendrocyte myelination through PTPsigma. Exp Neurol 247:113-121.

Perissinotto D, Iacopetti P, Bellina I, Doliana R, Colombatti A, Pettway Z, Bronner-Fraser M, Shinomura T, Kimata K, Morgelin M, Lofberg J, Perris R (2000) Avian neural crest cell migration is diversely regulated by the two major hyaluronan-binding proteoglycans PG-M/versican and aggrecan. Development 127:2823-2842.

Perlson E, Hanz S, Ben-Yaakov K, Segal-Ruder Y, Seger R, Fainzilber M (2005) Vimentin-dependent spatial translocation of an activated MAP kinase in injured nerve. Neuron 45:715-726.

Peters NS, Coromilas J, Severs NJ, Wit AL (1997) Disturbed connexin43 gap junction distribution correlates with the location of reentrant circuits in the epicardial border zone of healing canine infarcts that cause ventricular tachycardia. Circulation 95:988-996.

Pfeffer MA, Braunwald E (1990) Ventricular remodeling after myocardial infarction. Experimental observations and clinical implications. Circulation 81:1161-1172.

Pizzorusso T, Medini P, Berardi N, Chierzi S, Fawcett JW, Maffei L (2002) Reactivation of ocular dominance plasticity in the adult visual cortex. Science 298:1248-1251.

Poo MM (2001) Neurotrophins as synaptic modulators. Nat Rev Neurosci 2:24-32.

Porter KE, Turner NA (2009) Cardiac fibroblasts: at the heart of myocardial remodeling. Pharmacol Ther 123:255-278.

Properzi F, Asher RA, Fawcett JW (2003) Chondroitin sulphate proteoglycans in the central nervous system: changes and synthesis after injury. Biochem Soc Trans 31:335-336.

Protas L, Barbuti A, Qu J, Rybin VO, Palmiter RD, Steinberg SF, Robinson RB (2003) Neuropeptide Y is an essential in vivo developmental regulator of cardiac ICa,L. Circ Res 93:972-979.

Pu J, Boyden PA (1997) Alterations of Na+ currents in myocytes from epicardial border zone of the infarcted heart. A possible ionic mechanism for reduced excitability and postrepolarization refractoriness. Circ Res 81:110-119.

Pu J, Robinson RB, Boyden PA (2000) Abnormalities in Ca(i)handling in myocytes that survive in the infarcted heart are not just due to alterations in repolarization. J Mol Cell Cardiol 32:1509-1523.

Pulido R, Serra-Pages C, Tang M, Streuli M (1995) The LAR/PTP delta/PTP sigma subfamily of transmembrane protein-tyrosine-phosphatases: multiple human LAR, PTP delta, and PTP sigma isoforms are expressed in a tissue-specific manner and associate with the LAR-interacting protein LIP.1. Proc Natl Acad Sci U S A 92:11686-11690.

Raake PW, Zhang X, Vinge LE, Brinks H, Gao E, Jaleel N, Li Y, Tang M, Most P, Dorn GW, Houser SR, Katus HA, Chen X, Koch WJ (2012) Cardiac G-protein-coupled receptor kinase 2 ablation induces a novel Ca2+ handling phenotype resistant to adverse alterations and remodeling after myocardial infarction. Circulation 125:2108-2118.

Raivich G, Hellweg R, Kreutzberg GW (1991) NGF receptor-mediated reduction in axonal NGF uptake and retrograde transport following sciatic nerve injury and during regeneration. Neuron 7:151-164.

Randall WC, Szentivanyi M, Pace JB, Wechsler JS, Kaye MP (1968) Patterns of sympathetic nerve projections onto the canine heart. Circ Res 22:315-323.

Ranscht B (2000) Cadherins: molecular codes for axon guidance and synapse formation. Int J Dev Neurosci 18:643-651.

Rao MS, Sun Y, Escary JL, Perreau J, Tresser S, Patterson PH, Zigmond RE, Brulet P, Landis SC (1993) Leukemia inhibitory factor mediates an injury response but not a target-directed developmental transmitter switch in sympathetic neurons. Neuron 11:1175-1185.

Reichardt LF (2006) Neurotrophin-regulated signalling pathways. Philos Trans R Soc Lond B Biol Sci 361:1545-1564.

Richardson RJ, Grkovic I, Allen AM, Anderson CR (2006) Separate neurochemical classes of sympathetic postganglionic neurons project to the left ventricle of the rat heart. Cell Tissue Res 324:9-16.

Rockman HA, Koch WJ, Lefkowitz RJ (2002) Seven-transmembrane-spanning receptors and heart function. Nature 415:206-212.

Rodriguez-Tebar A, Dechant G, Barde YA (1990) Binding of brain-derived neurotrophic factor to the nerve growth factor receptor. Neuron 4:487-492.

Roger VL, et al. (2012a) Heart disease and stroke statistics--2012 update: a report from the American Heart Association. Circulation 125:e2-e220.

Roger VL, et al. (2012b) Heart disease and stroke statistics--2012 update: a report from the American Heart Association. Circulation 125:e2-e220.

Rolls A, Cahalon L, Bakalash S, Avidan H, Lider O, Schwartz M (2006) A sulfated disaccharide derived from chondroitin sulfate proteoglycan protects against inflammation-associated neurodegeneration. FASEB J 20:547-549.

Rubart M, Zipes DP (2005) Mechanisms of sudden cardiac death. J Clin Invest 115:2305-2315.

Ruit KG, Osborne PA, Schmidt RE, Johnson EM, Jr., Snider WD (1990) Nerve growth factor regulates sympathetic ganglion cell morphology and survival in the adult mouse. J Neurosci 10:2412-2419.

Saeki K, Ogawa S, Sadanaga T, Yoh S, Furuno I, Nakamura Y (1993) Sympathetic denervation of the epicardial border zone in the genesis of dispersion of refractoriness and arrhythmogenesis in a 7-day-old canine myocardial infarction model. Coron Artery Dis 4:775-782.

Said SI, Mutt V (1970) Polypeptide with broad biological activity: isolation from small intestine. Science 169:1217-1218.

Sapieha PS, Duplan L, Uetani N, Joly S, Tremblay ML, Kennedy TE, Di PA (2005) Receptor protein tyrosine phosphatase sigma inhibits axon regrowth in the adult injured CNS. Mol Cell Neurosci 28:625-635.

Scheer FA, Hu K, Evoniuk H, Kelly EE, Malhotra A, Hilton MF, Shea SA (2010) Impact of the human circadian system, exercise, and their interaction on cardiovascular function. Proc Natl Acad Sci U S A 107:20541-20546.

Schomig A, Richardt G (1990) Cardiac sympathetic activity in myocardial ischemia: release and effects of noradrenaline. Basic Res Cardiol 85 Suppl 1:9-30.

Schreiber RC, Hyatt-Sachs H, Bennett TA, Zigmond RE (1994) Galanin expression increases in adult rat sympathetic neurons after axotomy. Neuroscience 60:17-27.

SCHWARTZ PJ, MOTOLESE MARI, POLLAVINI GIOR, LOTTO ANTO, RUBERTI UGO, TRAZZI RINA, BARTORELLI CESA, ZANCHETTI ALBE, GROUP TISDP (1992) Prevention of Sudden Cardiac Death After a First Myocardial Infarction by Pharmacologic or Surgical Antiadrenergic Interventions. Journal of Cardiovascular Electrophysiology 3:2-16.

Shen Y, Tenney AP, Busch SA, Horn KP, Cuascut FX, Liu K, He Z, Silver J, Flanagan JG (2009) PTPsigma is a receptor for chondroitin sulfate proteoglycan, an inhibitor of neural regeneration. Science 326:592-596.

Sherman LS, Back SA (2008) A 'GAG' reflex prevents repair of the damaged CNS. Trends Neurosci 31:44-52.

Shi X, Habecker BA (2011) gp130 cytokines stimulate proteasomal degradation of tyrosine hydroxylase via extracellular signal regulated kinases 1 & 2. J Neurochem.

Shibata EF, Brown TL, Washburn ZW, Bai J, Revak TJ, Butters CA (2006) Autonomic regulation of voltage-gated cardiac ion channels. J Cardiovasc Electrophysiol 17 Suppl 1:S34-S42.

SHOLL DA (1953) Dendritic organization in the neurons of the visual and motor cortices of the cat. J Anat 87:387-406.

Siao CJ, Lorentz CU, Kermani P, Marinic T, Carter J, McGrath K, Padow VA, Mark W, Falcone DJ, Cohen-Gould L, Parrish DC, Habecker BA, Nykjaer A, Ellenson LH, Tessarollo L, Hempstead BL (2012) ProNGF, a cytokine induced after myocardial infarction in humans, targets pericytes to promote microvascular damage and activation. J Exp Med 209:2291-2305.

Silver J, Miller JH (2004) Regeneration beyond the glial scar. Nat Rev Neurosci 5:146-156.

Simula S, Lakka T, Kuikka J, Laitinen T, Remes J, Kettunen R, Hartikainen J (2000) Cardiac adrenergic innervation within the first 3 months after acute myocardial infarction. Clin Physiol 20:366-373.

Sirko S, von HA, Wizenmann A, Gotz M, Faissner A (2007) Chondroitin sulfate glycosaminoglycans control proliferation, radial glia cell differentiation and neurogenesis in neural stem/progenitor cells. Development 134:2727-2738.

Smith DS, Skene JH (1997) A transcription-dependent switch controls competence of adult neurons for distinct modes of axon growth. J Neurosci 17:646-658.

Snow DM, Brown EM, Letourneau PC (1996) Growth cone behavior in the presence of soluble chondroitin sulfate proteoglycan (CSPG), compared to behavior on CSPG bound to laminin or fibronectin. Int J Dev Neurosci 14:331-349.

Sofroniew MV (2005) Reactive astrocytes in neural repair and protection. Neuroscientist 11:400-407.

Sofroniew MV, Howe CL, Mobley WC (2001) Nerve growth factor signaling, neuroprotection, and neural repair. Annu Rev Neurosci 24:1217-1281.

Soleman S, Yip PK, Duricki DA, Moon LD (2012) Delayed treatment with chondroitinase ABC promotes sensorimotor recovery and plasticity after stroke in aged rats. Brain 135:1210-1223.

Solomon SD, Zelenkofske S, McMurray JJ, Finn PV, Velazquez E, Ertl G, Harsanyi A, Rouleau JL, Maggioni A, Kober L, White H, Van de Werf F, Pieper K, Califf RM, Pfeffer MA (2005) Sudden death in patients with myocardial infarction and left ventricular dysfunction, heart failure, or both. N Engl J Med 352:2581-2588.

Spach MS, Kootsey JM (1983) The nature of electrical propagation in cardiac muscle. Am J Physiol 244:H3-22.

Stanton MS, Tuli MM, Radtke NL, Heger JJ, Miles WM, Mock BH, Burt RW, Wellman HN, Zipes DP (1989) Regional sympathetic denervation after myocardial infarction in humans detected noninvasively using I-123-metaiodobenzylguanidine. J Am Coll Cardiol 14:1519-1526.

Streppel M, Azzolin N, Dohm S, Guntinas-Lichius O, Haas C, Grothe C, Wevers A, Neiss WF, Angelov DN (2002) Focal application of neutralizing antibodies to soluble neurotrophic factors reduces collateral axonal branching after peripheral nerve lesion. Eur J Neurosci 15:1327-1342.

Tamaoki M, Imanaka-Yoshida K, Yokoyama K, Nishioka T, Inada H, Hiroe M, Sakakura T, Yoshida T (2005) Tenascin-C regulates recruitment of myofibroblasts during tissue repair after myocardial injury. Am J Pathol 167:71-80.

Tang X, Davies JE, Davies SJ (2003) Changes in distribution, cell associations, and protein expression levels of NG2, neurocan, phosphacan, brevican, versican V2, and tenascin-C during acute to chronic maturation of spinal cord scar tissue. J Neurosci Res 71:427-444.

Tatemoto K, Rokaeus A, Jornvall H, McDonald TJ, Mutt V (1983) Galanin - a novel biologically active peptide from porcine intestine. FEBS Lett 164:124-128.

Thomas D, Kiehn J, Katus HA, Karle CA (2004) Adrenergic regulation of the rapid component of the cardiac delayed rectifier potassium current, I(Kr), and the underlying hERG ion channel. Basic Res Cardiol 99:279-287.

Thompson KM, Uetani N, Manitt C, Elchebly M, Tremblay ML, Kennedy TE (2003) Receptor protein tyrosine phosphatase sigma inhibits axonal regeneration and the rate of axon extension. Mol Cell Neurosci 23:681-692.

Toeda K, Nakamura K, Hirohata S, Hatipoglu OF, Demircan K, Yamawaki H, Ogawa H, Kusachi S, Shiratori Y, Ninomiya Y (2005) Versican is induced in infiltrating monocytes in myocardial infarction. Mol Cell Biochem 280:47-56.

Tom VJ, Kadakia R, Santi L, Houle JD (2009) Administration of chondroitinase ABC rostral or caudal to a spinal cord injury site promotes anatomical but not functional plasticity. J Neurotrauma 26:2323-2333.

Tona A, Bignami A (1993) Effect of hyaluronidase on brain extracellular matrix in vivo and optic nerve regeneration. J Neurosci Res 36:191-199.

Tonks NK (2006) Protein tyrosine phosphatases: from genes, to function, to disease. Nat Rev Mol Cell Biol 7:833-846.

Tuszynski MH, Gabriel K, Gage FH, Suhr S, Meyer S, Rosetti A (1996) Nerve growth factor delivery by gene transfer induces differential outgrowth of sensory, motor, and noradrenergic neurites after adult spinal cord injury. Exp Neurol 137:157-173.

Uchi J, Komukai K, Kusakari Y, Obata T, Hongo K, Sasaki H, Kurihara S (2005) alpha1-adrenoceptor stimulation potentiates L-type Ca2+ current through Ca2+/calmodulin-dependent PK II (CaMKII) activation in rat ventricular myocytes. Proc Natl Acad Sci U S A 102:9400-9405.

Valdivia HH, Kaplan JH, Ellis-Davies GC, Lederer WJ (1995) Rapid adaptation of cardiac ryanodine receptors: modulation by Mg2+ and phosphorylation. Science 267:1997-2000.

Vaseghi M, Gima J, Kanaan C, Ajijola OA, Marmureanu A, Mahajan A, Shivkumar K (2013) Cardiac Sympathetic Denervation In Patients With Refractory Ventricular Arrhythmias Or Electrical Storm: Intermediate And Long Term Follow Up. Heart Rhythm10.

Vaseghi M, Lux RL, Mahajan A, Shivkumar K (2012) Sympathetic stimulation increases dispersion of repolarization in humans with myocardial infarction. Am J Physiol Heart Circ Physiol 302:H1838-H1846.

Veeranna, Amin ND, Ahn NG, Jaffe H, Winters CA, Grant P, Pant HC (1998) Mitogen-activated protein kinases (Erk1,2) phosphorylate Lys-Ser-Pro (KSP) repeats in neurofilament proteins NF-H and NF-M. J Neurosci 18:4008-4021.

Verrier RL, Klingenheben T, Malik M, El-Sherif N, Exner DV, Hohnloser SH, Ikeda T, Martinez JP, Narayan SM, Nieminen T, Rosenbaum DS (2011) Microvolt T-wave alternans physiological basis, methods of measurement, and clinical utility--consensus guideline by International Society for Holter and Noninvasive Electrocardiology. J Am Coll Cardiol 58:1309-1324.

Viatchenko-Karpinski S, Gyorke S (2001) Modulation of the Ca(2+)-induced Ca(2+) release cascade by beta-adrenergic stimulation in rat ventricular myocytes. J Physiol 533:837-848.

Vo PA, Tomlinson DR (1999) The regeneration of peripheral noradrenergic nerves after chemical sympathectomy in diabetic rats: effects of nerve growth factor. Exp Neurol 157:127-134.

von HA, Sirko S, Faissner A (2006) The unique 473HD-Chondroitinsulfate epitope is expressed by radial glia and involved in neural precursor cell proliferation. J Neurosci 26:4082-4094.

Vracko R, Thorning D, Frederickson RG (1990) Fate of nerve fibers in necrotic, healing, and healed rat myocardium. Lab Invest 63:490-501.

Wallace MJ, Batt J, Fladd CA, Henderson JT, Skarnes W, Rotin D (1999) Neuronal defects and posterior pituitary hypoplasia in mice lacking the receptor tyrosine phosphatase PTPsigma. Nat Genet 21:334-338.

Wallace MJ, Fladd C, Batt J, Rotin D (1998) The second catalytic domain of protein tyrosine phosphatase delta (PTP delta) binds to and inhibits the first catalytic domain of PTP sigma. Mol Cell Biol 18:2608-2616.

Wan X, Laurita KR, Pruvot EJ, Rosenbaum DS (2005) Molecular correlates of repolarization alternans in cardiac myocytes. J Mol Cell Cardiol 39:419-428.

Wenk JF, Klepach D, Lee LC, Zhang Z, Ge L, Tseng EE, Martin A, Kozerke S, Gorman JH, III, Gorman RC, Guccione JM (2012) First evidence of depressed contractility in the border zone of a human myocardial infarction. Ann Thorac Surg 93:1188-1193.

Wenk JF, Sun K, Zhang Z, Soleimani M, Ge L, Saloner D, Wallace AW, Ratcliffe MB, Guccione JM (2011) Regional left ventricular myocardial contractility and stress in a finite element model of posterobasal myocardial infarction. J Biomech Eng 133:044501.

Werner A, Willem M, Jones LL, Kreutzberg GW, Mayer U, Raivich G (2000) Impaired axonal regeneration in alpha7 integrin-deficient mice. J Neurosci 20:1822-1830.

Wernli G, Hasan W, Bhattacherjee A, van RN, Smith PG (2009) Macrophage depletion suppresses sympathetic hyperinnervation following myocardial infarction. Basic Res Cardiol 104:681-693.

Wheeldon NM, McDevitt DG, Lipworth BJ (1993) Investigation of putative cardiac beta 3-adrenoceptors in man. Q J Med 86:255-261.

Wilson LD, Wan X, Rosenbaum DS (2006) Cellular alternans: a mechanism linking calcium cycling proteins to cardiac arrhythmogenesis. Ann N Y Acad Sci 1080:216-34.:216-234.

Wilson RF, Johnson TH, Haidet GC, Kubo SH, Mianuelli M (2000) Sympathetic reinnervation of the sinus node and exercise hemodynamics after cardiac transplantation. Circulation 101:2727-2733.

Wita K, Filipecki A, Bochenek T, Tabor Z, Myszor J, Turski M, Doruchowska A, Trusz-Gluza M (2012) Microvolt T-wave alternans predicts cardiac events after acute myocardial infarction in patients treated with primary percutaneous coronary intervention. Adv Med Sci 57:328-333.

Yamaguchi Y (2000) Lecticans: organizers of the brain extracellular matrix. Cell Mol Life Sci 57:276-289.

Yamaguchi Y (2001) Heparan sulfate proteoglycans in the nervous system: their diverse roles in neurogenesis, axon guidance, and synaptogenesis. Semin Cell Dev Biol 12:99-106.

Yao JA, Hussain W, Patel P, Peters NS, Boyden PA, Wit AL (2003) Remodeling of gap junctional channel function in epicardial border zone of healing canine infarcts. Circ Res 92:437-443.

Yarbrough TL, Lu T, Lee HC, Shibata EF (2002) Localization of cardiac sodium channels in caveolin-rich membrane domains: regulation of sodium current amplitude. Circ Res 90:443-449.

Yatani A, Shen YT, Yan L, Chen W, Kim SJ, Sano K, Irie K, Vatner SF, Vatner DE (2006) Down regulation of the L-type Ca2+ channel, GRK2, and phosphorylated phospholamban: protective mechanisms for the denervated failing heart. J Mol Cell Cardiol 40:619-628.

Yoshioka K, Gao DW, Chin M, Stillson C, Penades E, Lesh M, O'Connell W, Dae M (2000) Heterogeneous sympathetic innervation influences local myocardial repolarization in normally perfused rabbit hearts. Circulation 101:1060-1066.

Yue L, Feng J, Wang Z, Nattel S (1999) Adrenergic control of the ultrarapid delayed rectifier current in canine atrial myocytes. J Physiol 516 (Pt 2):385-398.

Zhang Y, Yeh J, Richardson PM, Bo X (2008) Cell adhesion molecules of the immunoglobulin superfamily in axonal regeneration and neural repair. Restor Neurol Neurosci 26:81-96.

Zhou FQ, Snider WD (2006) Intracellular control of developmental and regenerative axon growth. Philos Trans R Soc Lond B Biol Sci 361:1575-1592.

Zhou FQ, Walzer M, Wu YH, Zhou J, Dedhar S, Snider WD (2006) Neurotrophins support regenerative axon assembly over CSPGs by an ECM-integrin-independent mechanism. J Cell Sci 119:2787-2796.

Zhou S, Chen LS, Miyauchi Y, Miyauchi M, Kar S, Kangavari S, Fishbein MC, Sharifi B, Chen PS (2004) Mechanisms of cardiac nerve sprouting after myocardial infarction in dogs. Circ Res 95:76-83.

Zoubina EV, Smith PG (2000) Axonal degeneration and regeneration in rat uterus during the estrous cycle. Auton Neurosci 84:176-185.

Zuo J, Hernandez YJ, Muir D (1998) Chondroitin sulfate proteoglycan with neurite-inhibiting activity is up-regulated following peripheral nerve injury. J Neurobiol 34:41-54.

Zuo J, Neubauer D, Graham J, Krekoski CA, Ferguson TA, Muir D (2002) Regeneration of axons after nerve transection repair is enhanced by degradation of chondroitin sulfate proteoglycan. Exp Neurol 176:221-228.

Zygmunt AC, Goodrow RJ, Weigel CM (1998) INaCa and ICl(Ca) contribute to isoproterenol-induced delayed after depolarizations in midmyocardial cells. Am J Physiol 275:H1979-H1992.